# Integrating short- and long-term bioerosion processes in the Eastern Mediterranean Sea

Dissertation

zur Erlangung des Doktorgrades der Naturwissenschaften
(Dr. rer. nat.)

am Fachbereich Geowissenschaften
der Universität Bremen

vorgelegt von

Claudia Färber

Wilhelmshaven
Januar 2016

Gutachter:

Prof. Dr. André Freiwald
Senckenberg am Meer, Wilhelmshaven

Prof. Dr. Hildegard Westphal
Leibniz-Zentrum für Marine Tropenökologie (ZMT), Bremen

weitere Mitglieder der Prüfungskommission:

Prof. Dr. Heiko Pälike
Prof. Dr. Michal Kucera
Dr. Wolf-Achim Kahl
Neele Meyer

Datum des Kolloquiums: 1. Juni 2016

Name: Claudia Färber 28. 01.2016

Anschrift: Hamburger Str. 30, 26382 Wilhelmshaven

# Erklärung

---

Hiermit versichere ich, dass ich

1. die Arbeit ohne unerlaubte fremde Hilfe angefertigt habe,

2. keine anderen als die von mir angegebenen Quellen und Hilfsmittel benutzt habe

und

3. die den benutzten Werken wörtlich oder inhaltlich entnommenen Stellen als solche kenntlich gemacht habe.

Wilhelmshaven, den 28.01.2016

.....

(Unterschrift)

# Acknowledgements

This thesis is based on data resulting from the DFG project "Integrating short- and long-term bioerosion processes (Greece)" (Wi 3754/2-1), carried out from February 2013 until January 2016 at the research institute Senckenberg am Meer (SaM) in Wilhelmshaven.

First and foremost, I would like to thank my supervisors Prof. Dr. André Freiwald and Dr. Max Wisshak (SaM, Wilhelmshaven) for giving me the opportunity to carry out my Ph.D. in the project, for always supporting and encouraging me during the last three years, and having always an open door for questions and discussions. Further, I would like to thank Prof. Dr. Hildegard Westphal (ZMT, Bremen) for joining my thesis committee and for being the second examiner of this thesis.

I would like to express my deepest gratitude to Dr. Jürgen Titschack (MARUM, Bremen) for providing great support during micro-CT post-processing and many fruitful discussions, Dr. Nikoleta Bellou (HCMR, Greece) for supporting and joining our field trips to Rhodes, Prof. Dr. Richard Bromley and Ulla Asgaard for providing us the material from their long-term experiment, Dr. Karsten Ehrig and Dr. Bernhard Illerhaus (BAM, Berlin), for micro-CT scanning the samples from the long-term experiment, Dr. Daniel Baum (ZIB, Berlin) for providing powerful algorithms for micro-CT post-processing, Dr. Christine Schönberg (University of Western Australia, Crawley) for supporting sponge spicule extraction and identification, Dr. Karin Boos (MARUM, Bremen) and Dr. Marina Carreiro-Silva (University of the Azores) for providing expert statistical support, and Dr. Gudrun Radtke (HLNUG, Wiesbaden) and Prof. Dr. Stjepko Golubic (Boston University, Boston) for supporting the identification of microbioerosion traces. I thank the graduate school GLOMAR (MARUM, Bremen) for offering a broad range of helpful seminars and for conference funding, especially Dr. Christina Klose, Dr. Martina Loebl, and Dr. Karin Boos.

I sincerely thank my colleagues at the SaM, especially Nicol Mahnken for sputter-coating SEM samples and helping with all kind of logistics, Marco Persicke and Maik Wilsenack for technically supporting the preparation of the Rhodes experiment, Heike Waldau for administrative support, and Burkhard Köster for IT support. Neele Meyer is highly acknowledged for supporting the preparations of our first field trip during her internship and joining the second as a student assistant. Furthermore, I would like to thank Kei Matsuyama, Dr. Lydia Beuck, Torsten Janssen, Barbara Domenighini, Íris Sampaio, and all I cannot personally acknowledge here for help and support.

Finally, I would like to thank my family and friends, who always supported and encouraged me, especially during the last three years.

# Abstract

Bioerosion, the degradation of hard substrate by living organisms, is an integral process of the marine carbonate cycle, contributing to the recycling of carbonate substrates and helping to maintain the balance between construction and destruction in reef environments. Experimental studies on bioerosion are an important tool for carbonate budget calculations and palaeoenvironmental reconstruction. Most previous bioerosion experiments were conducted over a period of 1 to 2 years giving a detailed picture on microbioerosion in different geographical settings. Experimental studies on the long-term succession of macrobioeroders were previously limited to tropical coral reef systems.

Aim of this thesis was the integration of short- and long-term bioerosion processes in the Eastern Mediterranean Sea. Research on bioerosion in the Mediterranean Sea has a long tradition, but experimental studies are scarce and were previously restricted to the Western Mediterranean Sea. The Eastern Mediterranean Sea is an extreme environment, characterised by an ultra-oligotrophic nutrient regime and exceptionally high temperature and salinity conditions. Experimental data on Mediterranean bioerosion, hence, contributes important information for evaluating global patterns of bioerosion and for modelling the future impact of bioerosion. This is particularly relevant since bioerosion is considered to increase with ongoing ocean acidification, with potentially detrimental effects on carbonate-dominated ecosystems.

The main objectives were (1) to analyse the spatio-temporal variability of bioerosion in the Eastern Mediterranean Sea and its effect on the carbonate budget, (2) to assess the usability of the observed bioerosion traces for palaeoenvironmental reconstruction, and (3) to set the results in latitudinal and longitudinal context to previous bioerosion experiments. This was based on three experimental studies: (1) a carbonate cycling experiment with experimental platforms deployed for a summer, a winter, and one year along a bathymetric transect from 15 to 250 m water depth south-west off the Peloponnese Peninsula in the Ionian Sea, (2) a coastal bioerosion experiment with limestone substrates mounted for 1 and 2 years in the inter- to supratidal zone at the island of Rhodes, and (3) a long-term experiment with experimental blocks deployed for 1 to 14 years in 3 to 17 m water depth around Rhodes. Short-term bioerosion rates and traces were analysed by gravimetrical measurements and scanning electron microscopy, respectively. For the analysis of long-term bioerosion rates and traces micro-computed tomographic (micro-CT) analysis was chosen in a novel approach.

In total, 44 different bioerosion traces were observed that were assigned to bioeroding cyanobacteria, chlorophytes, fungi, foraminifera, bacteria, sponges, polychaetes, bivalves, gastropods, diatoms, sea urchins, chitons, and other previously unknown producers. The carbonate cycling experiment revealed that the distribution and boring intensity of microbioerosion agents in the Eastern Mediterranean Sea is mostly controlled by the availability of light in the water column, but secondarily subject to a distinct seasonal variability. The highest bioerosion activity was recorded in 15 m up-facing substrates in the shallow euphotic zone (mean 83 g $m^{-2}$ $yr^{-1}$), largely driven by phototrophic cyanobacteria, while towards the chlorophyte-dominated deep euphotic to dysphotic zone and the organotroph-dominated aphotic zone the intensity of bioerosion and diversity of bioerosion traces strongly decreased (mean 1.39 g $m^{-2}$ $yr^{-1}$ in 250 m). During summer, the bioeroding activity of phototrophic microbioeroders was significantly higher than during winter, stimulated by enhanced light availability due to more hours of daylight and increased irradiance angles.

Stable water column stratification and a resulting nutrient depletion in shallow water led to lower turbidity levels and caused a shift in the photic zonation that was reflected by more phototrophs being active at greater depth. The observed patterns in overall bioeroder distribution and abundance were mirrored by the calculated carbonate budget with bioerosion rates exceeding carbonate accretion rates in the shallow subtidal zone (-65 g $m^{-2}$ $yr^{-1}$).

Towards and within the supratidal zone, the coastal experiment revealed a distinct decrease of microbioerosion activity and diversity of bioerosion traces, with only initial bioerosion traces having been observed after 1 to 2 years. A higher vertical distribution of borings in substrates on the wind-exposed west coast than in substrates on the sheltered east coast, and thriving microbioerosion trace assemblages in water-filled solution pans in the supratidal zone indicated sea water supply as one of the limiting factors of coastal bioerosion. Although recent rocky coasts show a distinct colour zonation, produced by different bioeroding cyanobacteria, no distinct zonation of microbioerosion traces could be reconstructed. This is because in contrast to subtidal microbioerosion traces, which can assigned to their living trace makers by morphological characteristics, the taxonomical differentiation of coastal endoliths is mostly based on colour pigments. Because these are not preserved in the fossil record, makes the reconstruction of fossil rocky shore zonation patterns by means of microbioerosion traces difficult.

Although on the surrounding sea floor, boring bivalves and polychaetes were reported to be common, analysis of macrobioerosion traces from the long-term experiment revealed a dominance of boring sponges. An early community development stage was observed during the first 5 years of exposure, where first boring sponges settled, but produced low rates of macrobioerosion (1–220 g $m^{-2}$ $yr^{-1}$), followed by an intermediate stage when boring sponges formed large and more diverse cavity networks and bioerosion rates increased (309–650 g $m^{-2}$ $yr^{-1}$). After 14 years, 30 % of the block volumes were occupied by boring sponges, yielding to maximum bioerosion rates of 900 g $m^{-2}$ $yr^{-1}$. High spatial variability of macroborers and low numbers of replicates, however, prohibited clear conclusions about the onset of macrobioerosion equilibrium conditions. This underlines the need for further long-term experiments, especially outside the tropical realm, in order to quantify the actual impact of macrobioerosion on the marine realm.

# Zusammenfassung

Bioerosion, der Abbau von Hartsubstraten durch lebende Organismen, ist ein wichtiger Prozess im marinen Karbonatkreislauf, der zur Wiederverwertung karbonatischer Substrate beiträgt und mitverantwortlich ist die Balance zwischen Auf- und Abbau in Riffsystemen zu erhalten. Experimentelle Studien über Bioerosion sind ein wichtiges Werkzeug zur Ermittlung von Karbonatbudgets und der Paläoumweltrekonstruktion. Die meisten bisherigen Bioerosionsexperimente wurden über einen Zeitraum von 1 bis 2 Jahren durchgeführt und lieferten ein umfangreiches Bild über Mikrobioerosion in unterschiedlichen geographischen Regionen. Experimentelle Studien zu der Langzeitentwicklung von Makrobohrern beschränken sich bisher hingegen auf tropische Korallenriffsysteme.

Ziel dieser Arbeit war die Untersuchung von Kurz- und Langzeitbioerosionsprozessen im östlichen Mittelmeer. Die Erforschung von Bioerosionsprozessen im Mittelmeer hat eine lange Tradition, aber experimentelle Studien sind selten und beschränkten sich bisher auf das westliche Mittelmeer. Dabei ist das östliche Mittelmeer ein extremer Lebensraum, der sich durch ein ultra-oligotrophes Nährstoffregime auszeichnet und zudem durch auffallend hohe Wassertemperaturen und Salinitätsbedingungen charakterisiert ist. Experimentelle Daten über Bioerosion im Mittelmeer tragen deshalb maßgeblich zum Verständnis globaler Bioerosionsmuster und zur Modellierung des zukünftigen Einflusses von Bioerosion bei. Dies ist besonders wichtig, da angenommen wird, dass Bioerosion zukünftig durch Ozeanversauerung ansteigen wird und einen zunehmend schädlichen Effekt auf karbonatische Ökosysteme ausüben wird.

Die Hauptziele waren (1) die räumliche und zeitliche Variation von Bioerosion im östlichen Mittelmeer, sowie den Einfluss auf das Karbonatbudget zu ermitteln, (2) die Anwendung der gefundenen Bioerosionsspuren für Paläoumweltrekonstruktionszwecke zu prüfen und (3) die Ergebnisse in latitudinalen und longitudinalen Kontext zu bisherigen Bioerosionsexperimenten zu setzen. Dies basierte auf drei Bioerosionsexperimenten: (1) einem Karbonatkreislaufexperiment in dessen Rahmen Plattformen mit experimentellen Substraten für ein Sommer- und Winterhalbjahr, sowie ein ganzes Jahr entlang eines Tiefentransektes von 15 bis 250 m Wassertiefe südwestlich der Peloponnes Halbinsel im Ionischen Meer exponiert waren, (2) einem Bioerosionsexperiment an der Küste von Rhodos in dessen Rahmen Kalksubstrate für 1 bis 2 Jahre vom inter- bis in den supratidalen Bereich befestigt waren, und (3) einem Langzeitexperiment vor Rhodos, in dessen Rahmen experimentelle Blöcke für 1 bis 14 Jahre in 3 bis 17 m Wassertiefe exponiert waren. Kurzzeitliche Bioerosionsraten und -spuren wurden anhand gravimetrischer Methoden und Rasterelektronenmikroskopie ermittelt. Langzeitliche Bioerosionsraten und -spuren wurden erstmals in einem neuen Ansatz mittels Mikro-Computertomographie erfasst.

Insgesamt wurden 44 unterschiedliche Bioerosionsspuren beobachtet, die bioerodierenden Cyanobakterien, Chlorophyten, Pilzen, Foraminiferen, Bakterien, Schwämmen, Polychaeten, Muscheln, Schnecken, Diatomeen, Seeigeln, Käferschnecken und anderen bisher unbekannten Produzenten zugeordnet werden konnten. Das Karbonatkreislaufexperiment zeigte, dass die Verteilung und Bohrintensität von Mikrobioerodieren im östlichen Mittelmeer hauptsächlich durch die Verfügbarkeit von Licht in der Wassersäule gesteuert wird, aber sekundär eine deutliche saisonale Variabilität aufweist. Die höchste Bioerosionsrate wurde in nach oben ausgerichteten Substraten in 15 m Wassertiefe in der flachen euphotischen Zone gemessen (durchschnittlich 83 g $m^{-2}$ $yr^{-1}$), hauptsächlich gesteuert durch phototrophe Cyanobakterien, während Bioerosionsraten und die Diversität von

Bohrspuren mit Eintritt in die Chlorophyten-dominierte tiefe euphotische und dysphotische Zone, sowie die von Organotrophen-dominierte Zone stark zurückging. Während des Sommers war die Bioerosionsaktivität von phototrophen Mikrobioerodierern aufgrund höherer Wassertemperaturen, höherer absoluter Lichtintensitäten und niedriger Wassertrübung infolge niedriger Nährstoffkonzentrationen während der sommerlichen Schichtung der Wassersäule deutlich erhöht. Die beobachteten Muster in der Gesamtverteilung und Häufigkeit von bioerodierenden Organismen spiegelte sich auch im errechneten Karbonatbudget wieder, das durch einen deutlichen Überschuss an Bioerosion über Karbonatakkretion im Flachwasser gekennzeichnet war (-65 g $m^{-2}$ $yr^{-1}$).

In Richtung des Supratidals hingegen zeigte das Bioerosionsexperiment an der Küste einen deutlichen Abfall in der Aktivität bohrender Organismen und der Diversität von Bohrspuren, und es konnten nach 1 bis 2 Jahren lediglich initiale Bohrungen beobachtet werden. Eine höhere vertikale Verteilung von Bohrungen in Substraten an der wind-exponierten Westküste als an der wind-geschützten Ostküste, sowie florierende Bohrspuren in wassergefüllten Lösungspfannen im Supratidal deuteten die Verfügbarkeit von Meerwasser als Hauptlimitierungsfaktor von Küstenbioerosion an. Obwohl rezente Felsenküsten eine charakteristische Farbzonierung aufweisen, die durch unterschiedliche bioerodierende Cyanobakterien hervorgerufen wird, konnte keine Zonierung von Mikrobioerosionspuren rekonstruiert werden. Dies ist dadurch zu erklären, dass im Gegensatz zu subtidalen Mikrobioerosionsspuren, die ihren lebenden Erzeugern aufgrund morphologischer Kriterien zugeordnet werden können, die Klassifikation von küstenbewohnenden Endolithen hauptsächlich auf Pigmentvariationen beruht. Diese jedoch sind nicht im Fossilbericht überliefert, was eine Rekonstruktion von fossilen Küstenzonierungsmustern anhand von Mikrobohrern erschwert.

Während des Langzeitexperimentes wurden hauptsächlich Bohrspuren von Schwämmen beobachtet, obwohl auf dem Meeresboden auch bohrende Bivalven und Polychaeten sehr häufig waren. Während der ersten 5 Jahre wurden initiale Gemeinschaften mit niedrigen Bioerosionsraten beobachtet (1–220 g $m^{-2}$ $yr^{-1}$), die nach 6 bis 7 Jahren von den ersten größeren und diverseren Bohrschwammgemeinschaften abgelöst wurden, was zu einem deutlichen Anstieg der Bioerosionsraten führte (309–650 g $m^{-2}$ $yr^{-1}$). Nach 14 Jahren waren 30 % des Blockvolumens durch Bohrschwämme besiedelt, die zu maximalen Bioerosionsraten von 900 g $m^{-2}$ $yr^{-1}$ führten. Aufgrund der hohen räumlichen Variation von Makrobioerodierern konnte jedoch keine klare Aussage über das Einsetzen eines Makrobioerosionequilibriums getroffen werden. Dies unterstreicht die Notwendigkeit von weiteren Langzeitstudien, besonders außerhalb des tropischen Bereichs, um den tatsächlichen Einfluss von Makrobioerosion auf marine karbonatische Systeme besser erfassen zu können.

# Thesis outline

This thesis is organised in nine chapters. Chapter 1 provides an introduction into the process of bioerosion and presents the motivation and objectives of this thesis. Chapter 2 provides an overview about the environmental setting and the characteristics of the study sites. Chapter 3 presents the material and methods used in the course of this study. The scientific objectives as outlined in Chapter 1 are addressed within three manuscripts (Chapters 4–6) that are published in, submitted to, or in preparation for submission to international peer-review journals. Corresponding to the topic of this thesis, the manuscripts are arranged in chronological order reporting on bioerosion from seasonal to decadal scale:

Chapter 4: "Effects of water depth, seasonal exposure, and substrate orientation on microbial bioerosion in the Ionian Sea (Eastern Mediterranean)", Claudia Färber, Max Wisshak, Ines Pyko, Nikoleta Bellou, André Freiwald, published in PLoS ONE, 10(4), e0126495, doi: 10.1371/journal.pone.0126495.

- Content: This chapter presents the results from a carbonate cycling experiment that was carried out over ½ to 1 year in the Ionian Sea. Experimental platforms were deployed in 15, 50, 100, and 250 m water depth south-west of the Peloponnese Peninsula (Greece) in order to analyse the effects of water depth, seasonal exposure, and substrate orientation on microbioerosion. Bioerosion rates and traces were assessed by gravimetrical methods and scanning electron microscopy (SEM).
- Contributions: The experiment was initiated by MW, NB, and AF. The experiment was conceived and designed by MW and NB. The experiment was prepared and performed by IP, NB, and MW. Sample preparation, laboratory work, SEM analysis, and data analysis was carried out by CF and IP. The manuscript was written by CF with contributions of all co-authors.

Chapter 5: "Early succession of inter- and supratidal microbioerosion at rocky limestone coasts (Eastern Mediterranean Sea)", Claudia Färber, Nikoleta Bellou, André Freiwald, Max Wisshak, to be submitted to Palaeogeography, Palaeoclimatology, Palaeoecology.

- Content: This chapter presents the results from a bioerosion experiment that was conducted over 1 to 2 years at the rocky coast of the island of Rhodes (Greece). Experimental substrates were mounted along four transects across the intertidal and supratidal zones to investigate the spatio-temporal development of coastal bioerosion in the Eastern Mediterranean Sea. Bioerosion traces were analysed by SEM.
- Contributions: The experiment was initiated by MW, CF, and AF. The experiment was prepared by CF and MW. Fieldwork was carried out by CF, MW, and NB. Sample preparation, laboratory work, SEM analysis, and data analysis was carried out by CF. The manuscript was written by CF with contributions of all co-authors.

Chapter 6: "Long-term development of macrobioerosion in the Mediterranean Sea assessed by micro-computed tomography", Claudia Färber, Jürgen Titschack, Christine H.L. Schönberg, Karsten Ehrig, Karin Boos, Daniel Baum, Bernhard Illerhaus, Ulla Asgaard, Richard G. Bromley, André Freiwald, Max Wisshak, submitted to Biogeosciences.

- Content: This chapter presents results from the first long-term bioerosion experiment from the non-tropical realm, and showcases the use of micro-computed tomography (micro-CT) to study internal macrobioerosion. Experimental blocks were deployed

from 1 to 14 years in 3 to 17 m water depth off the rocky coast of Rhodes to monitor the pace at which bioerosion affects carbonate substrate and the sequence of colonisation by bioeroding organisms. Internal macrobioerosion was visualised and quantified by micro-CT and computer-algorithm based segmentation procedures. Boring sponge species were identified by sponge spicule analysis.

- Contributions: The experiment was initiated and performed by UA and RGB. Micro-CT analysis was carried out by KE and BI. Micro-CT post-processing was carried out by CF, JT, and DB. Sponge spicule analysis was carried out by CF and CHLS. The data was analysed by CF and KB. The manuscript was written by CF with contributions of all co-authors.

A concluding discussion and outlook of the findings of all three manuscripts is presented in Chapters 7 and 8, respectively. References for all chapters are provided in a comprehensive list in Chapter 9. Supplementary data for all manuscripts are provided in the Appendix.

# Contents

# 1 Introduction

## 1.1 The role of carbonate bioerosion in the marine realm

The term bioerosion was introduced by Neumann (1966) to describe the removal and destruction of hard substrate by living organisms. Bioerosion occurs from freshwater to marine environments affecting various types of substrates, which can be generally classified into three categories: (1) lithic substrates such as rock, biogenic skeletal material, and man-made material, (2) plant material such as wood, nuts, and leaves, and (3) osseous substrates such as bone and teeth (Bromley, 1994). However, the highest diversity and greatest ecological significance of bioeroding organisms is found in the marine realm, where bioerosion affects limestone rock grounds, carbonate hardgrounds, carbonate clasts from boulders to sand grains, and skeletons of animals and calcareous algae (Golubic et al., 1975). Marine carbonate bioerosion plays an important role in the marine carbonate cycle (Golubic et al., 1979; Ridgwell and Zeebe, 2005), contributing to the recycling of dead carbonate substrate into fresh calcareous sediment (Bromley, 1994), and helping to maintain the balance between construction and destruction in coral reef environments (e.g., Glynn, 1997).

### 1.1.1 Research on bioerosion

Today, research on bioerosion evolves a wide, interdisciplinary field of natural sciences at the interface of biology, palaeontology, geology, and geomorphology. Research on bioerosion has a long tradition and earliest studies were already carried at the beginning of the 19$^{th}$ century (Grant, 1826; Osler, 1826) — even long before the official definition by Neumann (1966). Until the 1970s, most studies were descriptive and focused on the taxonomic description of bioeroders (Schönberg and Tapanila, 2006). Since the 1980s, more and more studies investigated the mechanisms of bioerosion as well as its palaeontological perspectives, which included also the advancement of new techniques for exploring the microscopic record of bioerosion (Schönberg and Tapanila, 2006). One of the greatest advances was certainly the development of the "cast-embedding technique" (Golubic et al., 1970), allowing to preserve endoliths and their traces *in situ* and to make them optically accessible in three-dimensions. This method has been permanently developed and improved since then, and is still the standard procedure to visualise boring traces (see Chapter 3.2.1; Wisshak, 2012). Since the 1990s, a series of field experiments was carried out in order to investigate the effect and variability of bioerosion in different carbonate environments (see Chapter 1.1.3; Wisshak, 2006 for a review). At the same time, the utility of microbioerosion traces for palaeoenvironmental reconstruction was more and more improved and especially the investigation of microbioerosion trace assemblages (ichnocoenoses) has been recognised to be a strong tool for judging light availability and hence relative bathymetry in modern and ancient environmental settings (see Chapter 1.1.4 for further description; Wisshak, 2012 for a review).

In the last years, as part of the increasing recognition of the negative effects of climate change on marine ecosystems, more and more laboratory experiments were conducted. Declining pH and carbonate saturation state in the ocean caused by anthropogenic emission of greenhouse gas are known to significantly threaten growth and calcification rates of marine carbonate biota (e.g., Kroeker et al., 2010; Bates, 2014). Studies on marine carbonate biodegrading biota are comparatively new, however, revealing that bioerosion agents are

among the few organisms that profit from global change and enhanced bioerosion rates under ocean acidification scenarios have been reported, for instance, for microendoliths (Tribollet et al., 2009), and bioeroding sponges (e.g., Wisshak et al., 2012, 2013, 2014b; Fang et al., 2013; Stubler et al., 2014). Ongoing ocean acidification and global warming, hence, present a serious danger to carbonate factories such as coral reefs or red algae deposits (e.g., Hoegh-Guldberg et al., 2007; Basso and Granier, 2012), and experimental studies will become increasingly important for evaluating global patterns of bioerosion and for modelling future impacts of bioerosion on carbonate ecosystems (Kennedy et al., 2013).

In the following, short reviews about the ecology of bioerosion agents, previous experimental studies, and the application of bioerosion traces for palaeoenvironmental reconstruction are given, which are tailored to the objectives of this thesis. Further comprehensive and detailed information on the various aspects of bioerosion are provided in review papers on bioerosion in general (Warme, 1975; Tribollet et al., 2011), microbioerosion (Golubic et al., 1975; Wisshak, 2012), the stratigraphy of bioerosion (Bromley, 2004; Glaub and Vogel, 2004), and the palaeoecology of bioerosion (Bromley, 1994).

### 1.1.2 Ecology of bioerosion agents

In modern oceans, at least twelve phyla of animals, as well as several groups of plants and protozoans possess the ability to bioerode (Warme, 1975). This comprises external bioerosion by organisms that live outside the substrate (epiliths) or internal bioerosion by organisms that excavate the substrate (endoliths) (Golubic et al., 1981). This classification is further subdivided into euendoliths that actively bore a cavity, cryptoendoliths that passively nestle within existing cavities, and chasmoendoliths that occupy minute, nonbiogenic fissures (Golubic et al., 1981). The distinction between these habitats, however, is not always clear, because some organisms may belong to more than one category or may vary their habit during their life cycle (Golubic et al., 1975). Endolithic organisms are taxonomically classified as biotaxa either within the International Code of Botanical Nomenclature (ICBN; Greuter et al., 2000) or the International Code of Zoological Nomenclature (ICZN; International Commission on Zoological Nomenclature, 1999). Their traces are treated as ichnotaxa and are taxonomically covered by the ICZN as well. For the establishment of new ichnogenera or ichnospecies, the type material shall be fossilised, but recent traces may be identified and addressed as ichnotaxa (Bertling et al., 2006).

Traditionally, bioerosion agents are differentiated into microboring, macroboring, grazing, and attaching organisms (Fig. 1.1). The resulting traces are microborings, macroborings, grazing traces, and attachment scars. Microborings are less than a millimetre in size and show tunnel diameters of commonly less than a hundred microns, being produced by euendolithic cyanobacteria, green algae (chlorophytes), red algae (rhodophytes), fungi, foraminifera, and presumably, bacteria and archaea (Wisshak, 2012). Macroborings and grazing traces are larger than a millimetre in size and commonly visible with the naked eye. Macroboring agents include boring sponges, gastropods, various groups of worms (polychaetes, phoronids, sipunculids), bivalves, bryozoans, barnacles, and gastropods (Wilson, 2007). Grazers comprise gastropods, polyplacophorans, echinoderms, and fish (Tribollet et al., 2011). Attachment scars are produced, for instance, by foraminifera, brachiopods, and bivalves, attaching on hard substrates by etching (Bromley and Heinberg, 2006).

Bioeroding organisms are metabolically diverse and employ different feeding strategies (Tribollet et al., 2011). Endolithic cyanobacteria, chlorophytes, and rhodophytes are photoautotrophs and bore into substrates in order to find shelter from grazers (Radtke et

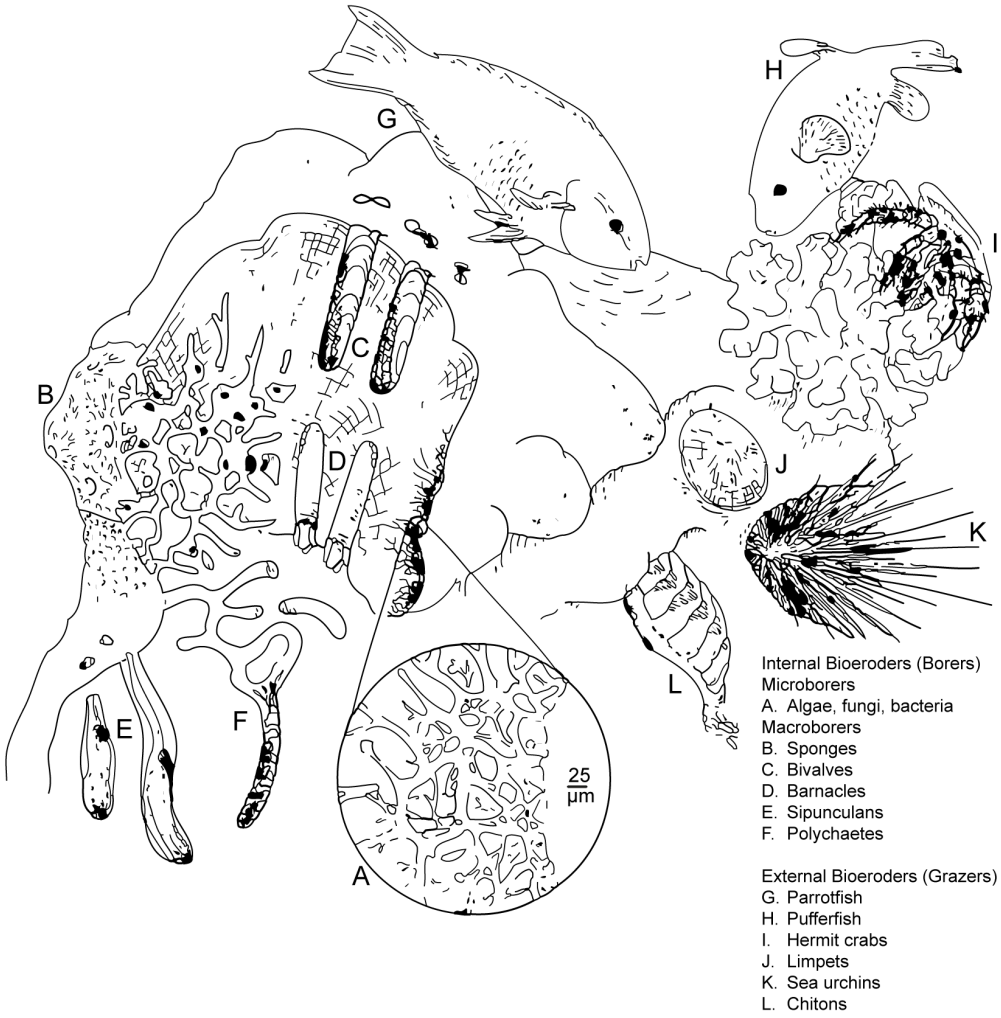


Figure 1.1 Variety of external and internal bioeroders that commonly attack coral skeletons (Glynn, 1997).

al., 1996). Endolithic marine fungi and bacteria are chemoheterotrophs and biodegrade calcareous shells in order to exploit mineralised organic matter or even other endolithic organisms as predators (Golubic et al., 2005). Macroborers are mostly filter feeders and dependent on the availability of nutrients in the water column (e.g., Smith et al., 1981), except some predatory gastropods that actively drill shells to feed on molluscs (Walker, 2007). Grazers are heterotrophs feeding on endo- and epilithic biofilms and algae with specialised mouthparts (Tribollet et al., 2011). The mechanisms of carbonate dissolution by endoliths, in contrast, are complex and still poorly understood. The observed variations in boring behaviour of microbial euendoliths indicate the existence of different mechanisms, which include calcium pumps, respiratory carbonic acid, or enzymes such as carbonic anhydrase (Garcia-Pichel, 2006; Garcia-Pichel et al., 2010 ;Tribollet, 2008; Tribollet et al., 2011). Many macroborers apply a combination of chemical and mechanical means to penetrate rocks and shells, such as boring sponges, who attach themselves onto the substrate and then penetrate by using etching cells to separate chips from the substrate (Tribollet et al., 2011). The synergistic effect between microbial euendoliths and grazers causes a vertical displacement of the

rock surface and increases the compensation depth for phototrophic endoliths (Tribollet et al., 2011). Without grazing, bioerosion by phototrophic euendoliths would remain limited to a few millimetres beneath the substrate surface.

Today, the best studied bioeroding organisms are sponges, echinoderms, and microeuendoliths (Schönberg and Tapanila, 2006). In modern seas, many microeuendoliths are eurythermal and have a cosmopolitan distribution, but certain taxa are stenotherm and occur within specific temperature limits (e.g., Wisshak and Porter, 2006; Bromley et al., 2007). Due to the photoautotrophic character of many euendoliths and their specific low-light tolerance limit and light optimum, the distribution of euendoliths in the water column follows a distinct vertical zonation: cyanobacteria dominate the shallow euphotic zone, chlorophytes are most abundant in the deep euphotic to dysphotic zone, and exclusively chemotrophs are able to thrive also in aphotic depths (Golubic et al., 1975; Perkins and Tsentas, 1976; Budd and Perkins, 1980; Akpan and Farrow, 1984; Günther, 1990). Most euendoliths are obligate open marine and strictly stenohaline, but also some euryhaline representatives have been identified that occur over a wide range of salinities from hypersaline lagoons to pure freshwater environments (e.g., Wisshak, 2012). In contrast to microborers, the distribution of macroboring and grazing agents is more complex and the occurrence of certain species can be related to several other factors such as substrate, depth, salinity, or temperature (e.g., Devescovi and Iveša, 2008; Schönberg, 2008). Not all macrobioeroders are cosmopolitans, but some, such as grazing fish, are restricted to tropical environments (see Wisshak, 2006 for a review of high-latitude bioerosion agents).

### 1.1.3 Spatio-temporal variability of marine bioerosion

In the last two decades, a series of experimental field studies has been conducted to investigate the succession and impact of bioerosion in different carbonate environments (Fig. 1.2, Table 1.1). Most experiments were carried out in the tropics investigating the interplay of carbonate producing and carbonate bioeroding organisms in coral reef ecosystems. These revealed that the succession of bioerosion agents is subject to a distinct temporal variability: in shallow-marine tropical waters, endolithic microborers (especially cyanobacteria) are among the initial agents of bioerosion infesting experimental substrates within a few days of exposure (Perkins and Tsentas, 1976; Kobluk and Risk, 1977). During the first months, microborers dominate over all other agents of bioerosion, but remain also an important component of the bioeroding community after 6 months through the interaction with grazers (Chazottes et al., 1995; Grange et al., 2015), and are considered to form fully established communities after 1 year of exposure (Tribollet and Golubic, 2005; Grange et al., 2015). First macroborers generally occur after 1 year of exposure, but are mostly represented by worms, while macroborers with longer developmental cycles such as boring sponges and bivalves need about 2 to 3 years to develop (Kiene and Hutchings, 1992, 1994; Pari et al., 2002; Tribollet and Golubic, 2005; Carreiro-Silva and McClanahan, 2012). Due to the high spatio-temporal variability, however, no macrobioerosion equilibrium has yet been identified.

Apart from the tropical realm, bioerosion experiments were previously restricted to 2 years of exposure, monitoring mainly microbioerosion. Based on bioerosion experiments in the North Atlantic, Wisshak et al. (2010) have shown that microbioerosion follows a distinct latitudinal gradient with highest values in the tropics (Vogel et al., 1996, 2000), intermediate levels in the warm-temperate (Wisshak et al., 2010, 2011), and lowest rates in the cold-temperate high latitudes (Wisshak, 2006). In parallel, also ichnodiversity decreases

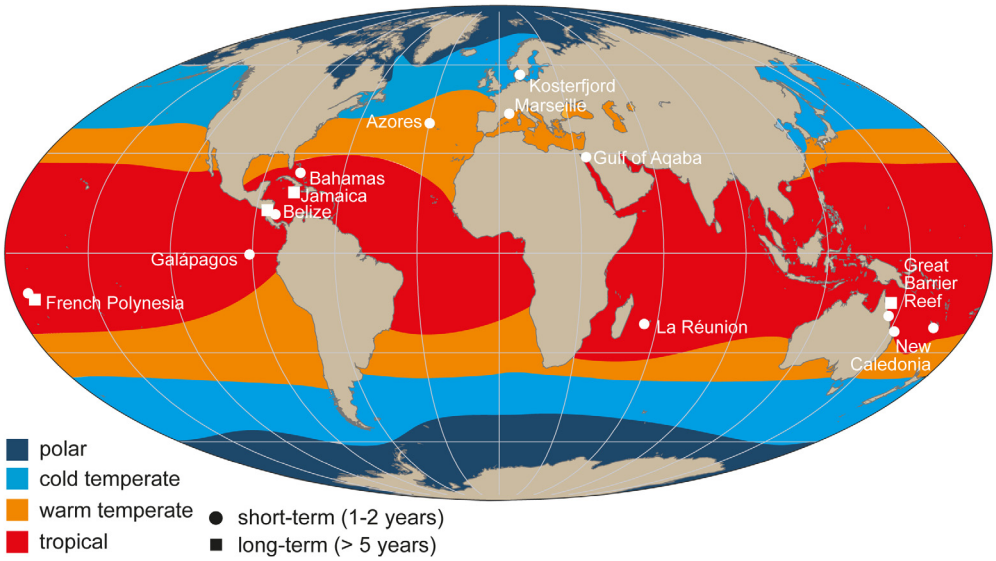


Figure 1.2 Study sites of previous quantitative bioerosion experiments in the marine biogeographical regions (modified and complimented after Wisshak (2006) and Lüning (1985); see Table 1.1 for references).

towards higher latitudes governed by the telescoping compression of the photic zonation as a result of light absorption by the more eutrophic conditions, declining angles of light influx, a stronger seasonal fluctuation in light availability, and lower water temperatures (Wisshak et al., 2011).

Within the water column, microbioerosion rates are generally highest in the well-illuminated euphotic zone and exponentially decrease with water depth, controlled by the vertical distribution of phototrophs (Wisshak et al., 2010). Highest ichnodiversity of microbioerosion was monitored in the shallow euphotic to deep euphotic zone (Wisshak et al., 2010, 2011). The effects of water temperature, salinity, and nutrients on microbioerosion, in contrast, are complex and often closely interlinked and thus difficult to distinguish (see Wisshak, 2012 for a review). In reef environments, the abundance and intensity of microbioerosion and macrobioerosion often shows a high spatial variability with respect to water depths, levels of nutrients, benthic cover, and numbers of grazing agents (e.g., Kiene and Hutchings, 1994; Chazottes et al., 2002; Carreiro-Silva and McClanahan, 2012).

### 1.1.4 Bioerosion in the fossil record

In the fossil record, bioerosion features are preserved as trace fossils and are useful indicators for palaeoenvironmental reconstruction (De Gibert et al., 2012; Wisshak, 2012). Among the oldest bioerosion traces are borings of cyanobacteria, which are known since the Proterozoic (Bromley, 2004; Glaub et al., 2007). Most microborings conform tightly with the body outlines of the organisms that produced them, and can be assigned to their living trace makers by a reasonably high degree of precision (Glaub et al., 2007). The interpretation of fossil microborings is supported by the study of modern counterparts, permitting to identify the microorganisms together with their trace, and to determine its distribution in relation to environmental and sedimentary conditions (Glaub et al., 2007). The combination of evolutionary longevity and environmental dependency makes microbioerosion traces useful indicators for palaeoenvironmental conditions, especially for judging light availability and hence relative bathymetry (e.g., Glaub et al., 2007; Wisshak, 2012). This is based on the

Table 1.1 Compilation of previous quantitative bioerosion experiments, modified and complemented after Wisshak (2006).

| Location | Exposure (months) | Reference |
|---|---|---|
| Belize | 1–2 | Carreiro-Silva et al. (2005, 2009, 2012) |
| | 12–60 | Lescinsky et al. (2008) |
| French Polynesia | 2–24 | Chazottes et al. (1995); Peyrot-Clausade et al. (1995a) |
| | 6–60 | Peyrot-Clausade et al. (1995b), Pari et al. (1998, 2002) |
| Reunion Island, Indian Ocean | 12 | Chazottes (1996); Chazottes et al. (2002) |
| Great Barrier Reef | 12–48 | Tribollet et al. (2002); Hutchings et al. (2005); Osorno et al. (2005) |
| | 6–24 | Kiene (1988) |
| | 3–49 | Davies and Hutchings (1983); Hutchings et al. (1992) |
| | 24–111 | Kiene (1985); Kiene and Hutchings (1992, 1994) |
| | 5–26 | Kiene (1997) |
| Galápagos | 15 | Reaka-Kudla et al. (1996) |
| New Caledonia | 1–12 | Grange et al. (2015) |
| Aqaba, Red Sea | 12–24 | Hassan (1998) |
| Bahamas | 3–24 | Vogel et al. (1996, 2000) |
| | 12 | Hoskin et al. (1986) |
| Azores | 3–24 | Wisshak et al. (2010, 2011) |
| Kosterfjord | 6–24 | Wisshak (2006) |
| Mediterranean Sea | 3–12 | Sartoretto (1998) |

photoautotrophic character of many euendoliths and their specific low-light tolerance limit and light optimum, resulting in a distinct vertical zonation pattern, which has been translated into a set of bathymetric index ichnocoenoses, defined by the co-occurrence of specific key ichnotaxa and supported by general characteristics of the ichnocoenoses (Glaub, 1994; Glaub et al., 2001; Vogel et al., 1995, 2008; Wisshak, 2012). A definition of a key ichnocoenosis for the supratidal, however, is still pending and also the application of endoliths for the reconstruction of palaeothermometry, palaeosalinity, and palaeotrophodynamics is more in its beginning (e.g., Wisshak, 2012).

Similar to microborings, also macroborings and grazing traces are well preserved in the fossil record. Macroborers can be dated back to the Proterozoic, but became more abundant in the Mesozoic (Bromley, 2004; Wilson et al., 2004). In contrast to microborings, the trace maker identification of macroborings is more difficult and leaves in some cases even the phylum in doubt (Bromley, 2004). In contrast to microborings, most marine macroborers are filter-feeders and their depth distribution has not been assessed as vigorously as for microboring organisms (Tribollet et al., 2011). Nevertheless, macroboring and grazing assemblages play a key role for rocky-coast recognition and are important tools for the reconstruction of palaeoshorelines (De Gibert et al., 2012).

## 1.2 Motivation and objectives

Aim of this study was the integration of short- and long-term bioerosion processes in the Eastern Mediterranean Sea. In the last years many bioerosion experiments were conducted investigating the impact of bioerosion in different carbonate ecosystems, but currently only few studies are available from non-tropical settings. Research on bioerosion in the Mediterranean Sea has a long tradition beginning with detailed taxonomical studies on bioeroding chlorophytes and cyanobacteria by Bornet and Flahault (1888, 1889) and Ercegovic (1927, 1929, 1932). During the late 1970s, Schneider (1976) investigated the microbial degradation of limestone coasts in the Eastern Mediterranean and Le Campion-Alsumard (1975, 1978, 1979) carried out a number of detailed systematic and experimental investigation on microendoliths in the region of Marseille in the Western Mediterranean Sea. Until now, quantitative data on Mediterranean bioerosion, however, are scarce and only available in form of short-term observations from the coast of Marseille (Le Campion-Alsumard, 1975, 1978, 1979; Sartoretto, 1998). The Eastern Mediterranean Sea is an extreme environment characterised by an ultra-oligotrophic nutrient regime and exceptionally high thermohaline conditions. Qualitative and quantitative data on Mediterranean bioerosion, hence, contribute important information for evaluating global patterns of bioerosion and for modelling future impacts of bioerosion (Kennedy et al., 2013).

The main objectives of this thesis were:

(1) To analyse the spatio-temporal variability of bioerosion in the Eastern Mediterranean Sea and to calculate its effect on the carbonate budget
(2) To assess the usability of the observed bioerosion traces as palaeoenvironmental indicators
(3) To set the results from the Eastern Mediterranean Sea in latitudinal and longitudinal comparison to previous bioerosion experiments

To answer these research questions, material from three bioerosion experiments in the Eastern Mediterranean Sea (Greece) was provided: (1) a carbonate cycling experiment with experimental platforms deployed for ½ to 1 year in 15 to 250 m water depth south-west off the Peloponnese, (2) limestone substrates mounted for 1 to 2 years in the inter- to supratidal zone at Rhodes, and (3) marble blocks deployed for 1 to 14 years in 3 to 17 m water depth around the island of Rhodes. The assessment of short-term bioerosion rates and traces was based on gravimetrical measurements and scanning electron microscopy. For the analysis of long-term bioerosion rates and traces micro-computed tomographic analysis was chosen in a novel approach.

# 2 The Mediterranean Sea

The Mediterranean Sea is a semi-enclosed basin, bordered by the landmasses of Europe and Asia in the north and east, and Africa in the south, and connected to the North Atlantic Ocean only by the narrow Straits of Gibraltar (width ca. 13 km, sill depth ca. 300 m), as well as to the Black Sea by the Dardanelles/Marmara Sea/Bosphorus system in the north-east and artificially via the Suez Canal to the Red Sea in the south-east. The Mediterranean Sea is composed of two major subbasins, the Western and Eastern Mediterranean Sea (Fig. 2.1). The Western Mediterranean Sea comprises the region between the Straits of Gibraltar and west of Sicily, including the Alborean, Balearic, Ligurian, and Tyrrhenian Sea. The Eastern Mediterranean Sea is composed of the Adriatic and Ionian Sea in the west and the Aegean Sea and Levantine Basin in the east, being separated by the Cretan Sea and the Cretan Straits. The Western and Eastern Mediterranean Sea are separated by the Straits of Sicily (width ca. 35 km, sill depth ca. 300 m) and the Straits of Messina (width ca. 3–8 km, depth ca. 250 m), representing a physical barrier, which significantly affects the biogeochemical processes within the eastern basin (Krom et al., 2012; Skliris, 2014).

In the following, short overviews about the climate, the oceanographic setting, and the carbonate factory of the Mediterranean Sea are given. Further comprehensive and detailed information are provided in review papers on the climate (e.g., Lionello et al., 2006, 2012), the thermohaline circulation (e.g., Robinson et al., 2001; Millot and Taupier-Letage, 2005; Skliris, 2014), the nutrient regime (Krom et al., 2012, 2014), and the primary productivity of the Mediterranean Sea (e.g., Stambler, 2014).

## 2.1 Climate and oceanography

In consequence of its semi-enclosed position, its location between the temperate zone to the north and the subtropical zone to the south, and its complicated morphology with many islands of different sizes, peninsulas, subbasins, narrow straits, and steep mountain ridges

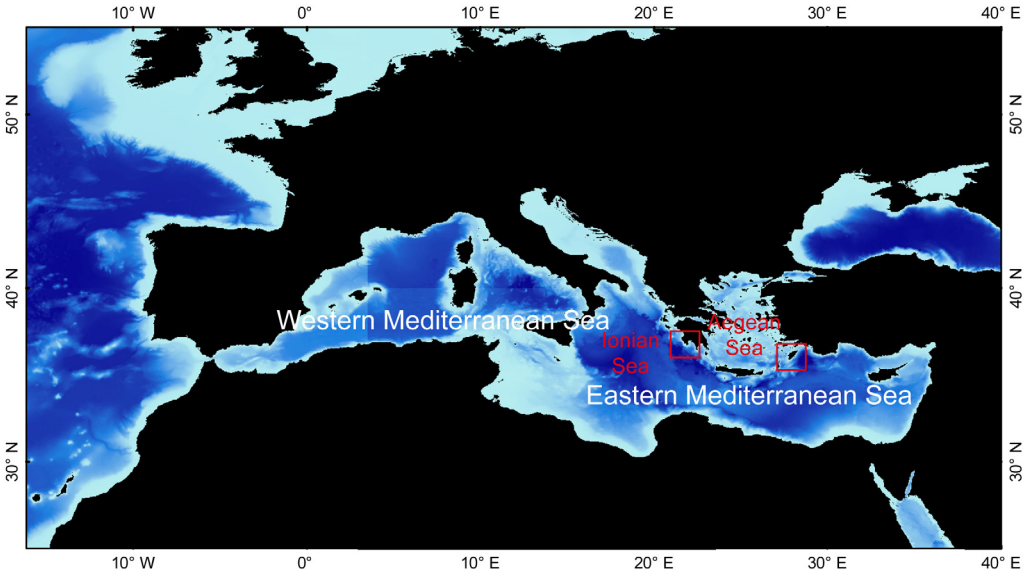


Figure 2.1 Map of the Mediterranean Sea and location of study sites during the present study. Bathymetric data were derived from the EMODnet Portal for Bathymetry (EMODnet, 2015).

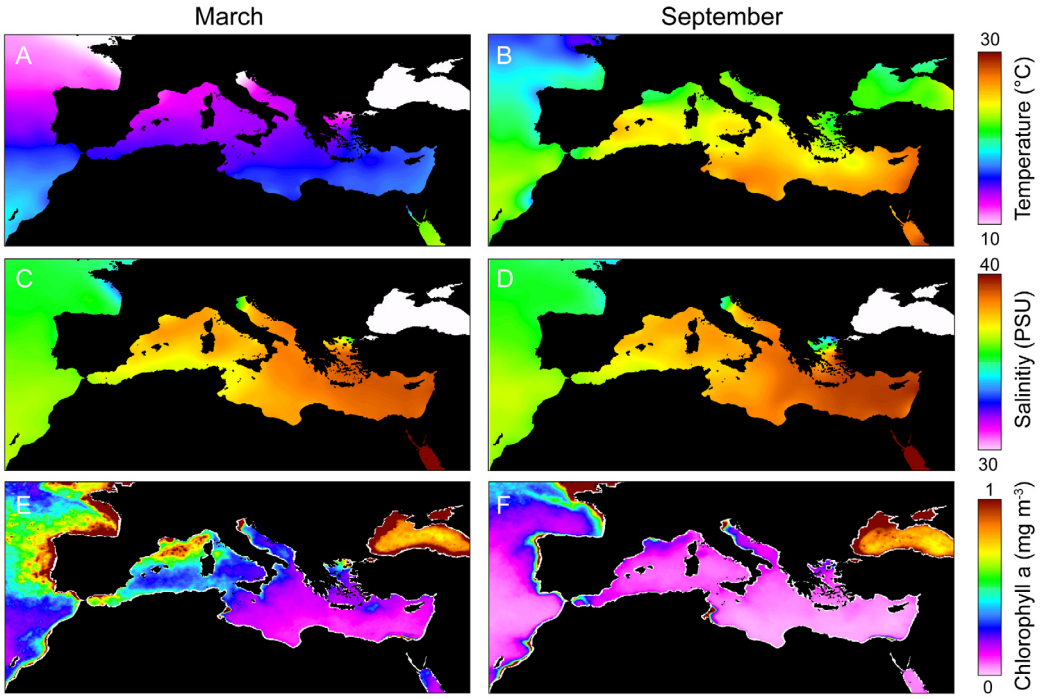


Figure 2.2 Average water temperature (A–B), salinity (C–D), and chlorophyll a (E–F) in the Mediterranean Sea during the coldest month March and the hottest month September. Water temperature and salinity (1955–2012) were derived from the World Ocean Database (Boyer et al., 2013), values of chlorophyll a (1997–2010) were produced with the Giovanni online data system (Acker and Leptoukh, 2007).

close to the coast, the Mediterranean Sea shows a complex oceanographic and climatic setting (e.g., Lionello et al., 2012). The Mediterranean climate can be generally defined as a mid-latitude temperate climate with hot and dry summers (May–October) and humid winters (November–April), but strong contrasts are present among different areas (e.g., Lionello et al., 2012). Also the Mediterranean wind fields show high variability on local and seasonal scale, but generally reach highest values during winter (e.g., Lionello et al., 2012).

Due to exceeding rates of evaporation over precipitation, the Mediterranean Sea in general, and the Eastern Mediterranean Sea in particular, are concentration basins with considerably higher sea surface temperature and salinity than the North Atlantic Ocean (Fig. 2.2A–D). The circulation of the Mediterranean Sea is complex and composed of three predominant and interacting cells: (1) an open vertical cell comprising the whole basin, (2) two closed vertical cells bounded within the western and eastern subbasins, and (3) several permanent and recurrent subbasin and mesoscale eddies, jets, and gyres (Robinson et al., 2001; Skliris, 2014). The open vertical cell is composed of inflowing low salinity Atlantic Surface Waters (100–200 m) that are transformed into Levantine Intermediate Water (LIW) through excessive heat loss and evaporation in the north-eastern Levantine Basin, spreading in opposite direction at intermediate depths (200–400 m), to finally exiting the Mediterranean Sea through the bottom layer at the Gibraltar Strait (Skliris, 2014; Fig. 2.3). The density contrast between highly saline Mediterranean Water and relatively fresh Atlantic Water drives an inverse estuarine (reverse thermohaline) circulation in the Straits of Gibraltar. Mediterranean water of high salinity exits into the Atlantic to balance the freshwater loss through the surface. The two closed thermohaline cells in the subbasins are driven by the formation of deep water, which was formerly considered to occur mainly

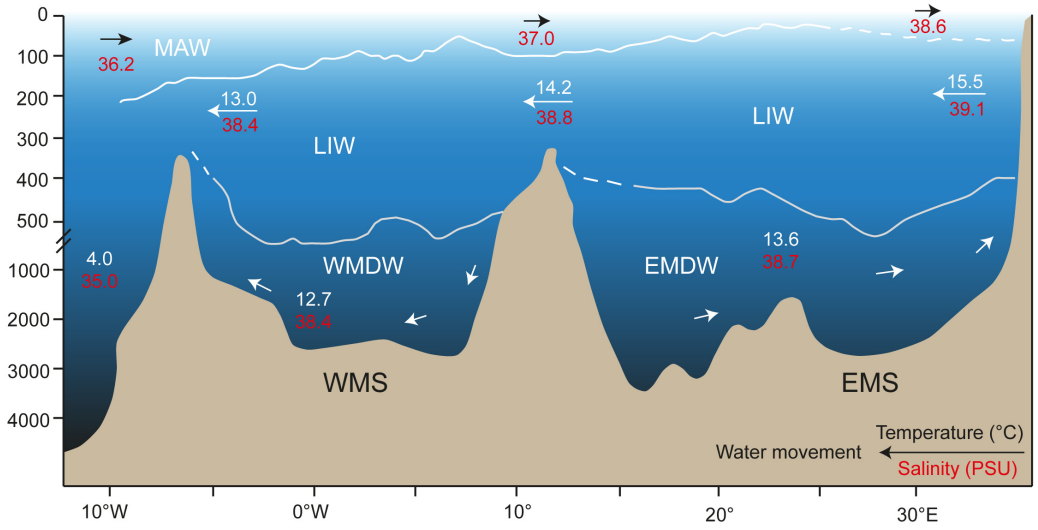


Figure 2.3 Vertical distribution of water masses in the Mediterranean Sea (WMS = Western Mediterranean Sea, EMS = Eastern Mediterranean Sea, MAW = Modified Atlantic Water, LIW = Levantine Intermediate Water, WMDW = Western Mediterranean Deep Water, EMDW = Eastern Mediterranean Deep Water (modified after Zavatarelli and Mellor, 1995 and UNEP/MAP, 2012).

during winter in the cyclonic gyre of the Gulf of Lions in the Western Mediterranean Sea and in the Southern Adriatic cyclonic gyre in the Eastern Mediterranean Sea (Skliris, 2014). In the last two decades, more localised features were discovered and climatic events identified that changed the main source of intermediate and deep water masses during a climatic event from the Adriatic to the Aegean Sea (Roether et al., 1996; Klein et al., 1999). Today, dense water formation in the Mediterranean Sea is known to be in addition associated with cascading of dense water over the continental shelf in the Gulf of Lions, the Adriatic Sea, and the Aegean Sea (Skliris, 2014). The broad-scale surface circulation is locally modified by intense mesoscale activity, such as gyres, eddies, and highly energetic currents that in some cases reach horizontal scales of 10–100 km penetrating into intermediate and bottom layers of the two subbasins (Millot and Taupier-Letage, 2005).

In consequence of the anti-estuarine circulation and the relatively young age of the water masses, the Mediterranean Sea in general, and the Eastern Mediterranean Sea in particular, are characterised by an ultra-oligotrophic setting, with nutrient concentrations in the deep water that are among the lowest measured anywhere in the oceans (Krom et al., 2014; Fig. 2.2E–F). Primary productivity in the Mediterranean is complex and continuously changes with temperature, salinity, nutrients, vertical mixing, and turbidity by winds (Stambler, 2014). In most parts of the Mediterranean Sea the annual phytoplankton blooms in the Eastern Mediterranean Sea start as soon as deep winter mixing occurs in early winter (December) and nutrients are supplied into the photic zone. The blooms continue throughout the winter months until spring (March) when the seasonal thermocline begins to form (Stambler, 2014). During summer stratification, warmer, less saline, surface water is separated from the deeper, colder, and more saline water inhibiting the flux of nutrients towards the surface layer, preventing autotrophic biomass accumulation in the surface layer (Stambler, 2014).

## 2.2 Carbonate factory

The Mediterranean Sea is part of the warm-temperate biogeographic province, which is mainly characterised by skeletal carbonate production, while non-skeletal carbonate precipitates are scarce (Betzler et al., 1997). Typical for a non-tropical fabric, the main carbonate producers in the Mediterranean Sea are red algae, bryozoans, molluscs, benthic foraminifera, and balanids (Carannante et al., 1988). On the inner to mid shelf generally two different types of substrates occur: (1) mobile or phytal substrates in low-energy settings and (2) hard- or rock grounds and phytal substrates in open-shelf systems (Betzler et al., 1997; Fig. 2.4).

In low-energy settings, the infralittoral is characterised by conglomeratic and sandy beaches (Fig. 2.4A), comprising extended sea grass meadows harbouring a diverse epiphytic flora and fauna of calcifying rhodophytes, brown algae, diatoms, bryozoans, hydrozoans, and foraminifera (Betzler et al., 1997). In the mediolittoral, only very few organisms with calcifying skeletons exist. In the circalittoral four characteristic facies types occur: the "détritique côtier", the "facies à prâlines", the maërl facies, and the "détritique du large". The "détritique côtier" represents an accumulation of calcified epiphytic organims derived from the infralittoral zone as well as branching, calcifying bryozoans. The "facies à prâlines" is dominated by rhodoliths being typically formed on isolated banks with strong bottom currents, clear water and no neritic influx. The maërl facies is dominated by branching red algae and a low diverse fauna with bivalves, polychaetes, echinoderms, and foraminifera, and typically occurs in water depths of 25–40 m in the Western and 60–65 m in the Eastern Mediterranean Sea. The "détritique du large" is the deepest facies, characterised by the deepest occurrences of rhodophyceans and deposits of siliclastic sands and bioclastic gravels. Typical faunal elements are hydrozoans, echinoids, scaphopods, polychaetes, and brachiopods.

On rocky shores with low to medium wave energy (Fig. 2.4B), the lower mediolittoral zone is characterised by the "trottoir algaire", comprising encrusting rhodophytes and a sciaphile (i.e., shade-loving) community of green and red algae on its lower flank (Betzler et al., 1997). The infralittoral is characterised by bioclastic sands dwelled by a diverse community of calcifying rhodophytes, chlorophytes, sea grass meadows, foraminifera, hydrozoans, bryozoans, ascidians, molluscs, polychaetes, and crustaceans. An important subfacies on horizontal rocky substrates is represented by a biocoenosis of brown algae (Cystoseiracea) triggering the growth of hemisciaphile (i.e., semi-shade loving) communities of rhodophytes, chlorophytes, encrusting foraminifera, hydrozoans, bryozoans, balanids, and serpulids. The circalittoral zone is dominated by hard substrates harbouring the sciaphile "coralligène" facies, which is typically composed of calcified rhodophyceans, brown algae, chlorophyceans, sponges, cnidarians, serpulids, brachiopods, bryozoans, echinoderm, ascidians, and bivalves. In contrast to the Western Mediterranean Sea, where calcified bryozoans are more abundant, echinoderms and ascidians are more important in the "coralligène" of the Eastern Mediterranean Sea. Basinward of the "coralligène", rocky substrates are in some places characterised by a specific filter-feeding fauna of sponges, cnidarians, madreporid corals, bryozoans, ascidians, echinoderms, and serpulids.

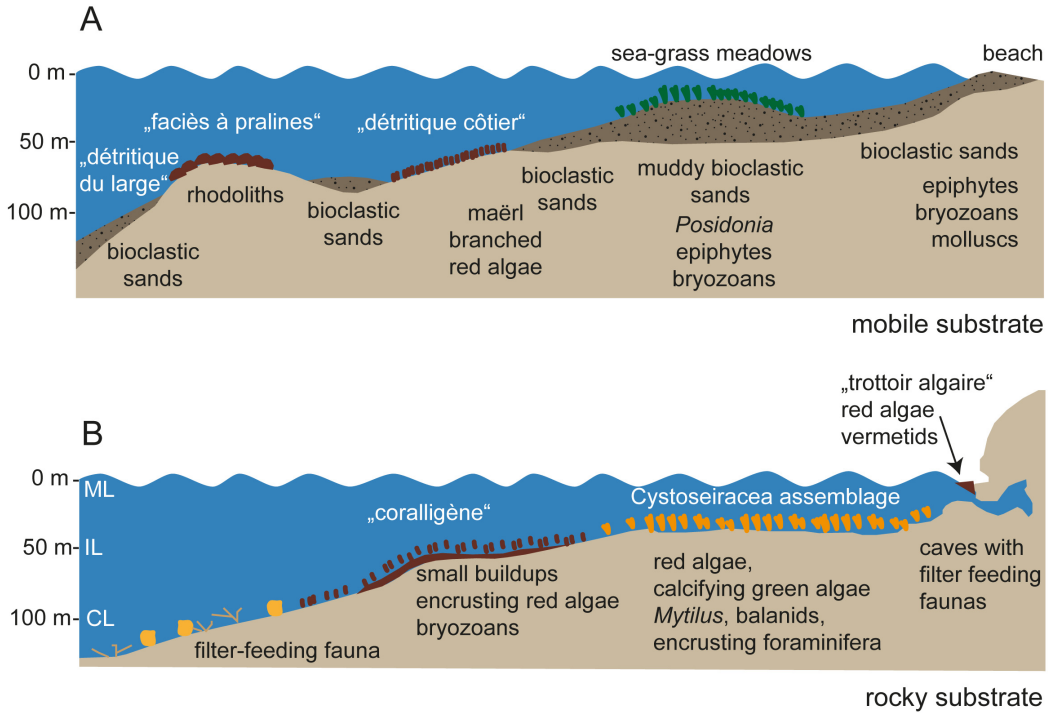


Figure 2.4 Simplified model of most important facies types in the Mediterranean Sea: (A) mobile or phytal substrates in low-energy settings and (B) hard- or rockgrounds and phytal substrates in open-shelf systems (ML = mediolittoral, IL = infralittoral, CL = circalittoral (modified from Betzler et al., 1997; after data from Pérès and Picard 1964, and Carannante et al. 1988).

## 2.3 Study sites

### 2.3.1 Peloponnese, Southern Ionian Sea

The carbonate cycling experiment was carried out close to the island Sapienza, south-west of the Peloponnese Peninsula in the Ionian Sea. The Ionian Sea is surrounded by the coasts of southern Italy, western Greece, and northern Africa and is connected with the Western Mediterranean Sea through the Strait of Sicily, to the east with the Levantine Basin through the Cretan Passage, and to the north with the Adriatic Sea through the Strait of Otranto (Nittis et al., 1993). The Ionian Sea is the largest basin in volume of the eastern Mediterranean Sea (~$10^6$ km$^3$) and includes the deepest parts of the Mediterranean Sea, the Hellenic Trench with depth exceeding 4000 m (Nittis et al., 1993; Stavrakakis et al., 2013). The Ionian Sea can be considered as a transition zone where water masses formed in the Levantine Sea, the Aegean Sea, and the Adriatic Sea meet and interact with water masses entering from the Western Mediterranean Sea through the Sicily Strait (Malanotte-Rizzoli et al., 1997).

The general water mass structure of the study site is characterised by Modified Atlantic Waters showing a salinity minimum in 30 to 200 m and Levantine Intermediate Waters in 200 to 600 m, indicated by a salinity maximum. During the summer, Ionian Surface Water clearly differs from Modified Atlantic Water by being saltier and warmer (Malanotte-Rizzoli et al., 1997). The area is far from any river discharge and characterised by exceptionally clear and oligotrophic water with low sedimentation rates (Khanaev and Kuleshov, 1992; Trimonis

and Rudenko, 1992). Values of surface irradiance calculated from light measurements of photosynthetically active radiation in the Ionian Sea suggest an approximate base of the euphotic and dysphotic zones in about 100 and 180 m, respectively (Mater Group, 2001).

### 2.3.2 Rhodes, Southern Aegean Sea

The long-term and the coastal bioerosion experiment were conducted at the island of Rhodes in the Southern Aegean Sea. The Dodecanese island of Rhodes is the largest of the Southern Sporades and located at the south-east border of the Aegean Sea, at a short distance to the Turkish coast. Rhodes extends in NE-SW direction, with a length of 77 km and a width of about 38 km (Mutti et al., 1970).

In a geological point of view, Rhodes is situated at the eastern end of a sedimentary arc consisting mainly of Mesozoic and Tertiary rocks folded and faulted during the Alpine orogeny, being covered by late Pliocene and Pleistocene sediments (Hanken et al., 1996). They comprise littoral, nearshore marine, clastic and limestone deposits as well as terrigenous pelagic muds and deep-water carbonates, being accumulated in a series of grabens or basins, where they formed complex facies mosaics, reflecting several regression and transgression cycles (Hanken et al., 1996). The climate of Rhodes is typical Mediterranean with six humid months (November–April) and six hot months (May–October). The mean annual temperature is about 19°C with total annual precipitation of 730 mm and in average 62 rain days per year (Mutti et al., 1970). During summer, mostly north-westerly winds prevail, during the winter winds from south-east.

The Aegean Sea is a semi-enclosed basin, connected with the Ionian and Levantine Basins through the eastern and western Straits of the Cretan Arc and in the north with the Sea of Marmara through the Dardanelles Strait and with the Black Sea through the Bosphorus Strait (Poulos et al., 1997; Zervakis et al., 2004). The general water mass structure of the Southern Aegean Sea is characterised by a surface layer of highly saline waters of Levantine origin, along with lower salinity Atlantic Water or modified Black Sea Water (Zervakis et al., 2004). The nutricline and the base of the euphotic zone are at about 100 m (Kucuksezgin et al., 1995), and the pycnocline is located at an average depth of about 25 m (Poulos et al., 1997).

# 3 Material and methods

## 3.1 Experimental setups

### 3.1.1 Carbonate cycling experiment

The carbonate cycling experiment was conducted from February 2008 to April 2009 south-west off the Peloponnese Peninsula in the Southern Ionian Sea (ca. 36.73 °N, 21.68 °E). In order to investigate the effects of water depth, seasonal exposure, and substrate orientation on carbonate bioerosion and accretion, twelve experimental platforms with experimental substrates on the up- and down-facing side were deployed along a bathymetric transect in 15, 50, 100, and 250 m water depth for a summer, a winter, and an entire year. The deployment of the summer and one year platforms was carried out onboard R/V Aegaeo on 28 February 2008. The summer platforms were recovered and replaced by the winter platforms after 226 days onboard R/V Philia on 11 and 12 October 2008. The winter and one year platforms were finally retrieved after 173 and 400 days, respectively, onboard R/V Philia on 2 April 2009. Platforms in 15 m were deployed by scuba divers, the deeper platforms by a remotely operated vehicle. Platforms in 15 m were deployed on rocky hard ground, the deeper platforms on sand-muddy soft ground.

The principle design of the experiment followed previous bioerosion experiments of Wisshak et al. (2010, 2011). Each platform was composed of a 54 x 60 cm PVC frame with four concrete filled PVC tube legs. In each orientation, six limestone and six PVC plates (10 x 10 x 1 cm) were mounted for the assessment of bioerosion and accretion rates, and three valves of the bivalve *Callista chione* for the investigation of bioerosion traces. Before deployment, limestone plates were sealed at all but the upper side with epoxy resin, and embedded in a socked of epoxy resin, in order to obtain bioerosion rates directly per surface and exposure time. *Callista* valves were embedded in a socket of epoxy resin, to minimise the danger or loss of substrates and to expose solely the inner pristine side of the valve to bioerosion agents. *Callista* was chosen on the one hand because it is a Mediterranean bivalve and represents thus a naturally growing substrate, and on the other, *Callista* shells have been shown to provide the most suitable substrate for casting purposes due to its dense aragonitic microstructure with comparatively little organic matrix (Wisshak, 2006).

In order to characterise the temperature variability and stratification of water masses during the experiment, on the down-facing side of each platform, a temperature data logger (Hobo Water Temp Pro v2, accuracy ±0.2 °C or Star Oddi Starmon-Mini, accuracy ±0.05 °C; 30 minute intervals) was fixed. After the winter, one 15 m platform was found turned over and was excluded from analysis. Due to data loss, no water temperatures are available from the 250 m winter deployment as well as from the entire one year deployment.

### 3.1.2 Coastal bioerosion experiment

The coastal bioerosion experiment was carried out from May 2013 to May 2015 at four limestone cliffs at the east and west coast of Rhodes, Greece: Agathi (36°10’ N, 28°6’ E), Lindos (36°6’ N, 28°5’ E), Kerameni (36°8’ N, 27°42’ E), and Monolithos (36°7’ N, 27°42’ E). These were previously identified as limestone outcrops on the Neotectonic Map of Greece 1:100 000 (Lekkas et al., 1993). In order to investigate the effects of water depth/aerial exposure, exposure time, and hydrodynamic site effects (wind-exposed versus sheltered) on

coastal bioerosion, a set of three shells of *Callista* and three limestone plates, each embedded in a socket of epoxy resin, were mounted along coastal transects in the intertidal (-0.25, 0, 0.25 m) and in the supratidal zone (0.75, 1.25, 3, 5, 7, and 10 m) below/above mean sea level. Mean sea level was defined by the upper limit of the red algae zone. In Agathi, additional substrates were mounted in four solution pans in the supratidal zone. Above water, substrates were mounted with dowels and stainless steel screws. Under water, substrates were fixed with cable ties. In order to monitor environmental conditions during the experiment, temperature data loggers (Star-Oddi Starmon Mini, accuracy ±0.05 °C and HOBO Water Temp Pro v1/v2, accuracy ±0.2 °C; 30 minute intervals) were mounted in -0.25 m water depth and in 10 m height (except Monolithos), as well as in solution pans. Data loggers were recovered after 1 year of exposure, experimental substrates after 1 and 2 years. The third set of substrates was left for long-term observations. Due to loss of many of those substrates in -0.25 m that were mounted with cable ties and did not survive the winter storms, substrates could be only retrieved in Lindos and Kerameni after 1 and 2 years, respectively. From solution pans, only the data logger in solution pan B could be recovered. Identification of karst features followed descriptions of Taboroši and Kázmér (2013). A photo documentation of each zone along the transects was undertaken above and under water.

### 3.1.3 Long-term bioerosion experiment

The long-term experiment was carried out from 1982 to 1996 at four limestone cliffs at the east and west coast of the island of Rhodes, Greece: (1) at the south and east edge of Ladiko Bay (36°19'5" N, 28°12'17" E; 36°19'10" N, 28°12'29" E), (2) south of Kolimbia (36°14'26" N, 28°9'44" E; 36°14'21" N, 28°9'47" E), (3) north of St. Paul's Bay near Lindos (36°5'17" N, 28°5'20" E), and (4) in Pyrgos (36°10'10" N, 27°43'55" E). All localities were characterised by limestone rock ground, either boulder fields or clean rock surfaces, and were free from local pollution. Annual monitoring in October showed no indication of interference of the experiment by human activities. In order to investigate the long-term succession of bioerosion agents and rates, in total, 46 marble and limestone blocks were deployed in 3 to 17 m water depth and retrieved by skin diving and using floatation devices. Recovered blocks were rinsed in fresh water and soft epiliths were removed. The blocks were subsequently photographed and dried. From all retrieved blocks, twelve were chosen from different depths (3 to 17 m) and exposure times (1 to 14 years), all with a surface area of 11 x 11 cm or more. Most of these showed no evidence for having been dislocated during the experiment, however, some blocks had slightly moved and for some the information about recovery date and/or water depth was incomplete. This was reviewed case by case, and ultimately the latter blocks were included in the study.

## 3.2 Visualisation and quantification of internal bioerosion

### 3.2.1 Scanning electron microscopy and digital light microscopy

Bioerosion traces in *Callista* shells from the short-term experiments were analysed as epoxy resin casts under the scanning electron microscope. Epoxy resin casts were prepared using the vacuum cast-embedding technique (e.g., Wisshak, 2012). For the preparation of the casts, shells were treated with 15 % hydrogen peroxide ($H_2O_2$) for a complete removal of fleshy epiliths. After drying, the shells were casted in epoxy resin (Araldite BY 158, Aradur 21) in a vacuum chamber (Struers CitoVac). After hardening, four surface and two

cross-sections were cut from each shell to allow a semi-quantitative quantification of bioerosion traces and determination of the actual penetration depth of the borings, respectively. Surface sections were fully decalcified in 5 % hydrogen chloride solution to exhibit the positive casts of the borings. Cross-sections were only partially etched about 20 seconds to prevent delicate casts from collapsing. After drying, casts were mounted with adhesive on SEM stubs, sputter-coated with gold, and analysed under the scanning electron microscope (VEGA3, TESCAN).

Bioerosion traces on the surface of limestone plates were documented with a digital light microscope (Keyence VHX-1000D). Prior to analysis, the plates were treated with 15 % $H_2O_2$ for complete removal of fleshy epiliths.

Bioerosion traces in *Callista* shells and limestone plates were semiquantified in the abundance classes 'very common', 'common', 'rare', and 'very rare'. Due to the removal of carbonate encrusters on limestone plates from the carbonate cycling experiment (see Chapter 3.2.2), the documentation of traces from limestone plates was potentially biased and thus excluded from statistical analyses, albeit listed in the bioerosion inventory.

### 3.2.2 Gravimetrical methods

Carbonate bioerosion and accretion rates from the carbonate cycling experiment were calculated in a gravimetrical approach via the difference in the weight of substrates before and after exposure, following the procedure in Wisshak (2006). Before deployment, substrate plates were dried for two weeks at 70 °C and weighed with a precision scale (limestone plates: Mettler Toledo Classic Plus PB3002-S, accuracy 10 mg; PVC plates: Mettler Toledo Classic AB 204-S, accuracy 0.1 mg). After recovery, all non-calcareous components were removed in 15 % $H_2O_2$ solution. Then the plates were again dried at 70 °C. From limestone substrates, all calcareous components were carefully removed with a scalpel under the binocular. Bioerosion rates were calculated from the weight difference of limestone plates before deployment and after removing calcareous components. Accretion rates were calculated from (1) the difference of the PVC plates before and after deployment and (2) from the weight of calcareous components, which were removed from the limestone plates. Net limestone erosion rates were calculated from the difference of accretion and bioerosion rates. All rates were expressed in gram per square metre per year (g $m^{-2}$ $yr^{-1}$).

### 3.2.3 Micro-computed tomography

For the visualisation and quantification of macrobioerosion traces from the long-term experiment, micro-computed tomographic (micro-CT) analysis was carried out in a novel approach. Micro-CT has the advantage that it is non-destructive and allows a volumetric quantification of bioerosion rates. To quantify bioerosion rates by gravimetrical means was not possible, because the weight before deployment was not available for all blocks. In order to yield spatial resolutions of about 70 µm, the blocks were cut with a rock saw to a size of 10 x 10 cm. The 7-year block was cut into three such replicates to obtain an impression of the spatial variability of bioerosion within a single block. In this way, a total of 14 samples was produced for micro-CT analysis.

Micro-CT scanning was carried out at the Bundesanstalt für Materialforschung und -prüfung (BAM), Berlin, Germany, using the 225 kV system (Badde and Illerhaus, 2008). An X-ray source voltage of 210 kV, a current of 90 µA, and a pre-filter of 1 mm copper was applied. Attenuation images were taken at smallest possible resolution due to specimen size.

To achieve the best signal-to-noise-ratio, 2400 projections over 360 degrees with a total measuring time of 16 h were taken. Images were reconstructed using BAM software generated from the original Feldkamp algorithm (Feldkamp et al., 1984). The resulting voxel size was 72 µm.

Post-processing of micro-CT data was conducted using the Amira software edition from Zuse Institute Berlin, ZIBAmira version 2014.51 (Stalling et al., 2005). In an initial segmentation step all encrusting epiliths on the surface of the blocks were excluded from the dataset using the *Segmentation Editor*. Limestone substrate was distinguished from the surrounding air and organic tissue (borings were partially filled by air and organic remains of the sponge) using the marker-based *Watershed segmentation* module. Segmentation of the borings from the space surrounding the block was carried out with the *AmbientOcclusionField* module (Baum and Titschack, subm.). Resulting micro-CT images of the blocks were cropped to uniform sizes of 90 x 90 x 18 mm with the *CropEditor* to obtain comparable volumes. The respective volumes of substrate and bioerosion per block were quantified with the *MaterialStatistics* module using the results from the latter segmentation. To quantify the total surface area of each block, bioerosion and substrate were selected together and the surface was calculated using the *SurfaceGen* module. After removing all other surfaces except the upper surface with the *SurfaceEditor* this surface area was quantified with the *SurfaceStatistics* module. To further evaluate the bioerosion constituents, a third segmentation step was performed based on a *DistanceMap* of the segmented bioerosion traces and using the *ContourTreeSegmentation* module to gain an automatic separation of bioerosion traces in the blocks (threshold: 0, persistence value: 0.05; see Titschack et al., 2015). Subsequently, the *ShapeAnalysis* module was used to parameterise each trace. The maximum trace extent defined microbioerosion patterns as < 1 mm and macrobioerosion patterns as > 1 mm, following the definition by Wisshak (2012). Bioerosion rates (including micro- and macrobioerosion; g $m^{-2}$ $yr^{-1}$) were calculated by multiplying the volume of bioerosion ($cm^3$) with the mean density of limestone/marble of 2.7 g $cm^{-3}$ (Schön, 2011) and expressing the result per surface area ($m^2$) per duration of exposure (years).

### 3.2.4 Sponge spicule analysis

For the identification of the trace makers of sponge borings in the experimental blocks from the long-term bioerosion experiment, sponge spicule preparations were made from dry sponge tissue. To extract the tissue from the equivalent positions as in micro-CT reconstructions, the blocks were broken with hammer and chisel, and tissue was carefully removed with a dissecting needle. Spicule preparations were made by digesting the sponge tissue in 68 % concentrated nitric acid in test tubes in a heated sand bath (60–70 °C) for about 2 h, then leaving the solutions in place over night without heat application. On the next day, acid-cleaned spicules were washed three times in distilled water and dehydrated three times in laboratory-grade ethanol, each wash occurring after centrifugation and pipetting off the supernatant. Spicules were then mounted for SEM analysis by drying aliquots of re-suspended spicules directly on SEM stubs, followed by sputter-coating with gold. Tylostyle measurements were obtained from 20 spicules per specimen. Spirasters and amphiasters were scarce and often broken, so that only five microscleres were measured where possible. Measurements were carried out using ImageJ v.1.48 (Rasband, 1997–2015).

### 3.2.5 Identification of bioerosion traces and boring sponges

Identification of bioerosion traces followed descriptions in Bromley (1970), Bromley and D'Alessandro (1983, 1984, 1989), Radtke (1991), Radtke and Golubic (2005), Schmidt (1992), Wisshak (2006), and Wisshak et al. (2011, 2014a). The identification of bioeroding sponges was mostly based on Rosell and Uriz (2002). In some cases, colour of the dry tissue helped with classification efforts (e.g., Christomanos and Norton, 1974), but in most cases species identification had to rely exclusively on spicules.

### 3.2.6 Statistical analyses

Detailed statistical analyses were carried out on data from the carbonate cycling experiment. An additional statistical evaluation of the data from the long-term bioerosion experiments was not considered feasible due to the limited amount of available blocks suitable for micro-CT analysis and the lack of replication. Statistical evaluation of the results from the coastal bioerosion experiment will be carried out when all remaining substrates will be recovered. Presently too many substrates showed only minor or no indication of bioerosion.

Due to the loss of the 15 m winter platform during the carbonate cycling experiment, overall tests of the effects of water depth, seasonal exposure, substrate orientation, and substrate type (the latter solely for accretion) on carbonate bioerosion and accretion along the complete transect were not feasible. Instead, data from 15 m was excluded from analysis and tests only carried out on data from 50–250 m. Prior to analysis, normality was tested and rejected ($p < 0.05$) by Shapiro-Wilk tests. Bioerosion and accretion rates were log(x+1) transformed and net limestone erosion rates (log(x+10). The effects of depth, exposure and orientation on bioerosion and net limestone erosion rates were tested by three-way permutational analysis of variance (PERMANOVA). The effects of depth, exposure, orientation, and substrate type on accretion rates were tested by four-way PERMANOVA. All PERMANOVA tests were based on a fixed factor design and calculated under 999 permutations.

Semiquantitative abundance data of bioerosion traces was translated into ranked abundance classes where 'very common' was transformed to an abundance value of 1000, 'common' to 100, 'rare' to 10, and 'very rare' to 1, following the procedure described in (Wisshak et al., 2011). In order to identify similarities among bioerosion traces multidimensional scaling analysis (MDS), in combination with a group-average cluster analysis based on Bray-Curtis similarity, and a similarity profile test (SIMPROF) was calculated (Clarke, 1993). One-way analysis of similarity (ANOSIM) was used to determine the significance of any clustering of bioerosion traces in the MDS ordination. Two-way ANOSIM was used to test the effects of depth, exposure, and orientation on bioerosion traces. Normality tests were carried out with SigmaPlot. PERMANOVA, MDS, and ANOSIM were calculated using the Primer+PERMANOVA software package (Anderson et al., 2008; Clarke and Gorley, 2006).

### 3.2.7 Environmental data

Complementary to measurements of water temperature during the short-term experiments, environmental data was derived from databases in order to gain a more complete picture of environmental conditions of the study sites in general and during the experiments. Data on water temperature and salinity for the whole Mediterranean Sea were derived from the

World Ocean Database (Boyer et al., 2013) and chlorophyll a data were produced with the Giovanni online data system (Acker and Leptoukh, 2007). The photic zonation of the Ionian Sea was reconstructed based on light measurements of photosynthetically active radiation from the MTP II-MATER database (Mater Group, 2001). Wind data of Rhodes were derived from the Integrated Surface Database Light (Smith et al., 2011) and was plotted with WRPlot View. Tidal data were derived from WXTide 32. Bathymetric data and maps were displayed in Ocean Data View (Schlitzer, 2014–2015) or derived from the EMODnet Portal for Bathymetry (EMODnet, 2015) and displayed with ESRI ArcGis 10.3.

# 4 Effects of water depth, seasonal exposure, and substrate orientation on microbial bioerosion in the Ionian Sea (Eastern Mediterranean)

Claudia Färber[1], Max Wisshak[1], Ines Pyko[2], Nikoleta Bellou[3], André Freiwald[1]

[1]Senckenberg am Meer, Abteilung Meeresforschung, Südstrand 40, 26382 Wilhelmshaven, Germany
[2]GeoZentrum Nordbayern, Fachgruppe Paläoumwelt, Universität Erlangen-Nürnberg, Loewenichstraße 28, 91054 Erlangen, Germany
[3]Hellenic Centre for Marine Research, Institute of Oceanography, 46.7 km Athens Sounio, 19003 Anavyssos, Greece

Published in PLoS ONE 10(4): e0126495, doi: 10.1371/journal.pone.0126495[1]

## Abstract

The effects of water depth, seasonal exposure, and substrate orientation on microbioerosion were studied by means of a settlement experiment deployed in 15, 50, 100, and 250 m water depth south-west of the Peloponnese Peninsula (Greece). At each depth, an experimental platform was exposed for a summer period, a winter period, and about an entire year. On the up- and down-facing side of each platform, substrates were fixed to document the succession of bioerosion traces, and to measure variations in bioerosion and accretion rates. In total, 29 different bioerosion traces were recorded revealing a dominance of microborings produced by phototrophic and organotrophic microendoliths, complemented by few macroborings, attachment scars, and grazing traces. The highest bioerosion activity was recorded in 15 m up-facing substrates in the shallow euphotic zone, largely driven by phototrophic cyanobacteria. Towards the chlorophyte-dominated deep euphotic to dysphotic zones and the organotroph-dominated aphotic zone the intensity of bioerosion and the diversity of bioerosion traces strongly decreased. During summer the activity of phototrophs was higher than during winter, which was likely stimulated by enhanced light availability due to more hours of daylight and increased irradiance angles. Stable water column stratification and a resulting nutrient depletion in shallow water led to lower turbidity levels and caused a shift in the photic zonation that was reflected by more phototrophs being active at greater depth. With respect to the subordinate bioerosion activity of organotrophs, fluctuations in temperature and the trophic regime were assumed to be the main seasonal controls. The observed patterns in overall bioeroder distribution and abundance were mirrored by the calculated carbonate budget with bioerosion rates exceeding carbonate accretion rates in shallow water and distinctly higher bioerosion rates at all depths during summer. These findings highlight the relevance of bioerosion and accretion for the carbonate budget of the Ionian Sea.

## 4.1 Introduction

Biological erosion of carbonate substrate is a key process during the (re)cycling of calcium carbonate and the formation of calcareous sediments in the ocean (Golubic et al., 1979; Ridgwell and Zeebe, 2005). Wherever fresh substrate becomes available it is rapidly colonised by pioneer microbial euendoliths, finding shelter from grazers and physical disturbance or seeking nutrition within the substrate (Golubic et al., 1975; Glaub et al., 2007; Tribollet et al., 2011). Mature microboring communities usually develop during the first 6 months of exposure (Chazottes et al., 1995; Tribollet and Golubic, 2005), while macroborers and grazers are considered to take more than 2–3 years to fully establish (Kiene and Hutchings, 1994). In order to investigate this succession and the effect of ecological conditions on bioerosion, intensive research has been carried out in the past years focusing mainly on tropical coral reef ecosystems (Hutchings, 1986; Pari et al., 1998, 2002; Chazottes et al., 2002). However, from bioerosion experiments conducted in the non-polar Atlantic Ocean it is known that bioerosion follows a distinct latitudinal gradient with highest intensities in the tropics (Hoskin et al., 1986; Vogel et al., 1996, 2000), intermediate levels in the warm-temperate (Wisshak et al., 2010, 2011), and lowest rates in the cold-temperate high latitudes (Wisshak, 2006). In modern oceans, many euendoliths are considered to show a cosmopolitan distribution (i.e. they occur worldwide in suitable habitats). For the bathymetric zonation of phototrophic euendoliths and the bioerosion trace assemblages they produce (ichnocoenoses), light was identified as main controlling factor (Glaub, 1994; Vogel et al., 1995, 2000; Glaub et al., 2001). In contrast, endolithic marine fungi are organotrophs biodegrading calcareous shells in order to exploit mineralised organic matter and are independent of light (Golubic et al., 2005). The knowledge on the effects of water temperature, salinity, inorganic nutrients, particulate organic matter, and the complex interplay of all these factors on microbial bioerosion is still limited (Wisshak, 2012).

In the Mediterranean Sea, ongoing eutrophication, pollution, warming, and ocean acidification are considered to magnify the intensity of bioerosion (Schönberg and Wisshak, 2014). In contrast to tropical settings, the main bioerosion agents are considered to be microendolithic cyanobacteria, chlorophytes, and fungi, alongside macroboring sponges, molluscs, and grazing sea urchins, while fish apparently do not play a significant role (Schönberg and Wisshak, 2014). Taxonomical studies on bioeroding cyanobacteria and chlorophytes have been carried out in the Mediterranean Sea since the late 19$^{th}$ century (Bornet and Flahault, 1888, 1889; Ercegovic, 1927, 1929, 1932). But experimental studies remain scarce and were mainly concentrated on the Marseilles region in the Western Mediterranean Sea (Le Campion-Alsumard, 1979; Sartoretto, 1998). From the sole bioerosion experiment conducted in the Eastern Mediterranean Sea, only preliminary results are presently published (Bromley et al., 1990).

The present study was part of a carbonate cycling experiment aiming to provide a budget of carbonate bioerosion versus accretion in the Ionian Sea. The Eastern Mediterranean Sea shows a high spatio-temporal variability with respect to water temperatures, salinity, nutrients, and primary productivity (Krom et al., 2014; Stambler, 2014). This provides prime conditions in order to investigate the effects of water depth, seasonal exposure, and substrate orientation on bioerosion and accretion. The experiment comprised twelve platforms with experimental substrates deployed along a bathymetric transect in 15, 50, 100, and 250 m. Per depth one platform was exposed for a summer period (February–October), a winter period (October–April), and about an entire year. In this paper, we report on the analysis of the effects of water depth, seasonal exposure, and substrate orientation on bioerosion

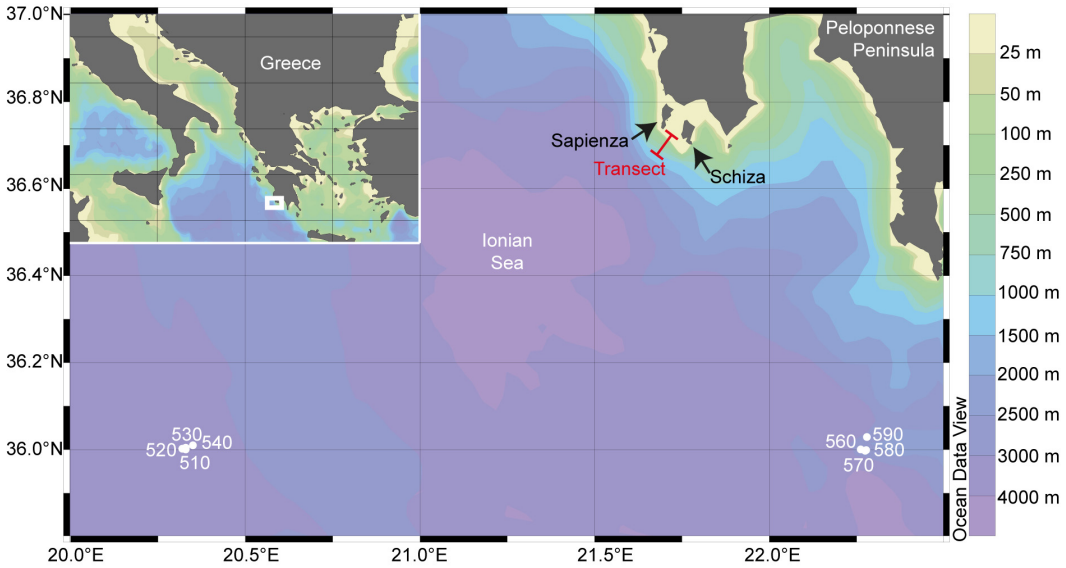


Figure 4.1 Location of the bathymetric transect (15, 50, 100, and 250 m) south-west of the Peloponnese Peninsula in the Ionian Sea. Numbers show the locations of light measurements that were carried out in the framework of the European Commission's Marine Sciences & Technology (MAST) program (Mater Group, 2001; Fig. A1). Base map displayed in Ocean Data View (Schlitzer, 2014–2015).

rates and traces, and discuss our results in context of the spatio-temporal environmental variability of the Ionian Sea.

## 4.2 Material and Methods

### 4.2.1 Ethics statement

The Hellenic Centre for Marine Research (HCMR) was consortium partner in the projects KM3NET (Contract No. 011937; EU-FP6), POSEIDON II (EFTA & Greek Ministry of National Economy) and POSEIDON III (Contract no. EL0048; EEA Grants) under which the cruises for this study were performed. The HCMR is a governmental research institute and belongs to the Ministry of Education and Religious affairs. Hence, it has the permit to obtain scientific fieldwork in Greek Seas and along the coastline and was represented during the cruises by co-author Nikoleta Bellou. Prior to the cruises the local authorities were informed about the planned experiment and the coordinates of the deployed experiment were provided. As no molecular biological analyses are planned to be performed no further permit and approval were needed.

### 4.2.2 Study site

The carbonate cycling experiment was carried out south-west of the Peloponnese Peninsula (Greece) in the Ionian Sea (ca. 36.73° N, 21.68° E, Fig. 4.1). The area is far from any river discharge and characterised by exceptionally clear and oligotrophic water with low sedimentation rates (Khanaev and Kuleshov, 1992; Trimonis and Rudenko, 1992). The general structure of water masses in the area is composed of Modified Atlantic Water that shows a subsurface minimum of salinity between 30–200 m water depth and Levantine Intermediate Water with a salinity maximum in 200–600 m (Malanotte-Rizzoli et al., 1997).

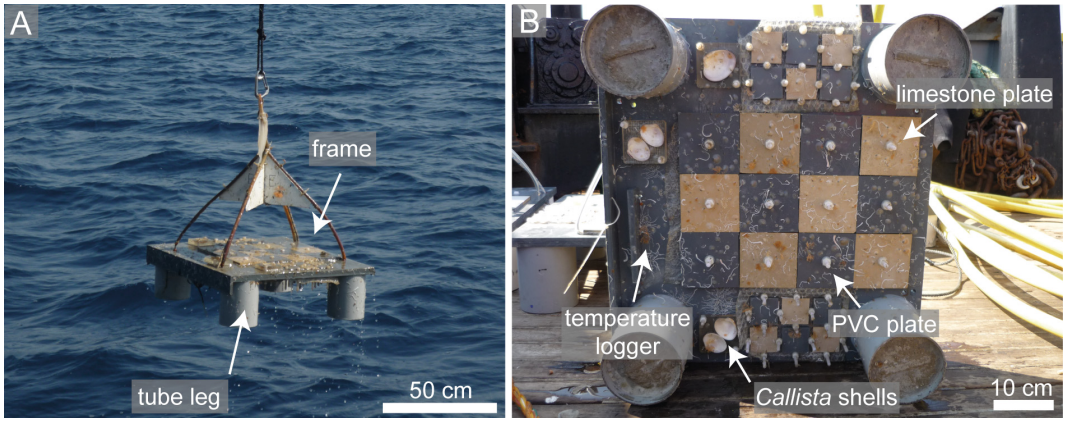


Figure 4.2 Photographs of an experimental platform. (A) Each platform is composed of a 54 x 60 cm PVC frame with four concrete filled PVC tube legs and experimental substrates on the up- and down-facing side. (B) View of the down-facing side of a platform equipped with limestone and PVC plates for the investigation of bioerosion and accretion rates, shells of the Mediterranean bivalve *Callista chione* for the analysis of bioerosion traces, and a water temperature data logger. Smaller PVC and limestone plates are mounted for the investigation of bacterial biofilms, which are not the scope of the present paper.

During summer, Ionian Surface Water clearly differs from Modified Atlantic Water by being saltier and warmer (Malanotte-Rizzoli et al., 1997). Values of surface irradiance calculated from light measurements of photosynthetically active radiation in the Ionian Sea that were carried out in the framework of the European Commission's Marine Sciences & Technology (MAST) program (Mater Group, 2001), suggest an approximate base of the euphotic and dysphotic zones in ca. 100 and 180 m, respectively (Fig. A1).

### 4.2.3 Experimental setup

The deployment of the summer and one year platforms was carried out onboard R/V Aegaeo on 28 February 2008. The summer platforms were recovered and replaced by the winter platforms after 226 days onboard R/V Philia on 11/12 October 2008. The winter and one year platforms were finally retrieved after 173 and 400 days, respectively, onboard R/V Philia on 2 April 2009. The 15 m platforms were deployed by scuba divers, the deeper platforms via remotely operated vehicle. Platforms in 15 m were deployed on rocky hard ground, the deeper platforms on sandy-muddy soft ground. After the winter, the 15 m platform was found turned over and was therefore excluded from analysis.

The principle design of the platforms is based on previous experiments in the Swedish Kosterfjord (Wisshak, 2006) and the Azores Archipelago (Wisshak et al., 2010, 2011, 2015). Each platform is composed of a 54 x 60 cm PVC frame with four concrete filled PVC tube legs and experimental substrates on the up- and down-facing side (Fig. 4.2). In each orientation, six limestone and six PVC plates (10 x 10 x 1 cm) were mounted for the assessment of carbonate bioerosion and accretion rates, as well as three shells of the Mediterranean bivalve *Callista chione*, embedded in a socket of epoxy resin, in order to expose solely the pristine inner side of the valve, for the investigation of bioerosion traces. Smaller PVC and limestone plates were mounted for the investigation of bacterial biofilms, which are not the scope of the present paper. On the down-facing side of each platform, a temperature data logger (Hobo Water Temp Pro v2, accuracy ±0.2 °C or Star Oddi Starmon-Mini, accuracy ±0.05 °C; 30 min. intervals) was fixed in order to characterise the temperature variability and stratification of water masses during the experiment. Due to data loss, no water

temperature measurements are available from the 250 m winter deployment as well as from the entire one year deployment.

### 4.2.4 Carbonate budget

Carbonate bioerosion and accretion rates were calculated via the difference in the weight of substrates before and after exposure. For this purpose, limestone and PVC plates were dried before deployment for two weeks at 70 °C and weighed with a precision scale (limestone plates: Mettler Toledo Classic Plus PB3002-S, accuracy 10 mg; PVC plates: Mettler Toledo Classic AB 204-S, accuracy 0.1 mg). After retrieval, all non-calcareous components were removed in 15 % hydrogen peroxide solution ($H_2O_2$). Then the plates were again dried at 70 °C. From limestone blocks, all calcareous components were carefully removed with a scalpel under the microscope. Bioerosion rates were calculated from the weight difference of limestone plates before deployment and after removing calcareous components. Accretion rates were calculated from the difference of the PVC plates before and after deployment, as well as from the weight of calcareous components, which were removed from the limestone plates. Net limestone erosion rates were calculated from the difference of carbonate accretion and bioerosion rates. All rates are given in gram per square metre per year ($g\ m^{-2}\ yr^{-1}$).

### 4.2.5 Bioerosion traces

Bioerosion traces in *Callista* shells were analysed by scanning electron microscopy (SEM). For this purpose, two shells each from the up- and down-facing side of each platform were selected. The third was stored in 4 % formaldehyde solution. For the preparation of epoxy resin casts of bioerosion traces, the shells were treated with $H_2O_2$ for a complete removal of fleshy epiliths, air dried, and casted in epoxy resin (Araldit BY 158, Aradur 21) in a vacuum chamber (Struers CitoVac). From each shell, four surface samples and two cross-sections were cut with a rock saw and decalcified in 5 % hydrochloric acid (cross-sections only partially). The epoxy resin blocks, now exhibiting the positive casts of the microborings, were sputter-coated with gold, and analysed under the SEM. Bioerosion traces on the surface of the limestone plates were documented with a digital light microscope (Keyence VHX-1000D).

Identification of bioerosion traces followed descriptions in Radtke (1991), Schmidt (1992), and Wisshak et al. (2011, 2014a). The bioerosion traces were ichnotaxonomically identified to ichnospecies level or described in informal nomenclature (e.g. 'Super thin form') and semiquantified in the abundance classes 'very common', 'common', 'rare', and 'very rare'. Due to the removal of carbonate encrusters, the documentation of traces from limestone plates was potentially biased and thus excluded from statistical analyses, albeit listed in the bioerosion inventory.

### 4.2.6 Statistical analyses

Due to the loss of the 15 m winter platform, overall tests of the effects of water depth, seasonal exposure, substrate orientation, and substrate type (the latter solely for accretion) on carbonate bioerosion and accretion along the complete transect were not feasible. Instead, 15 m rates were excluded from analysis and the tests only carried out for summer, winter, and one year bioerosion, accretion, and net erosion rates from 50–250 m. Prior to analysis, normality was tested and rejected ($p < 0.05$) by Shapiro-Wilk tests. Bioerosion and accretion rates were log(x+1) transformed and net limestone erosion rates log(x+10) transformed.

The effects of depth, exposure, and orientation on bioerosion and net limestone erosion rates were tested by three-way permutational analysis of variance (PERMANOVA). The effects of depth, exposure, orientation, and substrate type on accretion rates were tested by four-way PERMANOVA. All PERMANOVA tests were based on a fixed factor design and calculated under 999 permutations.

According to the procedure described in Wisshak et al. (2011), semiquantitative abundance data of bioerosion traces was translated into ranked abundance classes where 'very common' was transformed to an abundance value of 1000, 'common' to 100, 'rare' to 10, and 'very rare' to 1. In order to identify similarities among bioerosion traces multidimensional scaling analysis (MDS), in combination with a group-average cluster analysis based on Bray-Curtis similarity, and a similarity profile test (SIMPROF) was calculated (Clarke, 1993). Due to the loss of the 15 m winter platform, again only 50–250 m bioerosion traces were included. One-way analysis of similarity (ANOSIM) was used to determine the significance of any clustering of bioerosion traces in the MDS ordination. Two-way ANOSIM was used to test the effects of depth, exposure, and orientation on bioerosion traces. Normality tests were carried out with SigmaPlot. PERMANOVA, MDS, and ANOSIM were calculated using the Primer+PERMANOVA software package (Clarke and Gorley, 2006; Anderson et al., 2008).

## 4.3 Results

### 4.3.1 Water temperature

Water temperatures along the bathymetric transect were subject of a distinct seasonal variability (Fig. 4.3, Table A1). From April–November the water masses were highly stratified. Without the missing winter platform, the strongest fluctuation of 11 °C was observed in 15 m water depth, with a minimum of 15 °C in March–April, and a maximum of 26 °C in September. Water masses in 50 m showed a variability of 7 °C, with a minimum of 15 °C until May, an increase up to 20 °C until August, and a maximum of 22 °C in November. In 100 m, temperatures were comparatively constant at 15 °C until October, while from November a slight increase up to 18 °C was recorded. Although the winter period temperature data is missing at the 250 m site, the temperature trend at this depth suggests a constant temperature of 14.5 °C for the entire period of this study.

### 4.3.2 Carbonate budget

#### Bioerosion rates

Highest bioerosion rates were measured in 15 m up-facing substrates during summer and one year exposure (mean 83 g $m^{-2}$ $yr^{-1}$), showing a distinct decrease towards deeper water (Fig. 4.4A–C, Table A2). These values were about three-fold higher than in the 15 m down-facing substrates (mean 29 g $m^{-2}$ $yr^{-1}$). Three-way PERMANOVA of 50–250 m bioerosion rates revealed significant effects of depth and exposure (Table 4.1). Highest values of summer and one year bioerosion rates were reached in up-facing 50 m substrates (mean 32 g $m^{-2}$ $yr^{-1}$), while during the winter the bioerosion rates were distinctly lower (mean 8 g $m^{-2}$ $yr^{-1}$). In general, lowest values were measured in 250 m.

#### Accretion rates

In contrast to bioerosion, accretion rates on up-facing substrates in shallow water were low, but peaked on down-facing substrates in 15 and 50 m water depth (Fig. 4.4D–F, Table A2).

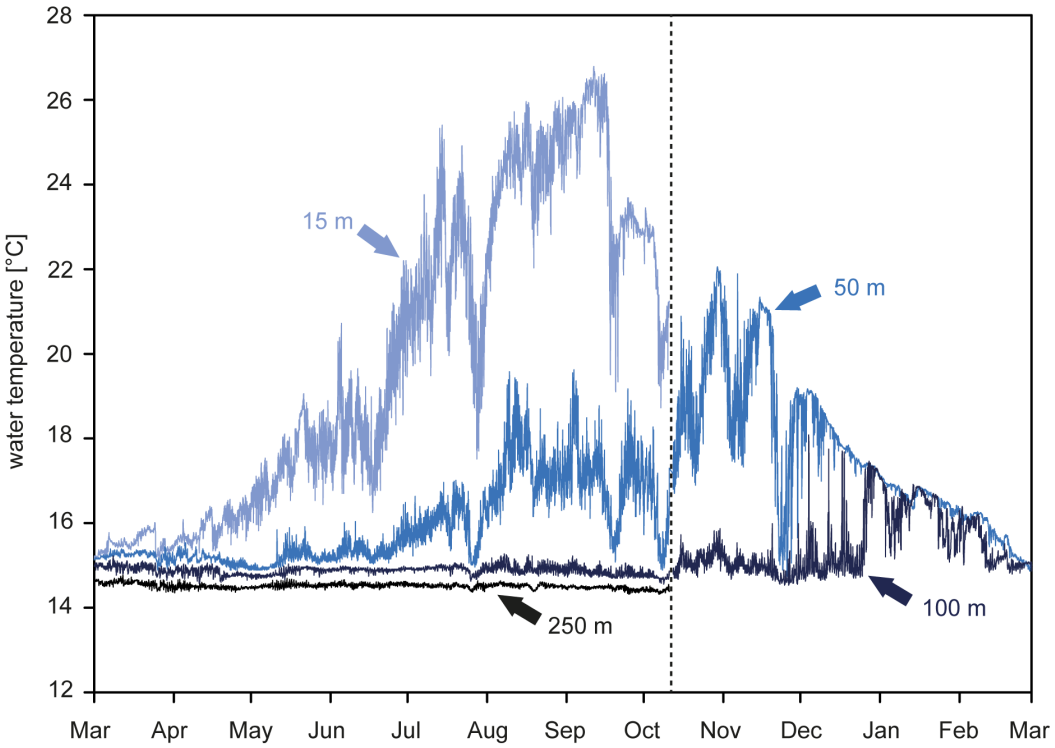


Figure 4.3 Water temperature measurement during the experiment from March 2008–2009. Dashed line marks the replacement from summer to winter platforms in October 2008. Due to platform and data loss, no water temperature is available for 15 and 250 m winter exposure, respectively.

Highest rates were observed on down-facing limestone and PVC substrates deployed in 50 m for one year (mean 241 g $m^{-2}$ $yr^{-1}$), and secondarily on 15 m limestone substrates (mean 213 g $m^{-2}$ $yr^{-1}$). During summer, carbonate production on those substrates was considerably lower (ca. 150–162 g $m^{-2}$ $yr^{-1}$). On 15 m down-facing substrates exposed for one year, the largest difference with regard to substrate composition was found with about five-fold higher carbonate accretion rates on PVC than on limestone substrates (mean 213 and 46 g $m^{-2}$ $yr^{-1}$). Four-way PERMANOVA of 50–250 m accretion rates revealed significant effects of depth, exposure, orientation, and substrate composition (Table 4.2). During summer and one year exposure, differences among carbonate accretion produced in 50 and 100 m were distinctly higher than during the winter. From 50–250 m, largest variability with regard to substrate orientation was observed on 50 m substrates during one year where about four-fold more carbonate was produced on down-facing than on up-facing substrates (mean 241 and 56 g $m^{-2}$ $yr^{-1}$). In 250 m water depth almost no carbonate was produced.

## Net limestone erosion rates

Calculated from the difference of accretion and bioerosion rates, net limestone erosion rates revealed a net loss of carbonate on 15 m up-facing substrates during summer and one year exposure (Fig. 4.4G–I, Table A2). For all other substrates a net gain of carbonate was recorded. Highest net production of carbonate was recorded in 50 m down-facing substrates during one year of exposure (mean 235 g $m^{-2}$ $yr^{-1}$). Highest net loss of carbonate was measured in 15 m up-facing substrates during one year exposure (mean -65 g $m^{-2}$ $yr^{-1}$).

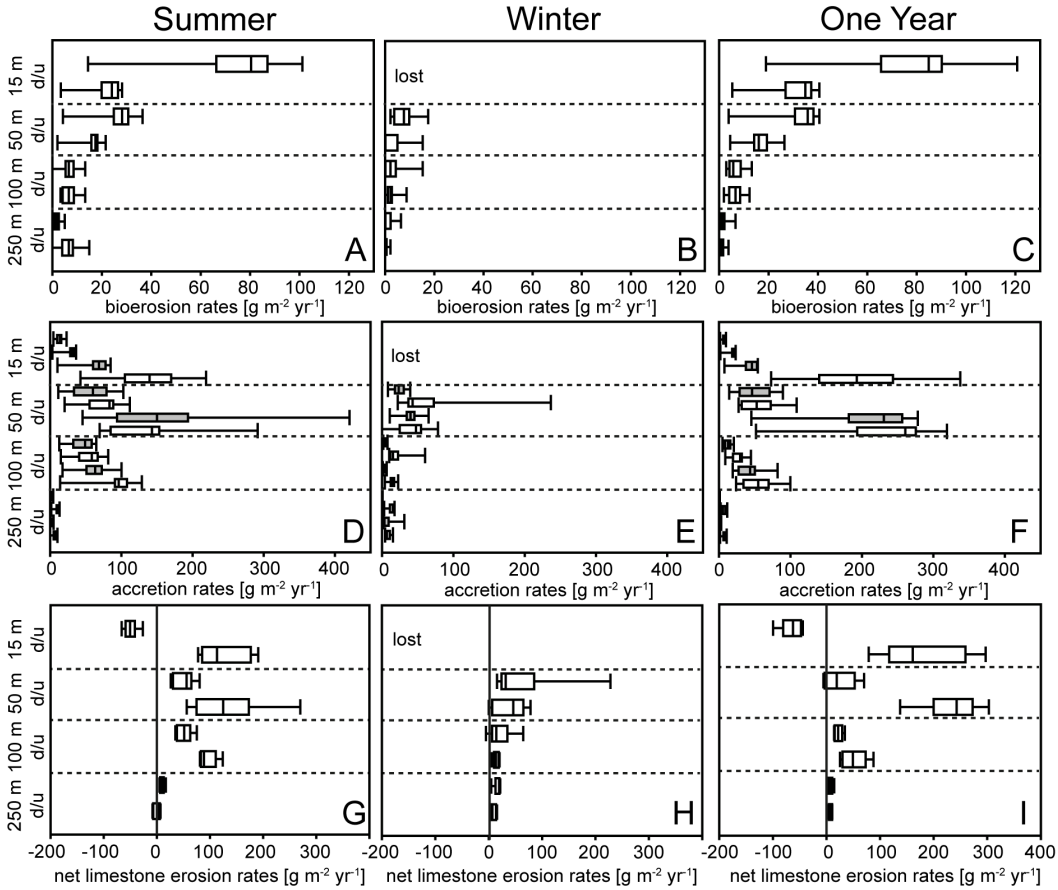


Figure 4.4 Box plots of bioerosion (A–C), accretion (D–F), and net limestone erosion rates (G–I) in up-facing (u) and down-facing (d) substrates from summer (A, D, G), winter (B, E, H), and one year exposure (C, F, I). Accretion is given for limestone (white) and PVC substrates (grey).

Three-way PERMANOVA showed that net limestone erosion rates in 50–250 m were significantly affected by water depth (Table 4.3). For exposure and orientation no effect was found.

### 4.3.3 Bioerosion traces

In *Callista* shells and limestone plates a total of 29 different bioerosion traces was observed (Fig. 4.5). These traces were attributed to 4 cyanobacterial microborings (Fig. 4.6A–E), 6 chlorophyte microborings (Fig. 4.6F–L), 6 fungal microborings (Fig. 4.7A–F), 6 microborings of other organotrophs (Fig. 4.7G–L), 3 macroborings (Fig. 4.8A–E), 3 attachment scars (Fig. 4.8F–H), and 1 grazing trace (Fig. 4.8I). SEM overviews and cross-sections on the same scale are illustrated for summer (Fig. 4.9), winter (Fig. 4.10), and one year exposure (Fig. 4.11).

The highest diversity of bioerosion traces was observed in 15 m up-facing substrates during one year of exposure, the lowest in substrates from 250 m water depth. During summer and one year exposure, up-facing substrates in 15 m were strongly colonised by cyanobacterial and chlorophyte microborings. Common were the cyanobacterial microborings *Fascichnus dactylus* and *Eurygonum nodosum* as well as the chlorophyte microboring *Rhopalia catenata*. Penetration depth was 15–100 µm. In 15 m down-facing substrates,

Table 4.1 Results of three-way permutational analysis of variance (PERMANOVA) testing effects of water depth, seasonal exposure, and substrate orientation on bioerosion rates from 50–250 m (statistically significant values are marked in bold.

| Source | df | SS | MS | Pseudo-F | P (perm) |
|---|---|---|---|---|---|
| Depth | 2 | 60.834 | 30.417 | 12.922 | **0.009** |
| Exposure | 2 | 39.932 | 19.966 | 8.482 | **0.008** |
| Orientation | 1 | 2.536 | 2.536 | 1.077 | 0.392 |
| Depth x Exposure | 4 | 25.400 | 6.350 | 2.698 | **0.031** |
| Depth x Orientation | 2 | 9.130 | 4.565 | 1.939 | 0.188 |
| Exposure x Orientation | 2 | 5.660 | 2.830 | 1.202 | 0.351 |
| Residual | 4 | 9.416 | 2.354 | | |
| Total | 17 | 152.910 | | | |

Table 4.2 Results of four-way permutational analysis of variance (PERMANOVA) testing effects of water depth, seasonal exposure, substrate orientation, and substrate type on accretion rates from 50–250 m (statistically significant values are marked in bold).

| Source | df | SS | MS | Pseudo-F | P (perm) |
|---|---|---|---|---|---|
| Depth | 2 | 271.940 | 135.970 | 75.014 | **0.002** |
| Exposure | 2 | 36.752 | 18.376 | 10.138 | **0.006** |
| Orientation | 1 | 12.062 | 12.062 | 6.655 | 0.025 |
| Substrate | 1 | 30.903 | 30.903 | 17.049 | **0.007** |
| Depth x Exposure | 4 | 36.875 | 9.219 | 5.086 | 0.031 |
| Depth x Orientation | 2 | 6.245 | 3.122 | 1.723 | 0.215 |
| Depth x Substrate | 2 | 18.664 | 9.332 | 5.148 | **0.020** |
| Exposure x Orientation | 2 | 6.647 | 3.324 | 1.834 | 0.212 |
| Exposure x Substrate | 2 | 4.113 | 2.057 | 1.135 | 0.424 |
| Orientation x Substrate | 1 | 7.466 | 7.466 | 4.119 | 0.061 |
| Depth x Exposure x Orientation | 4 | 12.365 | 3.091 | 1.705 | 0.191 |
| Depth x Exposure x Substrate | 4 | 10.952 | 2.738 | 1.510 | 0.244 |
| Depth x Orientation x Substrate | 2 | 4.589 | 2.294 | 1.266 | 0.356 |
| Exposure x Orientation x Substrate | 2 | 5.477 | 2.739 | 1.511 | 0.278 |
| Residual | 4 | 7.250 | 1.813 | | |
| Total | 35 | 472.300 | | | |

Table 4.3 Results of three-way permutational analysis of variance (PERMANOVA) testing effects of water depth, seasonal exposure, and substrate orientation on net limestone erosion rates from 50–250 m (statistically significant values are marked in bold)

| Source | df | SS | MS | Pseudo-F | P (perm) |
|---|---|---|---|---|---|
| Depth | 2 | 7.937 | 3.968 | 6.688 | **0.033** |
| Exposure | 2 | 1.202 | 0.601 | 1.013 | 0.435 |
| Orientation | 1 | 1.017 | 1.017 | 1.713 | 0.249 |
| Depth x Exposure | 4 | 2.518 | 0.630 | 1.061 | 0.470 |
| Depth x Orientation | 2 | 2.075 | 1.038 | 1.749 | 0.223 |
| Exposure x Orientation | 2 | 1.882 | 0.941 | 1.586 | 0.259 |
| Residual | 4 | 2.373 | 0.593 | | |
| Total | 17 | 19.004 | | | |

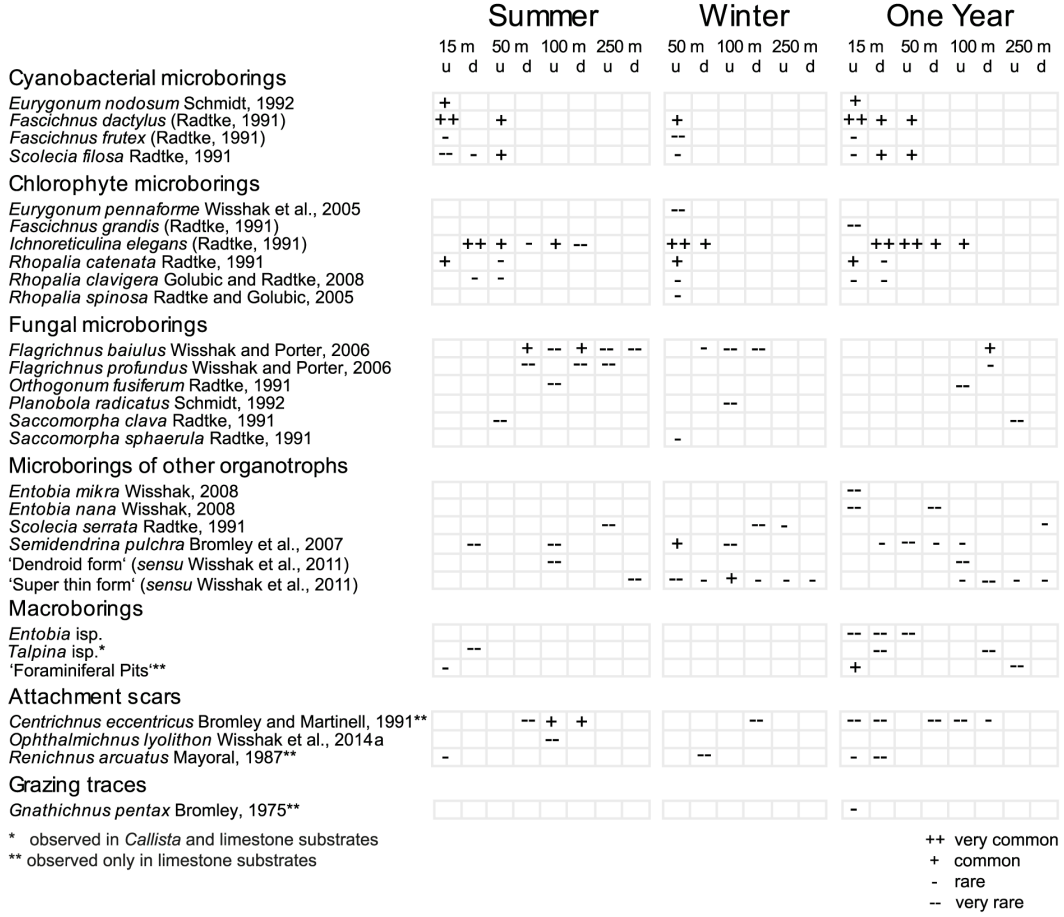


Figure 4.5 The inventory of bioerosion traces for the various water depths, substrate orientations (u = up-facing, d = down-facing), and exposure (summer, winter, and one year), categorised by trace types.

cyanobacterial microborings were still common, but chlorophyte microborings became more abundant. Frequently galleries of the chlorophyte trace *Ichnoreticulina elegans* were observed. Mean boring depth was 10 µm with only few galleries surpassing 50 µm.

Multivariate analysis of bioerosion traces from 50–250 m separated three significantly different main clusters (ANOSIM R = 0.875, p = 0.001) and two subclusters (ANOSIM R = 1, p = 0.001; Fig. 4.12; see Fig. A2 for underlying cluster analysis). Two-way ANOSIM showed that the occurrence of bioerosion traces was significantly affected by water depth and secondarily by orientation (Table 4.4). Cluster 1 contained bioerosion traces from up-facing 50 m summer, winter, and one year substrates, down-facing 50 m winter and one year substrates, and up-facing 100 m summer and one year substrates. In these substrates cyanobacterial and chlorophyte microborings dominated. The subclusters 1a and 1b further revealed a significant difference among bioerosion traces developed in 50 m up-facing substrates during winter and one year exposure, and those developed in 50 m down-facing winter and one year, and 100 m up-facing summer and one year substrates. Common traces in both subclusters were the chlorophyte microborings *I. elegans*. The major difference among these subclusters was the common occurrence of cyanobacterial microborings *F. dactylus* and *S. filosa* in subcluster 1a, while in subcluster 1b cyanobacteria were absent. Up-facing 50 m summer substrates differed from those in subcluster 1a and 1b showing commonly specimens of *F. dactylus* and *S. filosa*, but less *I. elegans*. Secondarily in 50 m up-facing

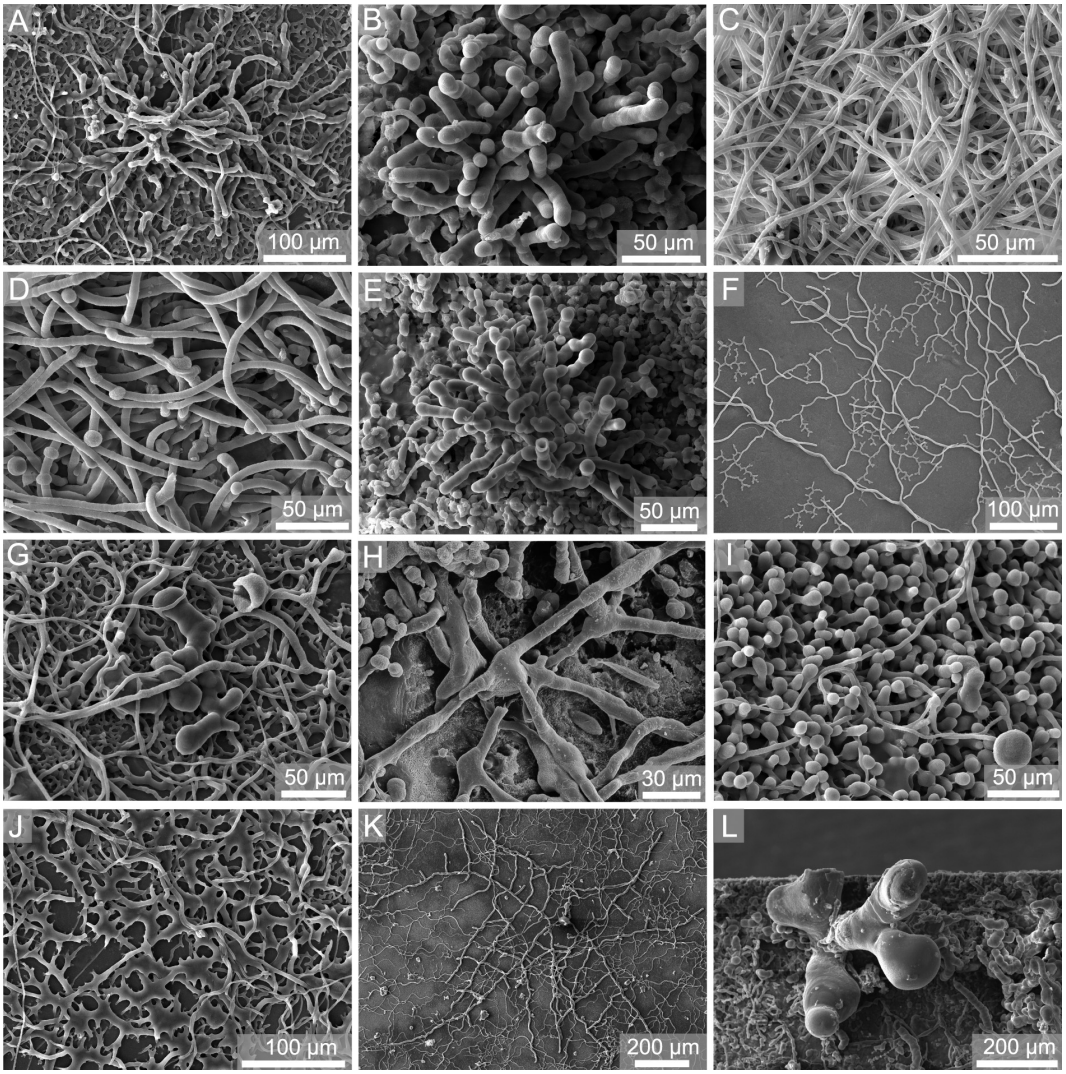


Figure 4.6 SEM images of epoxy-resin casts taken from *Callista* shells showing cyanobacterial (A–E) and chlorophyte (F–L) microborings. (A–B) *Fascichnus dactylus*, 50 m up, winter and 15 m up, one year, (C) *Scolecia filosa*, 15 m up, one year, (D) *Eurygonum nodosum*, 15 m up, one year, (E) *Fascichnus frutex*, 15 m up, one year, (F–G) *Ichnoreticulina elegans*, 100 m up, summer and 50 m up, winter, (H) *Rhopalia catenata*, 15 m up, summer, (I) *Rhopalia clavigera*, 50 m up, winter, (J) *Rhopalia spinosa*, 50 m up, winter, (K) *Eurygonum pennaforme*, 50 up, winter, (L) *Fascichnus grandis*, 15 m up, one year.

winter substrates common specimens of the foraminiferan trace *Semidendrina pulchra* were observed. In 100 m up-facing winter substrates filaments of the 'super thin form' were common. Mean boring depth in 50 m up-facing substrates was still about 25 µm with few galleries surpassing 150 µm. In all other substrates the boring intensity was very low. Cluster 2 contained bioerosion traces from 50 m and 100 m down-facing summer substrates and 100 m down-facing one year substrates. Typical were various specimens of the fungal microborings *Flagrichnus baiulus*. Cyanobacterial microborings were absent. With respect to chlorophyte microborings, only few galleries of *I. elegans* were detected. The boring intensity was very low. Cluster 3 included bioerosion traces from 100 m up- and down-facing winter and all 250 m substrates. Solely fungal microborings and those of other organotrophs were observed. Cyanobacterial and chlorophyte microborings were absent. Borings

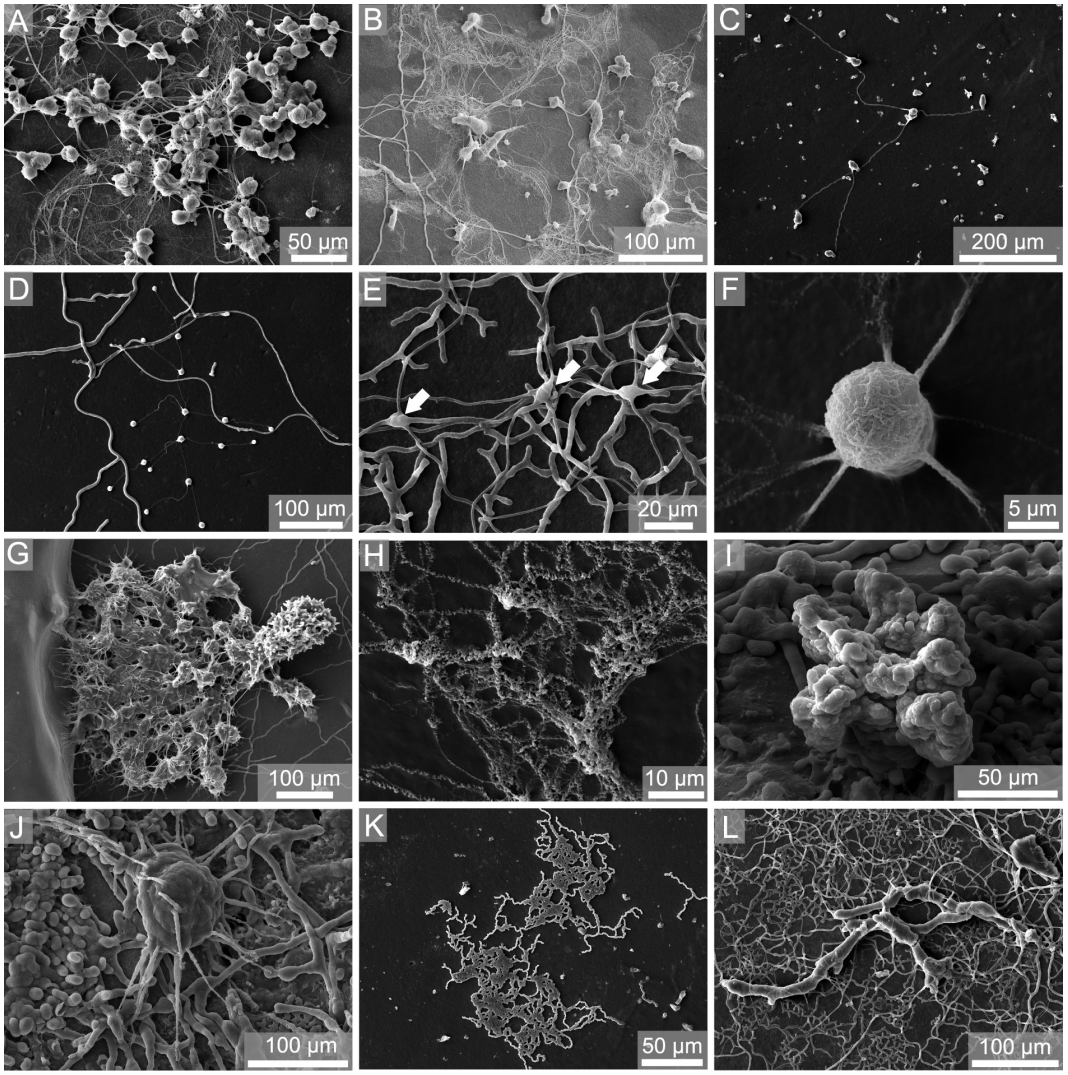


Figure 4.7 SEM images of epoxy-resin casts taken from *Callist*a shells showing fungal microborings (A–F) and traces of other organotrophs (G–L). (A) *Flagrichnus baiulus*, 50 m down, summer, (B) *Flagrichnus profundus*, 50 m down, summer, (C) *Saccomorpha clava*, 250 m up, one year, (D) *Saccomorpha sphaerula*, 50 m up, winter, (E) *Orthogonum fusiferum* (arrows mark swellings), 100 m up, one year, (F) *Planobola radicatus*, 100 m up, winter, (G) *Semidendrina pulchra*, 50 m down, winter, (H) 'Super thin form', 250 m down, winter, (I) *Entobia mikra*, 15 m up, one year, (J) *Entobia nana*, 15 m up, one year, (K) *Scolecia serrata*, 250 m up, winter, (L) 'Dendroid form 1', 100 m up, one year.

were scarce and represented by galleries of fungal microborings *F. baiulus* and *F. profundus*, and the organotroph traces *Scolecia serrata* and 'super thin form'. The boring intensity again was very low.

Excluded from statistical analyses, some conspicuous bioerosion traces were observed on limestone substrates. In 15 m up-facing one year plates, various small 'foraminiferal pits' were found, in which commonly tests of foraminiferans were preserved *in situ*. On 100 m up- and down-facing summer limestone plates, commonly the anomiid bivalve attachment scar *Centrichnus eccentricus* occurred. The echinoid grazing trace *Gnathichnus pentax* and initial sponge boring traces *Entobia mikra*, *E. nana*, and *Entobia* isp. were first observed during one year exposure.

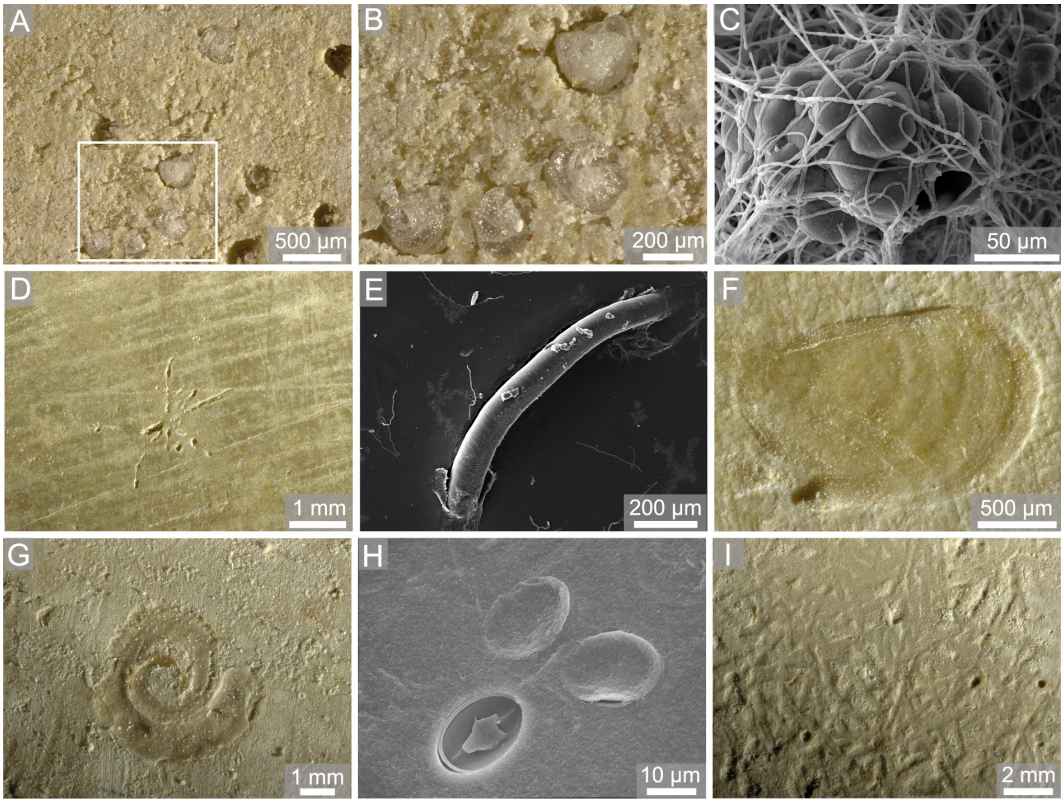


Figure 4.8 Light microscopic (A–B, D, F–G, I) and SEM images (C, E, H) of limestone blocks and *Callista* shells showing macroborings (A–E), attachment scars (F–H), and grazing traces (I). (A–B) 'Foraminiferal Pits', 15 m up, one year, (C) *Entobia* isp., 15 m down, one year, (D–E) *Talpina* isp., 50 m down, winter and summer, (F) *Centrichnus eccentricus*, 100 m down, summer, (G) *Renichnus arcuatus*, 15 m up, one year, (H) *Ophthalmichnus lyolithon*, 100 m up, summer, (I) *Gnathichnus pentax*, 15 m up, one year.

## 4.4 Discussion

### 4.4.1 Effect of water depth

Our settlement experiment demonstrates that carbonate bioerosion and accretion in the Ionian Sea strongly vary with water depth. The comparison of bioerosion rates and traces showed that the highest bioerosion activity occurs in shallow water being caused by the boring activity of cyanobacteria and chlorophytes, while towards the fungal and organotrophic euendolith-dominated deeper water the bioerosion intensity strongly decreases (Fig. 4.4, 4.5). This general bathymetrical pattern is in good agreement with previous settlement experiments conducted at the Great Barrier Reef (Vogel et al., 2000) and in the Azores Archipelago (Wisshak et al., 2010). The restriction of phototrophic cyanobacteria and chlorophytes to shallow water originates from their specific low-light tolerance limit and light optimum, while fungi and organotrophic euendoliths are light independent and able to thrive also in aphotic depths (Golubic et al., 1975; Perkins and Tsentas, 1976; Budd and Perkins, 1980; Akpan and Farrow, 1984; Günther, 1990). Microendolithic ichnocoenoses have long been identified to be a strong tool for judging light availability and hence relative bathymetry in both modern and ancient environmental settings (Wisshak, 2012). According to the set of bathymetric index ichnocoenoses that was developed in order to reconstruct photic conditions in palaeoenvironments (Glaub, 1994; Glaub et al., 2001; Vogel

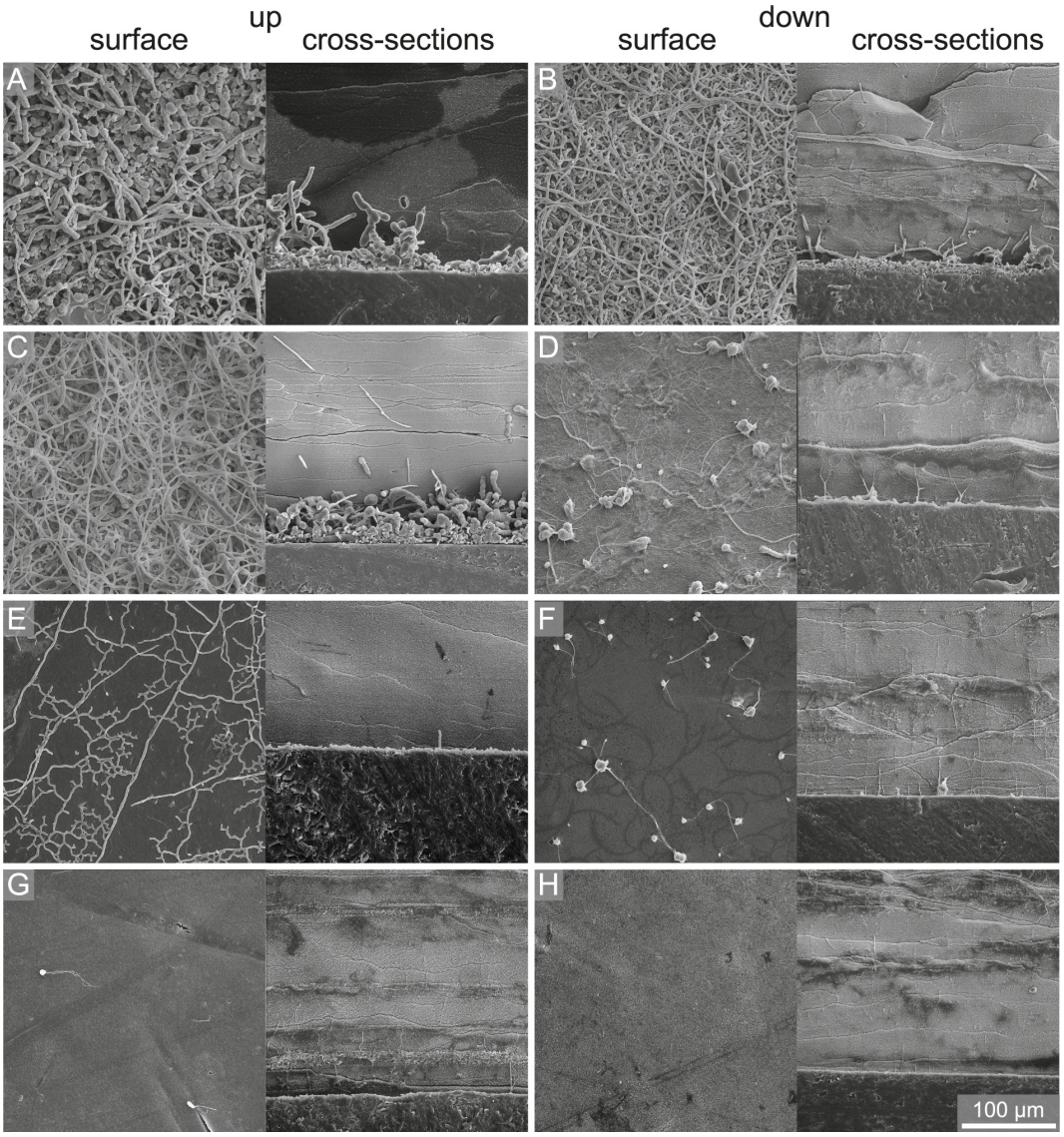


Figure 4.9 SEM images of summer samples of surface and cross-sections showing the degree of bioerosion with water depth and substrate orientation. (A) 15 m up, (B) 15 m down, (C) 50 m up, (D) 50 m down, (E) 100 m up, (F) 100 m down, (G) 250 m up, and (H) 250 m down.

et al., 1995, 2000; Wisshak, 2012), the dominance of the microboring trace index ichnotaxa *F. dactylus* and *R. catenata* in 15 m corresponds to typical shallow euphotic zone III ichnocoenoses from shallow subtidal ranges. In substrates deployed in 50 m water depth the common occurrence of *F. dactylus*, *S. filosa*, *I. elegans*, and few *S. clava* microborings reflects a transition between shallow euphotic zone III to deep euphotic ichnocoenoses. In 100 m the very common index ichnotaxon *I. elegans* and fungal microborings form a typical dysphotic ichnocoenosis, albeit *S. clava* was not observed. The exclusive occurrence of organotrophic microborings in 250 m substrates in the aphotic zone corresponds to typical aphotic ichnocoenoses although the index ichnotaxon *S. clava* was rare and *O. lineare* was not found. The low abundance and absence of these ichnotaxa is, however, not surprising, as they are known from other experiments to show only initial borings even after 1 and 2 years of exposure (Wisshak, 2006; Wisshak et al., 2011).

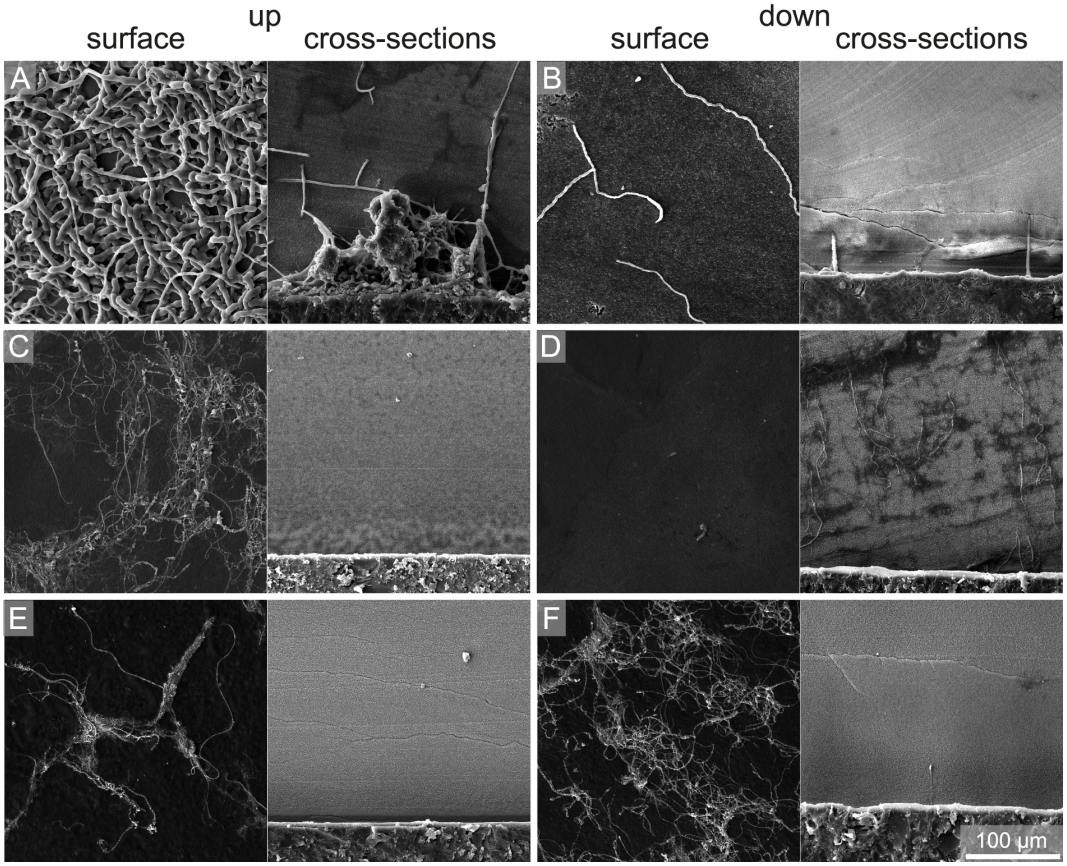


Figure 4.10 SEM images of winter samples of surface and cross-sections showing the degree of bioerosion with water depth and substrate orientation. (A) 50 m up, (B) 50 m down, (C) 100 m up, (D) 100 m down, (E) 250 m up, and (F) 250 m down.

In comparison to previous experiments from the Mediterranean Sea, the distribution of cyanobacterial and chlorophyte microborings from our experiment corresponds well with microbial endoliths observed during two colonisation experiments in the region of Marseilles in the Western Mediterranean Sea. Along a bathymetric transect from the supralittoral down to 190 m (Le Campion-Alsumard, 1979), the occurrence of the endolithic cyanobacteria *Mastigocoleus testarum*, *Hyella caespitosa*, and *Plectonema terebrans* down to 30, 60, and 80 m depth is in good agreement with their corresponding traces *E. nodosum*, *F. dactylus*, and *S. filosa* reported here from 15 and 50 m. The endolithic chlorophytes *Eugomontia sacculata*, *Phaeophila dendroides*, and *Ostreobium quekettii* occurred down to 80 and 100 m depth, which also corresponds well to the traces *R. clavigera*, *R. catenata*, and *I. elegans* we found down to 50 and 100 m. In a further colonisation experiment on rhodolith concretions in 10–60 m water depth (Sartoretto, 1998), *H. caespitosa* was restricted to 10 m, *P. tenebrans* and *M. testarum* were found down to 20 m, and solely *O. quekettii* reached down to 60 m. The comparison of the bathymetric distribution of those microendoliths suggests a certain resemblance of the photic zonation in the Eastern and Western Mediterranean Sea.

A detailed description of calcareous epiliths was beyond the scope of our study and detailed information on carbonate production in the Eastern Mediterranean Sea is not available. A comparison with carbonate production on the Balearic Platform in the Western

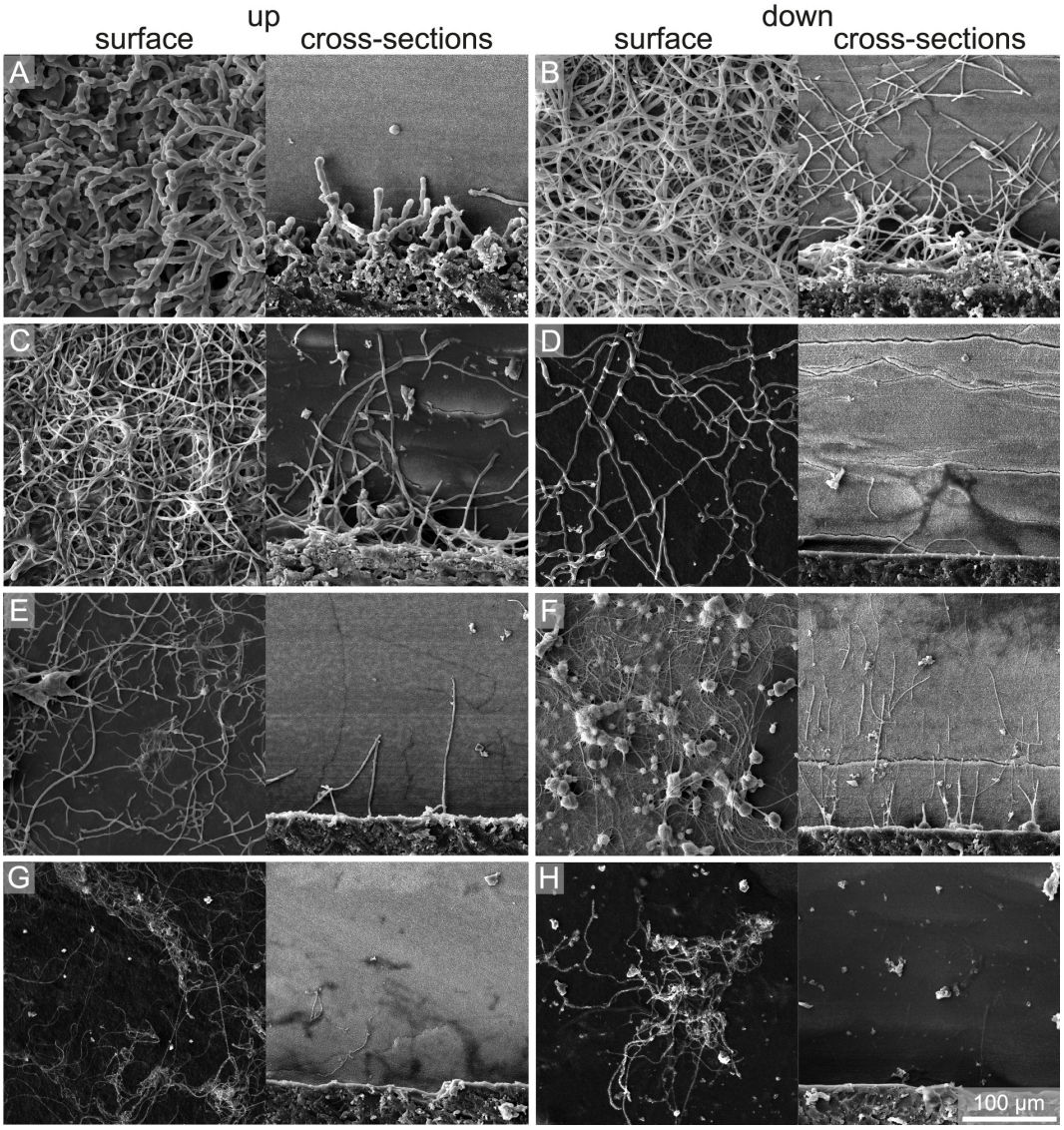


Figure 4.11 SEM images of one year samples of surface and cross-sections showing the degree of bioerosion with water depth and substrate orientation. (A) 15 m up, (B) 15 m down, (C) 50 m up, (D) 50 m down, (E) 100 m up, (F) 100 m down, (G) 250 m up, and (H) 250 m down.

Mediterranean Sea (Fornós and Ahr, 2006), where large amounts of carbonate are produced in the bryozoan and red algae facies of the middle ramp environment (ca. 30–90 m water depth), suggests that highest carbonate accretion rates in 50 m depth found in our study might likewise be produced by such low-light adapted epiliths.

In total, the calculation of net limestone erosion rates from the difference of carbonate bioerosion and accretion demonstrates the enormous effect of bioerosion on the carbonate budget of the Ionian Sea. While in deeper water (50–250 m) the net loss of carbonate by bioerosion is compensated by carbonate production, bioerosion rates exceed accretion in shallow water (15 m). In a similar settlement experiment along a more extended bathymetric transect in the Azores (Wisshak et al., 2010), highest mean bioerosion rates (456 g $m^{-2}$ $yr^{-1}$) were measured in the intertidal zone, whereas limestone accretion rates (7 g $m^{-2}$ $yr^{-1}$) were

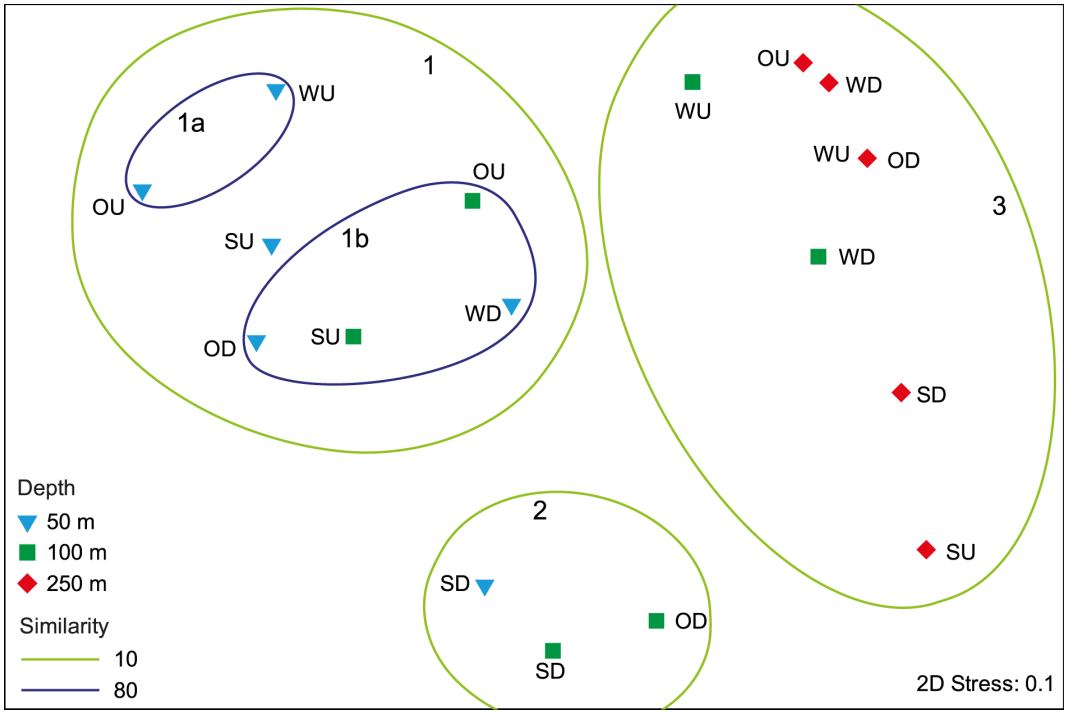


Figure 4.12 Multidimensional scaling plot (MDS) comparing summer, winter, and one year bioerosion traces observed in up- and down-facing substrates in 50–250 m water depth. Three main clusters (1, 2, 3) and two subclusters (1a, 1b) are separated with a Bray-Curtis similarity of 10 and 80, respectively. See Fig. A2 for underlying cluster analysis (S = summer, W = winter, O = one year; U = up-facing, D = down-facing).

low (i.e. net limestone erosion rate of -449 g $m^{-2}$ $yr^{-1}$). This indicates that we might also expect increasing net loss of carbonate towards and in the intertidal zone in the Ionian Sea.

### 4.4.2 Effect of seasonal exposure

The comparison of summer and winter platforms revealed a distinct seasonal effect on bioerosion and accretion. In 50 m, bioerosion rates of cyanobacteria and chlorophytes were distinctly higher during summer than during winter deployment (Fig. 4.4). With regard to bioerosion traces, the absence of *I. elegans* borings in 100 m winter substrates indicates a shift in light supply from a dysphotic ichnocoenosis during summer to an aphotic ichnocoenosis during winter (Fig. 4.5). These observations suggest a distinct seasonal variability in phototrophic microbioerosion, which is likely related to the reduction of absolute light availability during winter due to fewer hours of daylight and lower angles of irradiance. Both factors, however, do not alter the photic zonation, which is based on relative light levels (expressed in percentage of surface irradiance). Seasonal shifts of the photic zonation, in contrast, could originate from seasonal fluctuation in water turbidity. Turbidity effects on bioerosion were described from reef environments in Jamaica, where different light penetration regimes revealed marked variations in the bathymetric range of sediment microboring communities (Perry and Macdonald, 2002). Seasonal variations in the turbidity regime of the Eastern Mediterranean Sea could be associated with the observed seasonal variability of water masses (Fig. 4.3). Mean winter temperatures of 15 °C agree with values reported for Modified Atlantic Water between 30–200 m in the Ionian Sea during winter (Malanotte-Rizzoli et al., 1997). Also the strong increase of water temperatures in 15 m is a

Table 4.4 Results of two-way permutational analysis of similarity (ANOSIM) testing effects of water depth, seasonal exposure, and substrate orientation on bioerosion traces from 50–250 m (statistically significant values are marked in bold).

| Comparison | Factor | R | p |
|---|---|---|---|
| Depth x Orientation | Depth | 0.500 | **0.002** |
| | Orientation | 0.302 | **0.046** |
| Depth x Exposure | Depth | 0.472 | **0.011** |
| | Exposure | -0.019 | 0.515 |
| Orientation x Exposure | Orientation | -0.099 | 0.651 |
| | Exposure | 0.033 | 0.415 |

typical phenomenon in the Ionian Sea where Ionian Surface Water clearly differs from the underlying Modified Atlantic Water due to surface heating (Malanotte-Rizzoli et al., 1997). In general, summer stratification conditions are considered to cause a depletion of particles and dissolved nutrients and a reduction of primary production in surface water in the Mediterranean Sea (Stambler, 2014). During winter, in contrast, the euphotic zone is enriched in nutrients by vertical mixing and plankton blooms resulting in higher water turbidity and could thus cause a shift of the photic zonation towards shallower water.

In addition to this indirect effect of water temperature on phototrophic bioerosion, higher water temperatures during summer may also directly increase the activity of phototrophic endoliths. Many phytoplankton cellular processes are temperature dependent and especially cyanobacterial growth rates are considered to be favoured by increasing water temperatures (Paerl and Huisman, 2008). During the experiment highest temperatures of about 26 °C were measured during September in 15 m water depth, where mostly cyanobacterial microborings were observed. In contrast to light, many euendoliths in modern seas are eurythermal and have a cosmopolitan distribution, and the evaluation of microborings as a palaeotemperature and/or palaeolatitude indicator is still in its infancy (Wisshak, 2012). Optimal growth rates as well as lower and upper temperature limits of phototrophs are likely to be species specific and not presented for phototrophic microendoliths. Nevertheless, we suspect that in addition to the indirect effects of higher light availability and water transparency during summer stratification, water temperature might also directly enhance phototrophic microbioerosion during hot summer temperatures.

The difference among summer and winter bioerosion rates in 100 m depth was small. However, we observed a distinct seasonal difference in the abundance of the probable thraustochytrid fungal microboring *F. baiulus*, which was found in large quantities during summer. In contrast to cyanobacteria and chlorophytes, marine fungi are organotrophs that biodegrade calcareous shells in order to exploit mineralised organic matter and are independent of light supply (Golubic et al., 2005). Previously *Flagrichnus* borings were only described from non-tropical settings and were therefore suggested as an indicator for low (palaeo)temperatures (Wisshak and Porter, 2006). The presence of *F. baiulus* during summer could be explained by the observation that substrates deployed in 50 and 100 m were exposed to comparatively low temperatures of 15–19 °C, while during winter a distinct increase up to 22 °C in 50 m and 17 °C in 100 m was observed. A similar seasonal pattern was observed for thraustochytrid fungi in Mediterranean sandy habitats, where highest fungal densities were recorded in late spring and decreased during autumn–winter (Bongiorni and Dini, 2002). But the latter authors concluded that besides temperature other environmental

factors such as particulate and/or dissolved organic matter could have contributed to the seasonal pattern they observed.

Another microboring that is considered to be indicative of cold-water conditions is the probable endolithic foraminiferan trace *S. pulchra* (Bromley et al., 2007). In contrast to *F. baiulus*, this trace was found during our experiment mostly in 50 m winter substrates, where a distinct increase of water temperature up to 22 °C was recognised. For the suspension feeding foraminiferans, enhanced nutrient availability during winter could be related with higher amounts of inorganic nutrients during the winter plankton blooming period. However, we assume that similar to thraustochytrid fungi the occurrence of foraminifera is likely dependent on the interaction of several environmental parameters.

The minor difference between summer and one year bioerosion rates and microbioerosion traces suggests that the main settlement of microendoliths on one year substrates has taken place already during summer exposure. This corresponds to observations on coral reef ecosystems (Chazottes et al., 1995; Tribollet and Golubic, 2005), where microboring communities are considered to mature within 6 months of exposure. However, our results show that this applies only for summer exposure, while during the winter bioerosion rates the succession is strongly reduced. Due to practical reasons, summer exposure was about 50 days longer than winter exposure. Nevertheless, the observed differences in ichnocoenosis composition between the summer and winter period (e.g. *F. baiulus*) is unambiguous and very unlikely to have been caused by the minor difference in exposure period alone.

### 4.4.3 Effect of substrate orientation

In comparison to water depth and exposure, only a minor effect of orientation was found. On the up-facing side in 15 m the dominance of the index ichnotaxa *F. dactylus* and *R. catenata* microboring traces corresponds to typical shallow euphotic zone III ichnocoenoses from shallow subtidal ranges (Fig. 4.5). On the 15 m down-facing side, in contrast, the dominance of *I. elegans* and only few *R. clavigera* microborings represent a deep euphotic ichnocoenosis. In substrates deployed in 50 m water depth, the common occurrence of *F. dactylus*, *S. filosa*, *I. elegans*, and few *S. clava* microborings reflects deep euphotic ichnocoenoses on the up-facing side. On the down-facing side, the absence of *R. catenata*, but dominance of *I. elegans* and fungal traces are indicative for a dysphotic ichnocoenosis (although the index ichnotaxon *S. clava* was not observed). These findings suggest a distinct change in light supply among up- and down-facing substrates, which does not originate from a change in the photic zonation, but from shading effects on the down-facing side of the platform.

The inverse trend of higher bioerosion rates in up-facing substrates and higher accretion rates in down-facing substrates (Fig. 4.4) was similarly observed in a settlement experiment in the Azores Archipelago (Wisshak et al., 2010, 2015). Their study found that in addition to lower bioerosion pressure the main factors for the preferential settlement of calcareous epiliths on down-facing substrates were shading, negative phototactic larval behaviour, lower predation pressure, lower competition with epiphytes, and lack of sediment smothering. However, dense epilithic colonisation on down-facing substrates could also hinder the settlement and activity of bioeroders (Wisshak et al., 2010).

## 4.5 Conclusions

In conclusion, our study shows that bioerosion and accretion in the Ionian Sea were mostly affected by water depth and secondarily by seasonal exposure. Substrate orientation played

a minor role. Elevated temperatures and high absolute light intensities during summer due to more hours of daylight and increased irradiance angles promoted phototrophic microbioerosion by endolithic cyanobacteria and chlorophytes in shallow water. Plankton blooms during winter mixing, in contrast, likely led to a seasonal variability in water turbidity and thus resulted in a shift of the photic zonation. Altogether, these variations revealed pronounced differences in the composition and bathymetric range of summer versus winter microbioerosion ichnocoenoses as well as linked rates of bioerosion. The observed patterns in overall bioeroder distribution and abundance were mirrored by the calculated carbonate budget with bioerosion rates exceeding carbonate production rates in shallow water and distinctly higher bioerosion rates at all depths during summer.

## Acknowledgements

We thank the crew of R/V Aegaeo, R/V Philia, and the underwater team of HCMR for their assistance during the cruises. Catherine Maillard, Michele Fichaut, and Béatrice Milosavljevic from IFREMER are thanked for providing the MATER Database. We acknowledge Marina Carreiro-Silva for helping with statistical analyses and Sara Niedenzu for microscope assistance.

# 5 Early succession of inter- and supratidal microbioerosion at rocky limestone coasts (Eastern Mediterranean Sea)

Claudia Färber[1], Nikoleta Bellou[2], André Freiwald[1], Max Wisshak[1]

[1]Senckenberg am Meer, Abteilung Meeresforschung, Südstrand 40, 26382 Wilhelmshaven, Germany
[2]Hellenic Centre for Marine Research, Institute of Oceanography, 46.7 km Athens Sounio, 19003 Anavyssos, Greece

To be submitted to Palaeogeography, Palaeoclimatology, Palaeoecology

## Abstract

Bioerosion significantly contributes to the shaping of limestone coasts. Here, we present results from a bioerosion experiment that was carried out to investigate the spatio-temporal development of coastal bioerosion in the Eastern Mediterranean Sea. Experimental substrates were mounted along four transects across the intertidal and supratidal zones at limestone coasts at the island of Rhodes (Greece). After 1 and 2 years of exposure, 15 different bioerosion traces were observed that were mainly produced by euendolithic cyanobacteria and chlorophytes. The highest ichnodiversity was recorded in the lower intertidal zone and strongly decreased towards and within the supratidal zone. In contrast to the upper intertidal and lower supratidal zone, bioerosion trace assemblages in the lower intertidal zone were already fully developed after 1 to 2 years and substrates on the wind-exposed west coast showed a higher vertical distribution of borings than substrates on the sheltered east coast. Thriving microboring assemblages of cyanobacteria and chlorophytes were observed in water-filled solution pans. This indicates sea water supply as one of the limiting factors of coastal bioerosion. While most microbioerosion traces can be assigned to their living trace maker from morphological characteristics, coastal endoliths are classified based on pigment variations, which are not provided in the fossil record. This makes the reconstruction of fossil rocky shore zonation patterns by means of microbioerosion traces difficult.

## 5.1 Introduction

Rocky coasts are extreme environments that account for over 33 % of the world's oceanic coastline today (Johnson, 1988). Due to extreme and changing conditions rocky coasts provide various microenvironmental niches that are dwelled by different benthic organisms producing characteristic zonation patterns (e.g., Stephenson and Stephenson, 1949). While in storm-wave environments at high latitudes, mechanical wave action plays a dominant role, biological and chemical erosion prevail at mid- and low latitudes (e.g., De Waele and Furlani, 2013). Bioerosion comprises external bioerosion by grazing organisms that live outside the substrate removing it in the process of seeking food, and internal micro- and macrobioerosion agents (euendoliths) that actively excavate the substrate for seeking shelter or nutrition (Golubic et al., 1975). In the fossil record, bioeroders leave characteristic traces that can

be assigned to their living trace maker by a high degree of confidence (e.g., Wilson, 2007; Wisshak, 2012). On modern rocky coasts, euendolithic cyanobacteria produce a characteristic colour zonation (e.g., Schneider, 1976; Hoffman, 1985; Radtke et al., 1996; Radtke and Golubic, 2011). Microbioerosion ichnocoenoses have been shown to be a strong tool for judging light availability and hence relative bathymetry, but the record on coastal microbioerosion traces is scarce and a supratidal ichnocoenosis has not yet been defined (see Wisshak, 2012 for a review).

In the last years many bioerosion experiments have been conducted showing that microbioerosion is subject to a distinct spatio-temporal variability. In shallow-marine tropical environments, microborers (especially cyanobacteria) can reach stable communities within 1 year of exposure (Chazottes et al., 1995; Tribollet and Golubic, 2005; Grange et al., 2015), while establishment of macrobioeroders and grazers is considered to take several years (e.g., Kiene and Hutchings, 1992, 1994; Pari et al., 2002; Tribollet and Golubic, 2005; Carreiro-Silva and McClanahan, 2012). Based on bioerosion experiments in the North Atlantic, Wisshak et al. (2010) have shown that microbioerosion follows a distinct latitudinal gradient with highest values in the tropics (Vogel et al., 1996, 2000), intermediate levels in the warm-temperate (Wisshak et al., 2010, 2011), and lowest rates in the cold-temperate high latitudes (Wisshak, 2006). In the Mediterranean Sea, ongoing eutrophication, pollution, warming, and ocean acidification are considered to magnify the intensity of bioerosion (Schönberg and Wisshak, 2014). Research on bioerosion in the Mediterranean Sea has a long tradition (Bornet and Flahault, 1888, 1889; Ercegovic, 1927, 1929, 1932), but bioerosion experiments were previously limited to the Western Mediterranean Sea (Le Campion-Alsumard, 1979). Experimental data on bioerosion in the Eastern Mediterranean Sea is comparatively new investigating bioerosion along a bathymetric transect in the Ionian Sea as well as the long-term development of macrobioerosion at Rhodes (Färber et al., 2015, subm.). Here, we present results from a bioerosion experiment that was carried out across the rocky coast of Rhodes (i) to provide an inventory of coastal microbioerosion traces, (ii) to describe the initial succession of microbioerosion traces from the intertidal to the supratidal zone, (iii) to evaluate the dependency of the zonation patterns on hydrodynamic force and exposure time, and (iv) to analyse the feasibility of microbioerosion traces for the reconstruction of fossil rocky shore zonation patterns.

## 5.2 Materials and Methods

### 5.2.1 Study sites

The bioerosion experiment was carried out at four localities at the east and west coast of the island of Rhodes, Greece: Agathi (36°10’ N, 28°6’ E), Lindos (36°6’N, 28°5’E), Kerameni (36°8’N, 27°42’E), and Monolithos (36°7’N, 27°42’E; Fig. 5.1). These were previously identified as limestone outcrops on the Neotectonic Map of Greece 1:100 000 (Lekkas et al., 1993). Rhodes is characterised by the typical Mediterranean-type of climate with a cool and rainy period from November–May, and a hot and rather dry period from May–September. In general, annual maximum sea surface temperatures (>24 °C) occur around August and minimum in February (<13 °C). Sea surface salinity values (PSU scale) vary seasonally, ranging from less than 31 to more than 39 (Poulos et al., 1997). Due to the anti-estuarine circulation of the Mediterranean Sea, in which nutrient-depleted surface water flow in, the Eastern Mediterranean Sea has an ultra-oligotrophic regime (Krom et al., 1992). Due to its restricted position from the Atlantic Ocean, the Mediterranean Sea

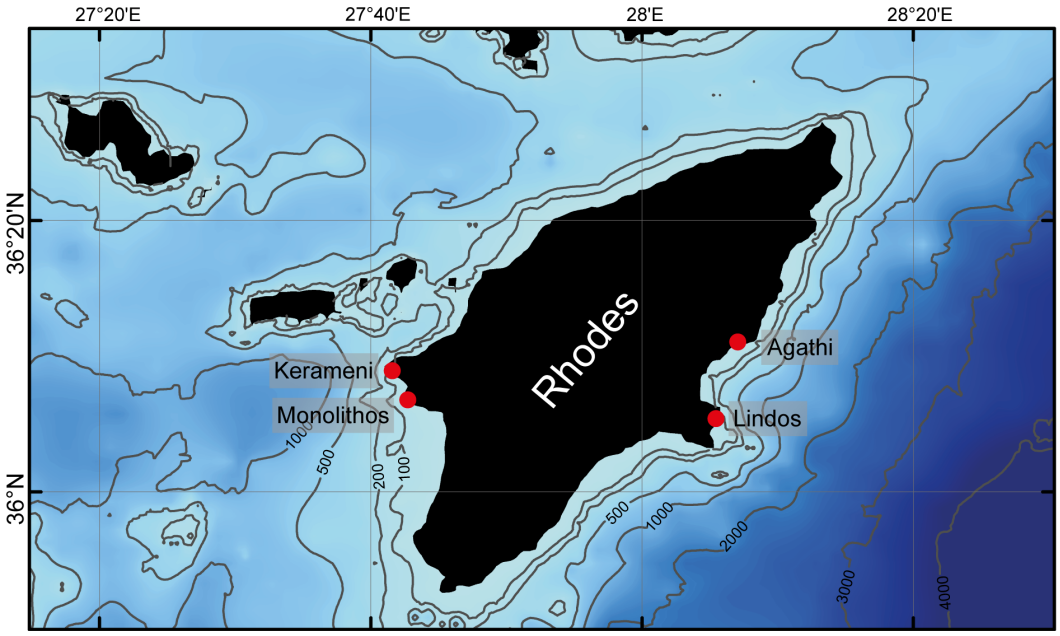


Figure 5.1 Location of the bioerosion experiment at four sites at the east and west coast of the island of Rhodes in the Eastern Mediterranean Sea. Bathymetric data were derived from the EMODnet Portal for Bathymetry (EMODnet, 2015).

is a microtidal environment with a tidal range of only about 40 cm in the South Aegean Sea (Fig. 5.2A). The wind field at Rhodes is dominated by south-west winds producing significantly higher wave exposure on the western side of the island (Fig. 5.2B).

### 5.2.2 Experimental setup

For the analysis of bioerosion traces, a set of three shells of the Mediterranean bivalve *Callista chione* and three limestone substrates, each embedded in sockets of epoxy resin, were mounted along coastal transects in the intertidal (-0.25, 0 and 0.25 m) and in the supratidal zone (0.75, 1.25, 3, 5, 7, and 10 m) below/above mean sea level. Mean sea level was defined by the upper limit of the red algae zone. In Agathi, additional substrates were mounted in four solution pans in the supratidal zone (solution pans A, B, C, and D). Above water, substrates were mounted with dowels and stainless steel screws. Under water, substrates were fixed with cable ties. For the measurement of air and water temperature, data loggers (Star-Oddi Starmon Mini, accuracy ±0.05 °C and HOBO Water Temp Pro v1/v2, accuracy ±0.2 °C; 30 min. intervals) were mounted in -0.25 m water depth and in 10 m height (except Monolithos), as well as in solution pans. Data loggers were recovered after 1 year of exposure, experimental substrates after 1 and 2 years. The third set of substrates was left for long-term observations. Due to loss of many of those substrates that were mounted with cable ties and did not survive the winter storms, at -0.25 m, substrates could be only retrieved in Lindos and Kerameni after 1 and 2 years, respectively. From solution pans, only the data logger in solution pan B could be recovered. Identification of karst features followed descriptions of Taboroši and Kázmér (2013). A photo documentation of each zone along the transects was undertaken above and under water.

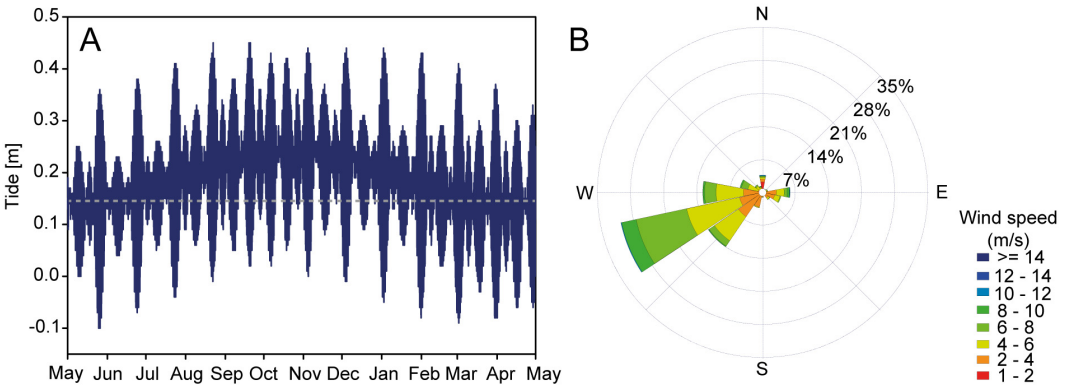


Figure 5.2 (A) Tidal interval at Rhodes from May 2013–2014 derived from WXTide 32. Dashed line marks mean sea level. (B) 30 year summary of wind data collected at Rhodes airport (Diagoras) from 1983–2012 derived from the Integrated Surface Database Light (Smith et al., 2011) and plotted with WRPlot View.

### 5.2.3 Bioerosion traces

Bioerosion traces in *Callista* shells were visualised as epoxy resin casts following the procedure described in Wisshak (2012). For the preparation of the casts, the shells were rinsed in 15 % hydrogen peroxide solution for a complete removal of fleshy epiliths, air dried, and embedded in epoxy resin (Araldit BY 158, Aradur 21) in a vacuum chamber (Struers CitoVac). From each shell, four surface samples and two cross-sections were cut with a rock saw and decalcified in 5% hydrochloric acid. Cross-sections were etched only partially for 20 seconds to prevent delicate casts from collapsing and to aid the recognition of the actual penetration depth of the endoliths in context of the shell. The epoxy resin blocks, now exhibiting the positive casts of the microborings, were sputter-coated with gold, and analysed under the scanning electron microscope (SEM, VEGA3 TESCAN). Bioerosion traces on the surface of the limestone plates were documented with a digital light microscope (Keyence VHX-1000D).

Identification of microbioerosion traces followed descriptions of Radtke and Golubic (2005), Wisshak (2006), and Wisshak et al. (2011). All bioerosion traces were ichnotaxonomically identified to ichnospecies level, or described in informal nomenclature (e.g., 'cyanobacterial etching trace'), and semiquantified in the abundance classes 'very common', 'common', 'rare', and 'very rare'.

## 5.3 Results

### 5.3.1 Water and air temperature

During the experiment, water and air temperatures were subject to distinct temporal variability (Fig. 5.3A–B, Table B1). Air temperature showed comparatively similar values across the localities with highest values observed in Agathi during August (42 °C) and lowest in Lindos during December (7 °C). Mean air temperature was 22 ± 6 °C. With respect to water temperature, distinctly higher values were recorded at the east coast than at the west coast during summer, an effect that diminished during winter. Highest water temperatures were measured in Lindos during August (30 °C), lowest values in Kerameni during December (7 °C). Mean water temperature was 21 ± 4 °C. Temperature measurements in

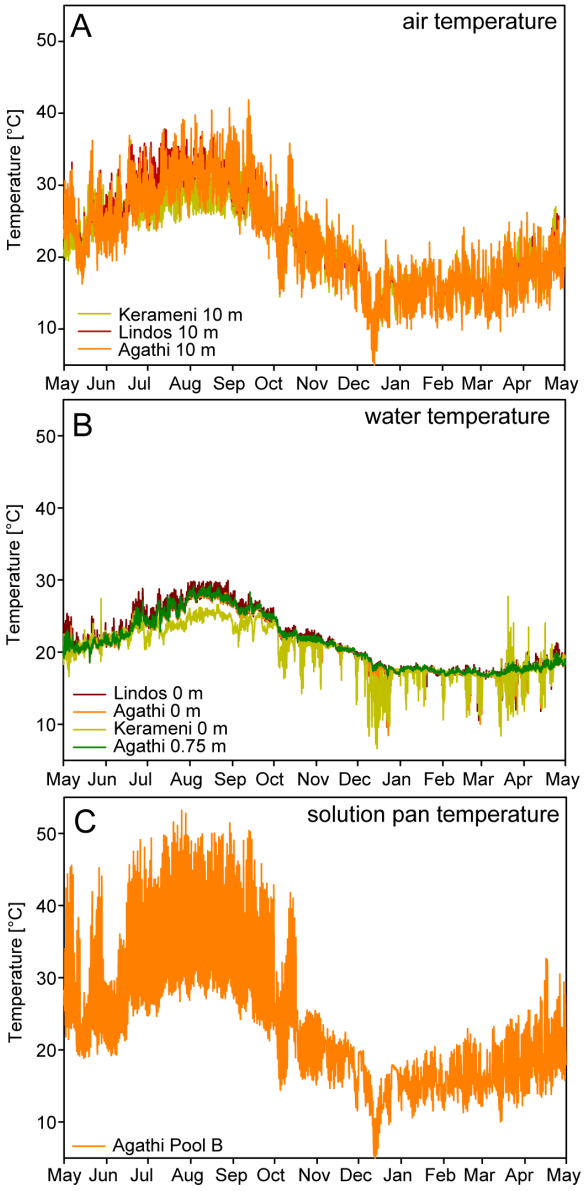


Figure 5.3 Fluctuations of (A) air temperature, and (B) water temperature in the intertidal zone at the various experimental sites and (C) in the solution pan B in Agathi during the experiment from May 2013 to May 2014.

solution pan B in Agathi revealed enormous temperature fluctuations with maximum values of 50 °C during August and minimal 2 °C in December (Fig. 5.3C).

### 5.3.2 Coastal zonation

The rocky limestone coast of Rhodes was characterised by a distinct zonation with respect to the colour of the substrate surface, encrustations, surface relief, and the associated macrofauna (Fig. 5.4–5.8). An overview about all four transects is provided in Fig. 5.9. Below mean sea level, in the lower intertidal zone, the rock surface was found densely covered

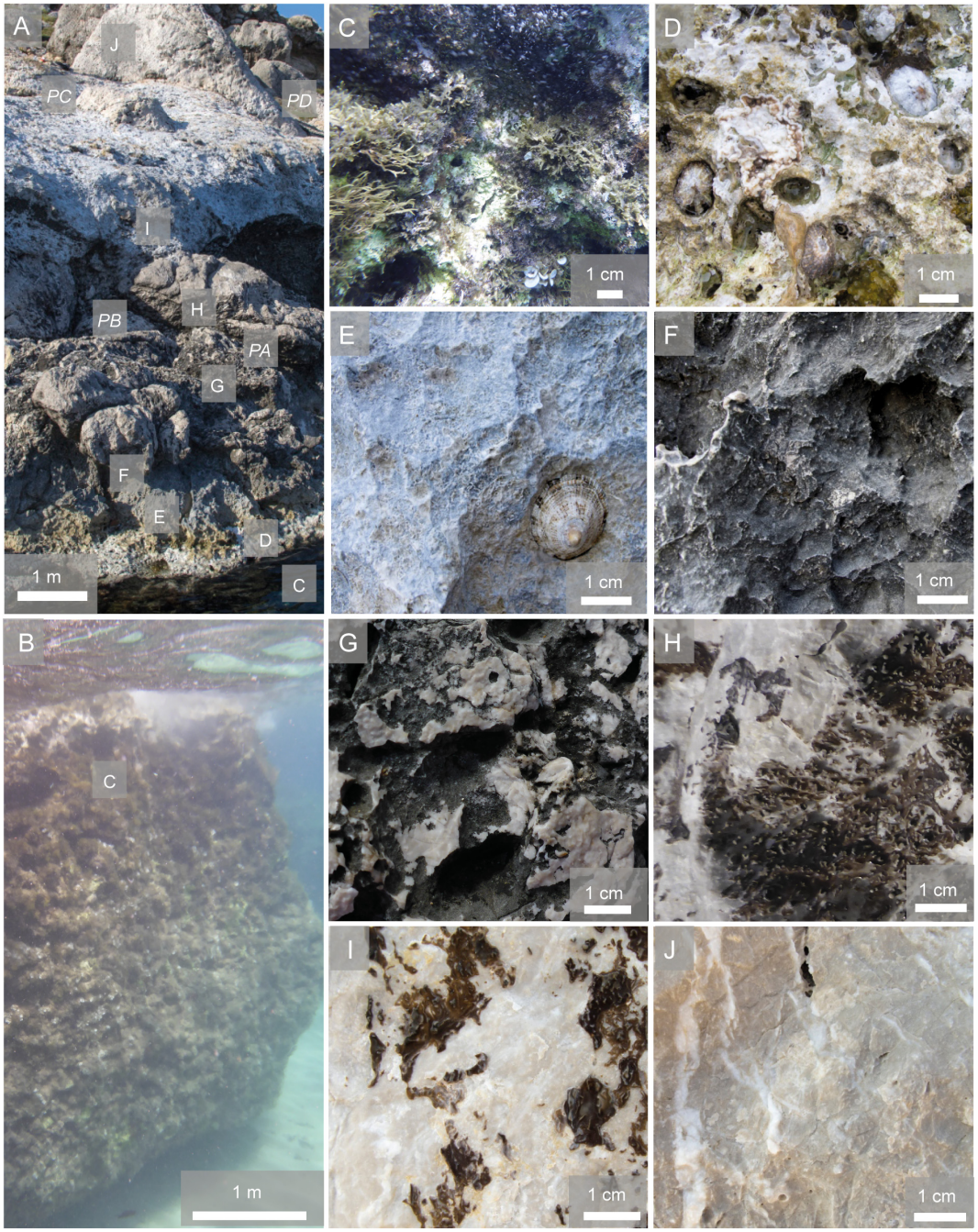


Figure 5.4 Photographs of the profile in Agathi. (A–B) Overview, (C) algae turf, (D) strongly pitted rock with white-beige encrustation, patellid gastropods and balanids, (E) slightly pitted blue-grey rock surface with few patellid gastropods, (F–G) strongly pitted rocks with black encrustations bare limestone with smooth rock surface, (H–I) brown rock varnish, (J) bare limestone. Italic signatures indicate positions of solution pans A (*PA*), B (*PB*), C (*PC*), D (*PD*).

with red and green algae turf (Fig. 5.4C, 5.6C, 5.7C, 5.8C). Mytilid bivalves, serpulid worms, balanids, boring sponges, and vermitid gastropods were very common.

Above mean sea level, in the upper intertidal zone, the rock surface was strongly pitted and covered by beige-white encrustations (Fig. 5.4D, 5.6D–E, 5.7D–E, 5.8D–E). In general, this


Figure 5.5 Photographs of solution pans in Agathi and distance to the shore line. For position of each solution pan see Fig. 5.4. (A) Solution pan A, 2 m, (B) B, 4 m, (C) C, 8 m, (D), D, 10 m.

zone showed a thickness of about 50 cm, except in Lindos where it was condensed to about 25 cm (Fig. 5.9). Patellid gastropods and barnacles were common. In Monolithos, the lower part of the upper intertidal zone was characterised by a distinct intertidal notch and karren structures in the upper part (Fig. 5.8A, E). In the lower supratidal zone, the colouration of the rock surface distinctly varied between the localities. In Agathi and Monolithos, in the lowermost part the rock surface showed a distinct blue-grey colouration (about 0.5 m in thickness), possessing a slightly pitted surface and being rarely covered by patellid gastropods (Fig. 5.4E). In Lindos, the rock surface was strongly pitted and covered by orange-brown lichens (Fig. 5.6F). Above, at all localities the rock surface was covered by black encrustations (about 0.5 m) and strongly pitted (Fig. 5.4F–G, 5.6G–H, 5.7F–G, 5.8F). Above the black zone, in Monolithos, additionally brown encrustations were observed showing only minor surface relief (about 0.75 m; Fig. 5.8G). In the upper part of the lower supratidal zone, the coverage of the rock surface decreased and became patchy. Partially brown, polished coatings were developed (Fig. 5.4H–I, 5.6H, 5.7H, 5.8H–I). In the upper supratidal zone, only bare limestone was exposed (Fig. 5.4J, 5.6I–J, 5.7I–J, 5.8J). In Kerameni distinct karren structures and solution pits occurred (Fig. 5.7I–J). Solution pans in Agathi were located in the lower supratidal (A and B) and upper supratidal zone (C and D; Fig. 5.4A). All solution pans showed a distinctly overhanging upper margin (Fig. 5.5). During deployment and recovery, solution pans A, B, and C showed filling with water, solution pan D was empty. Below the water line, solution pans showed distinct black biofilms and salt encrustation. The vegetation line distinctly varied among the localities (Fig. 5.9). In Agathi and Lindos

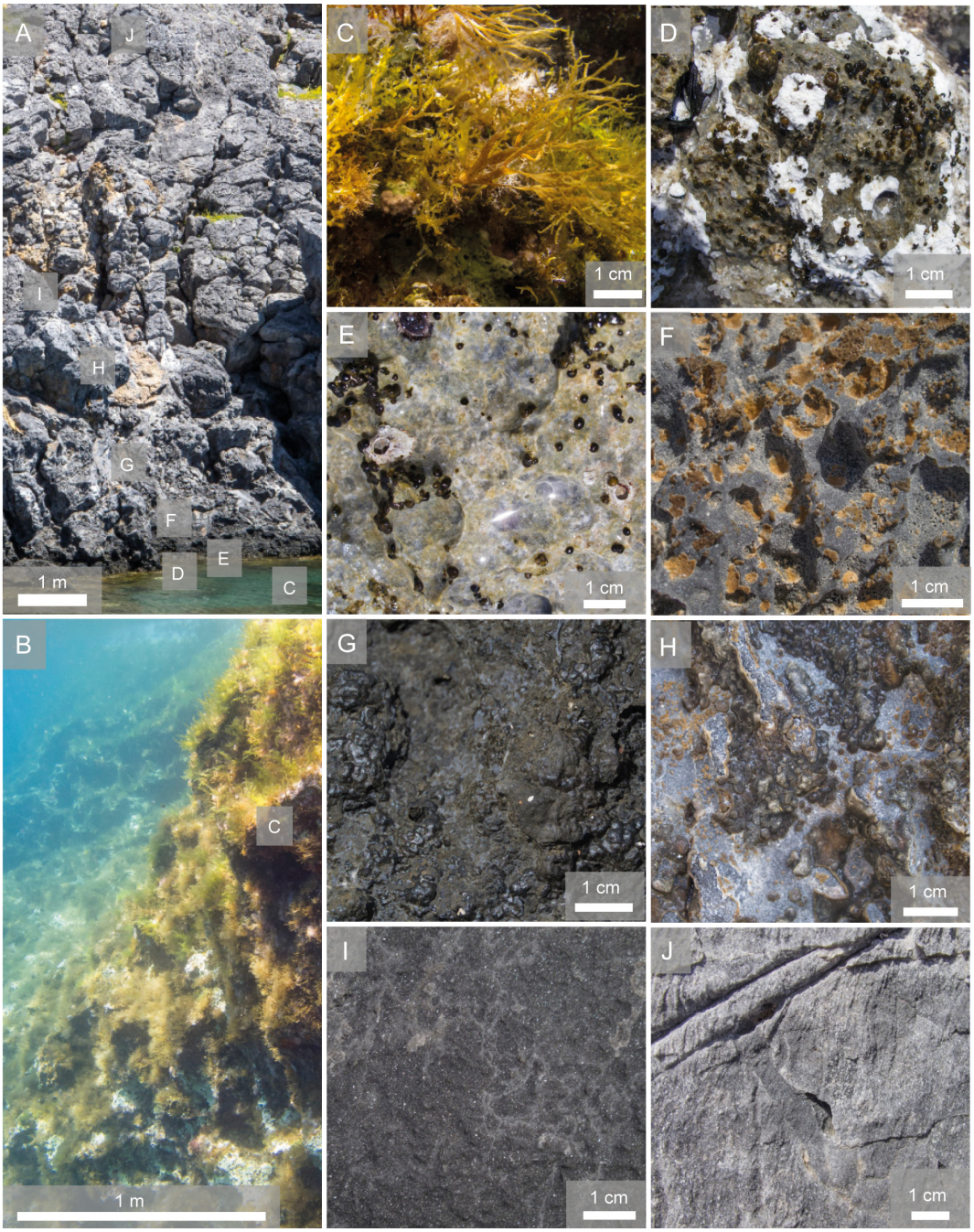


Figure 5.6 Photographs of the profile in Lindos. (A–B) Overview, (C) algae turf, (D–E) pitted rock surface with white-beige encrustations, gastropods and balanids, (F) strongly pitted rock surface with lichen encrustations, (G–H) black-brown encrustations, (I–J) bare limestone with smooth rock surface.

first vegetation was observed at about 7–8 m, in Kerameni at about 15 m, and at about 20 m in Monolithos.

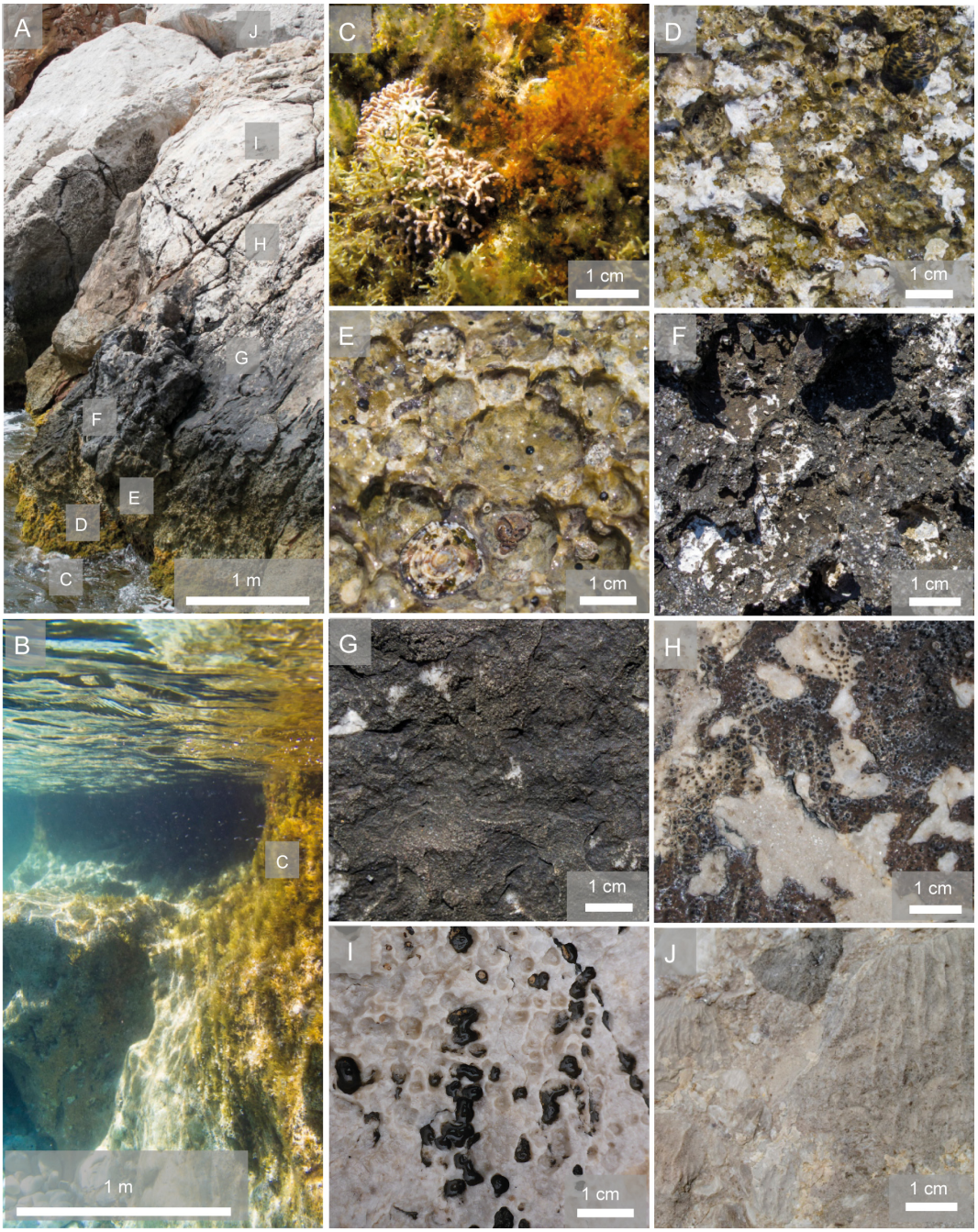


Figure 5.7 Photographs of the profile in Kerameni. (A–B) Overview, (C) algae turf, (D–E) strongly pitted surface with white-beige encrustations, gastropods and balanids, (F–G) strongly pitted surface with black encrustations, (H) brown rock varnish, (I) bare limestone with solution pits and (J) karren structures.

### 5.3.3 Bioerosion traces

In *Callista* shells and limestone plates a total of 14 different bioerosion traces were observed (Fig. 5.10). These traces were attributed to 7 cyanobacterial microborings (Fig. 5.11A–J), 1 cyanobacterial etching trace (Fig. 5.11K–L), 4 chlorophyte microborings (Fig. 5.12A–G), 1 fungal microboring (Fig. 5.12H), and 1 grazing trace (Fig. 5.12I). SEM overviews and cross-sections on the same scale are presented for the sections in Agathi, Lindos,

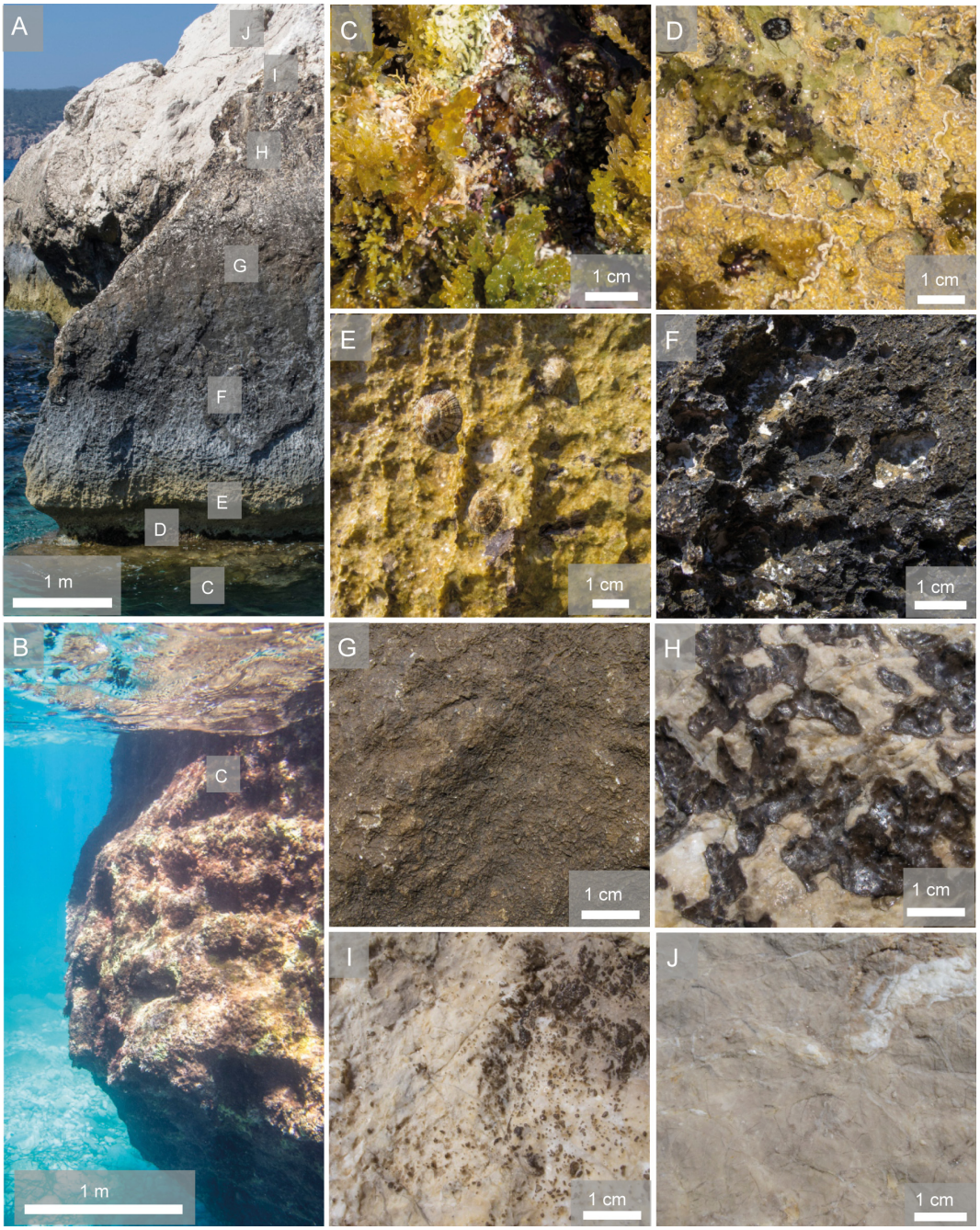


Figure 5.8 Photographs of the profile in Monolithos. (A–B) Overview, (C) algae turf, (D) strongly pitted rock surface with white-beige encrustation, gastropods and balanids, (E) strongly pitted rock surface with white-beige encrustations and karren structures, (F) strongly pitted rock surface with black encrustations, (G) slightly pitted rock surface with brown encrustations, (H–I) bare limestone with polished surface, (J) bare limestone with smooth rock surface.

Kerameni, and Monolithos after 1 and 2 years (Fig. 5.13, 5.14), as well as for solution pans in Agathi (Fig. 5.15).

The highest diversity of bioerosion traces was monitored in -0.25 and 0 m substrates showing intense bioerosion being mostly represented by the cyanobacterial microborings

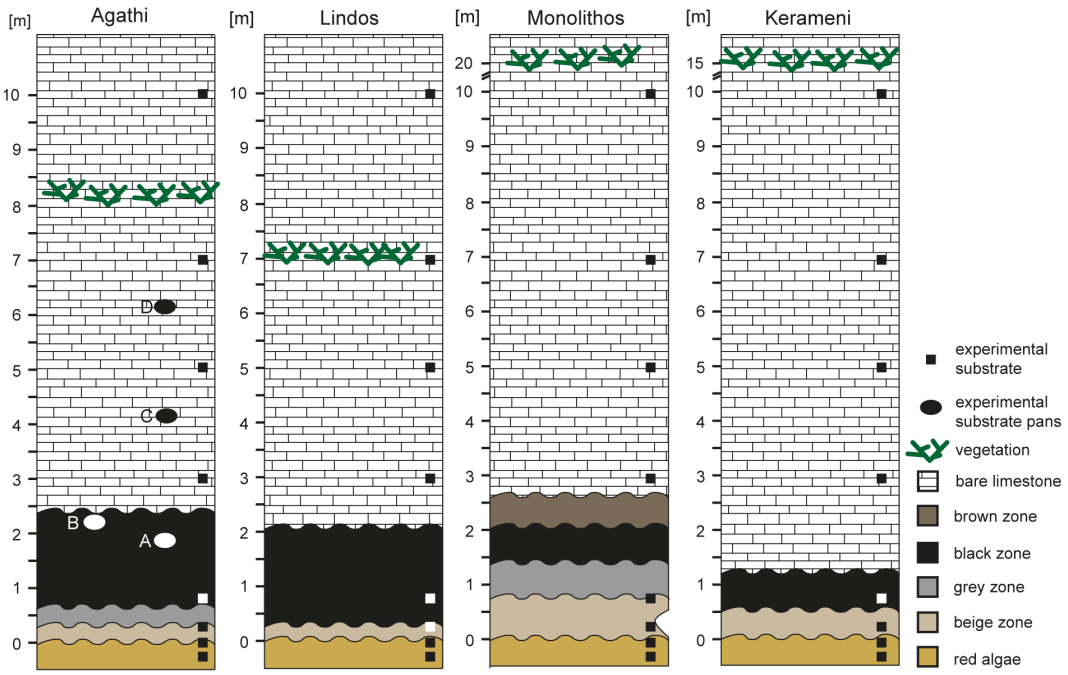


Figure 5.9 Schematic section showing zonation patterns observed at the four localities on the east (Agathi, Lindos) and west side (Monolithos, Kerameni) of Rhodes. Mean sea level corresponds with the upper limit of the red algae zone.

*Fascichnus dactylus*, *F. frutex*, and *Eurygonum nodosum*, the chlorophyte microborings *Ichnoreticulina elegans* and *Rhopalia catenata*, and the fungal microboring *Orthogonum fusiferum*. In these substrates the largest boring depth was reached (50–500 µm).

Towards the upper intertidal and supratidal zone, the ichnodiversity strongly decreased and a distinctly differed between the east and west coast. At the east coast, no bioerosion traces were observed in substrates exposed above 0 m, except in solution pans (see below). In Kerameni and Monolithos, in contrast, bioerosion traces were recorded up to 0.75 and 1.25 m, respectively, whereby a distinct increase in colonisation density from 1 to 2 years was recognised. After 1 year, in 0.25 m substrates in Kerameni solely initial bioerosion traces, mostly *R. catenata* were observed. After 2 years, in contrast, the substrates showed shallow, but consistent microborings, mostly in form of *F. dactylus* and *Planobola*. On few substrates the sea urchin grazing trace *Radulichnus inopinatus* was developed. In 0.75 m after 1 year no microborings were found, after 2 years, initial specimens of *F. frutex* occurred. In addition, cyanobacterial etching traces were observed in 0.25 and 0.75 m substrates after 1 and 2 years. Similarly in Monolithos, after 1 year only rare initial microbioerosion was developed, while after 2 years the substrates showed intense bioerosion with *E. nodosum* and *F. dactylus*. In contrast to Kerameni, after 1 year also in 0.75 and 1.25 m first borings were found. After 2 years, no borings occurred in 0.75 m and only initial bioerosion in 1.25 m. Above 1.25 m in general no bioerosion traces were monitored on vertical walls. In substrates mounted in solution pans in Agathi, a distinct suite of bioerosion traces was observed, as well as a decrease in bioerosion intensity from solution pan A to D with increasing distance and elevation from the mean sea level. In solution pan A, already after 1 year commonly the cyanobacterial and chlorophyte traces *F. dactylus* and *R. catenata* were developed. In solution pan B only few specimens of *F. dactylus* and *R. catenata* were observed after 1 year, after 2 years the substrates were shallow, but consistently bioeroded

| 1 Year | Agathi | | | | Lindos | | Kerameni | | Monolithos | | | |
|---|---|---|---|---|---|---|---|---|---|---|---|---|
| | 0 m | Pan A | Pan B | Pan C | -0.25 m | 0 m | 0 m | 0.25 m | 0 m | 0.25 m | 0.75 m | 1.25 m |
| Cyanobacterial microborings | | | | | | | | | | | | |
| *Eurygonum nodosum* Schmidt, 1992 | | | | | | -- | - | | | | | |
| *Fascichnus dactylus* (Radtke, 1991) | ++ | + | -- | -- | ++ | + | + | - | ++ | - | - | -- |
| *Fascichnus frutex* (Radtke, 1991) | ++ | | | | - | + | + | -- | + | | | |
| *Fascichnus rogus* (Radtke, 1991) | | | | | | | -- | -- | | | | |
| *Planobola* isp. | | | | | | + | - | | | - | | |
| *Planobola macrogata* Schmidt, 1992 | | | | | - | | | | | | | |
| *Scolecia filosa* Radtke, 1991 | | | | | | | | | | | | |
| Etching trace | | | | | | | | | | | | |
| 'Cyanobacterial etching trace' | | | | | | | | - | | | | |
| Chlorophyte microborings | | | | | | | | | | | | |
| *Eurygonum pennaforme* Wisshak et al. 2005 | | | - | | | | | -- | | | | |
| *Fascichnus grandis* (Radtke, 1991) | | | | | -- | | | | | | | |
| *Ichnoreticulina elegans* (Radtke, 1991) | | | | | ++ | | | | | | | |
| *Rhopalia catenata* Radtke, 1991 | | + | | | | ++ | ++ | + | - | - | | |
| Fungal microborings | | | | | | | | | | | | |
| *Orthogonum fusiferum* Radtke, 1991 | -- | | | | -- | -- | -- | | + | | | |
| Grazing trace | | | | | | | | | | | | |
| *Radulichnus inopinatus* Voigt, 1977* | | | | | | | | | | + | | |

| 2nd Year | Agathi | | | | Lindos | | Kerameni | | | Monolithos | | |
|---|---|---|---|---|---|---|---|---|---|---|---|---|
| | 0 m | Pan A | Pan B | Pan C | 0 m | -0.25 m | 0 m | 0.25 m | 0.75 m | 0 m | 0.25 m | 1.25 m |
| Cyanobacterial microborings | | | | | | | | | | | | |
| *Eurygonum nodosum* Schmidt, 1992 | | | | | | + | - | | | + | + | |
| *Fascichnus dactylus* (Radtke, 1991) | + | -- | | | -- | + | + | + | | + | + | -- |
| *Fascichnus frutex* (Radtke, 1991) | ++ | -- | | -- | + | ++ | - | | -- | ++ | | |
| *Fascichnus rogus* (Radtke, 1991) | | | | | | | | | | | | |
| *Planobola* isp. | -- | -- | | | - | | - | + | | | | |
| *Planobola macrogata* Schmidt, 1992 | | | | | | | | | | | | |
| *Scolecia filosa* Radtke, 1991 | -- | -- | | | | + | | -- | | + | | |
| Etching trace | | | | | | | | | | | | |
| 'Cyanobacterial etching trace' | | | | | | | | | - | | | |
| Chlorophyte microborings | | | | | | | | | | | | |
| *Eurygonum pennaforme* Wisshak et al. 2005 | | | | | | | | | | | | |
| *Fascichnus grandis* (Radtke, 1991) | | | | | | | | | | | | |
| *Ichnoreticulina elegans* (Radtke, 1991) | | | | | - | | | | | - | | |
| *Rhopalia catenata* Radtke, 1991 | + | + | + | | ++ | | ++ | + | | - | | |
| Fungal microborings | | | | | | | | | | | | |
| *Orthogonum fusiferum* Radtke, 1991 | -- | | | | - | + | - | | | + | | |
| Grazing trace | | | | | | | | | | | | |
| *Radulichnus inopinatus* Voigt, 1977* | | | | | | | | + | | | | |

*observed on limestone substrates

++ very common
+ common
- rare
-- very rare

Figure 5.10 The inventory of bioerosion traces for the various sites and water depths categorised by trace types for 1 and 2 years of exposure. Substrates that did not contain any bioerosion traces are not listed.

by *R. catenata*. In solution pan C only very few galleries of *F. dactylus* occurred. In solution pan D no bioerosion traces were observed. The boring depth in all solution pans was very low (0–10 µm).

## 5.4 Discussion

### 5.4.1 Succession of microbioerosion across the rocky coast

The rocky coast of Rhodes shows a distinct variability in rock surface colouration and relief, which is contributed by different types of bioeroding organisms (Schneider, 1976). While in general, the colouration and relief of the rock surface observed at Rhodes are in good agreement with corresponding studies around the globe (e.g., Schneider, 1976; Hoffman, 1999; Radtke and Golubic, 2011), our experiment demonstrates that the development of microbioerosion traces at limestone coasts is subject to a high spatio-temporal variability also on a local scale. During the experiment, the lowermost substrates were mounted in the lower intertidal zone regularly wetted during high tide and vegetated by algae turf. This zone corresponds to the lower intertidal subzone of Hoffman (1985) and the “notch”

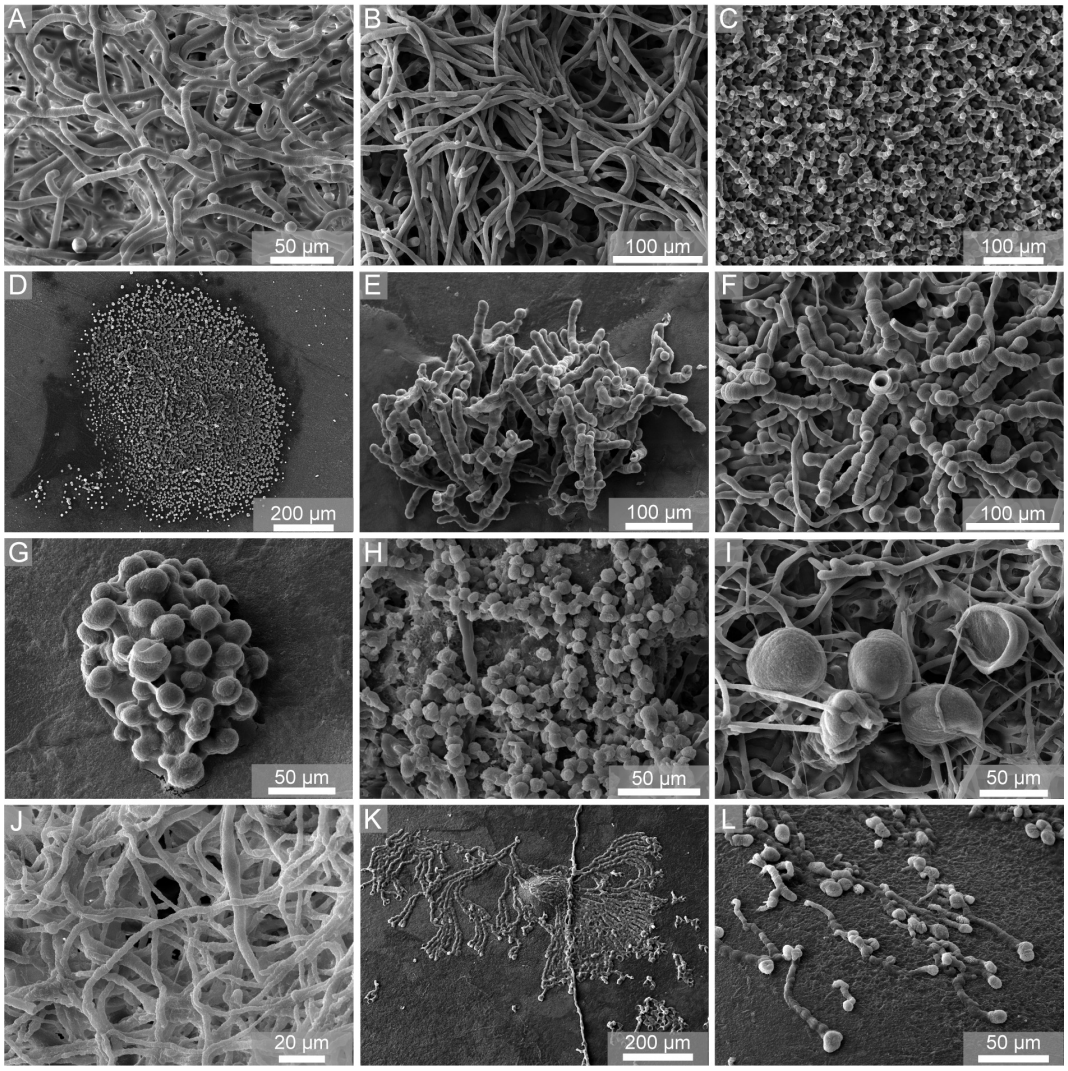


Figure 5.11 SEM images of epoxy-resin casts taken from *Callista* shells showing cyanobacterial microborings (A–J) and cyanobacterial etching traces (K–L). (A) *Eurygonum nodosum*, 0.25 m, Monolithos, 2 years, (B) *Fascichnus dactylus*, elongate appearance, 0 m, Agathi, 1 year, (C) *F. dactylus*, short appearance, 0 m, Kerameni, 1 year, (D) initial colony of *F. dactylus*, 0.75 m, Monolithos, 1 year, (E) initial colony of *F. dactylus*, 0.25 m, Kerameni, 2 year, (F) *Fascichnus frutex*, 0 m, 1 year, Agathi, (G) *Fascichnus rogus*, 0.25 m, Kerameni, 1 year, (H) *Planobola* isp., solution pan A, Agathi, 2 years, (I) *Planobola macrogata*, -0.25 m, Lindos, 1 year, (J) *Scolecia filosa*, 0 m, Monolithos, 2 years, (K–L) 'Cyanobacterial etching trace', 0.25 m, Kerameni, 1 year.

of Schneider (1976). In the lower intertidal zone, we monitored the highest ichnodiversity and a dominance of the cyanobacterial traces *F. dactylus*, *F. frutex*, *E. nodosum*, *S. filosa*, *I. elegans*, and the chlorophyte trace *R. catenata*. These traces mainly correspond to the endolithic cyanobacteria *Hyella caespitosa*, *Plectonema terebrans*, and *Mastigocoleus testarum* and chlorophytes *Ostreobium quekettii* and *Phaeophila dendroides*, which were observed by Le Campion-Alsumard (1979) in the lower mediolittoral around Marseilles and by Hoffman (1985) at Bermuda. At the Bahamas, Radtke et al. (1996) documented a dominance of rhodophyte algae and the chlorophyte *O. quekettii*, being likely an effect of shaded conditions in the notch. The comparison of 1 and 2 year bioerosion traces did not show any significant increase in the abundance of microborings, indicating stable communities. This is in good agreement with other studies on subtidal bioerosion, where in shallow

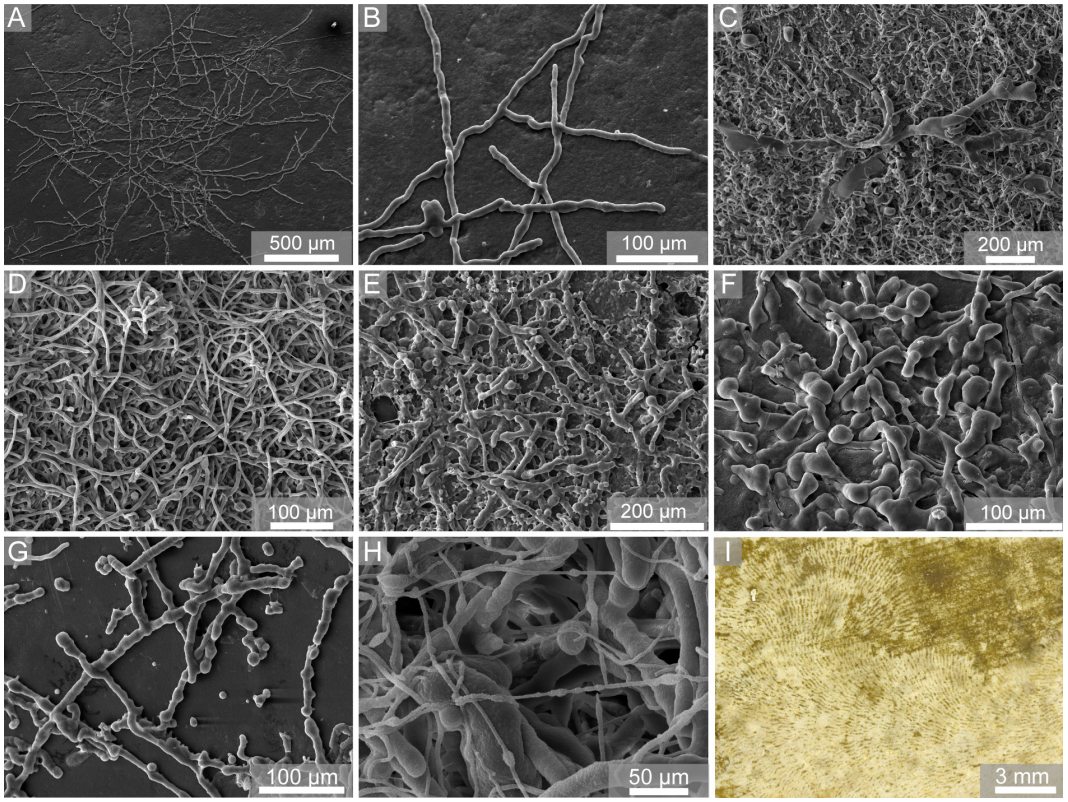


Figure 5.12 SEM images of epoxy-resin casts taken from *Callista* shells and light-microscopic image taken from a limestone plate showing chlorophyte (A–G) and fungal microborings (H) and a grazing trace (I). (A–B) *Eurygonum pennaforme*, solution pan B, Agathi, 1 year, (C) *Fascichnus grandis*, -0.25 m, Lindos, 1 year, (D) *Ichnoreticulina elegans*, -0.25 m, Lindos, 1 year, (E) *Rhopalia catenata*, 0 m, Lindos, 1 year, (F) *Rhopalia catenata*, solution pan A, Agathi, 2 years, (G) initial galleries of *R. catenata*, 0.25 m, Kerameni, 1 year, (H) *Orthogonum fusiferum*, -0.25 m, Kerameni, 2 years, (I) *Radulichnus inopinatus*, 0.25 m, Monolithos, 1 year.

ranges, cyanobacterial and chlorophyte bioerosion was stable after 1 year of exposure (e.g., Chazottes et al., 1995; Tribollet and Golubic, 2005), which we ascribe to constant water supply and comparatively short exposure to aerial conditions.

In the upper intertidal zone, the rock surface was covered by beige-white encrustations, comparable to the upper intertidal subzone of Hoffman (1985) and the "white" and "yellow brown zone" of Schneider (1976). At some parts of our profiles, a separation into a white and a beige zone would have been also feasible, but this boundary was not consistently developed and often difficult to pursue. In the upper intertidal zone, bioerosion traces were only observed at west side localities. Common bioerosion traces were *F. dactylus*, *E. nodosum*, *Planobola* isp., and *R. catenata*, which correspond to the cyanobacteria *H. caespitosa*, *Solentia foveolarum*, *M. testarum*, and *P. terebrans*, which were found by Schneider (1976), Le Campion-Alsumard (1979), Hoffman (1985), and Radtke et al. (1996). In contrast to the lower intertidal zone, the upper intertidal zone is exposed to aerial conditions for longer times during sea level low stand, and is thus stronger affected by evaporation processes, but receives spray or moist by larger waves (Hoffman, 1985; Radtke and Golubic, 2011). The dominance of bioerosion traces in west side substrates is likely an effect of more frequent wetting due to higher hydrodynamic force on the wind exposed side supporting larvae settlement and growth higher above mean sea level. However, also on the east side the colouration of rock surfaces indicates endolithic colonisation and we expect substrates to

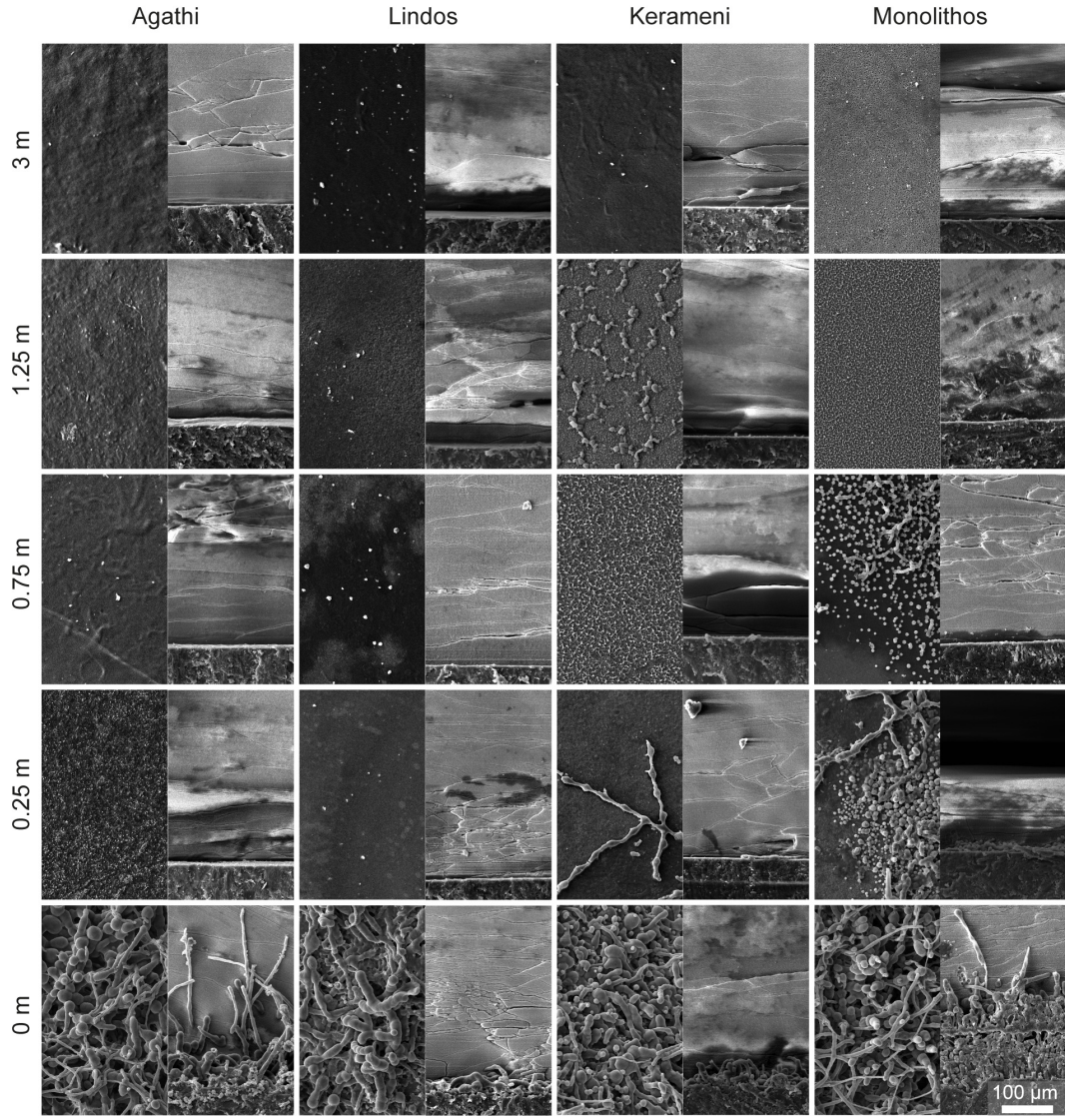


Figure 5.13 The development of bioerosion traces in shells of the bivalve *Callista chione* at the various depth stations in Agathi, Lindos, Kerameni, and Monolithos after 1 year of exposure. In general, no bioerosion traces were above 3 m during the experiment and are thus not displayed here.

be settled with ongoing exposure. The rock surface of the upper intertidal subzone shows a characteristic surface relief of karren structures and intertidal notches that indicates extensive grazing activity. The synergistic effect of grazing on euendoliths is an important process for the erosion of rocky coasts, because without grazing bioerosion would be halted or at least slowed down a few millimetres within the rock where light reaches the compensation level (Radtke et al., 1996). In our experimental substrates only few grazing traces were observed. However, we assume that with ongoing exposure grazing traces and macroborings will be found. This has been similarly documented in coral reef systems, where grazers and macroborers generally need about 2–3 years to develop (Tribollet and Golubic, 2005).
In the lower supratidal zone, the appearance of the rock surface distinctly varied between the localities. In general, however, the black zone occurring at all localities corresponds to the upper limit of the lower supratidal subzone of Hoffman (1985) and the dark-brown zone

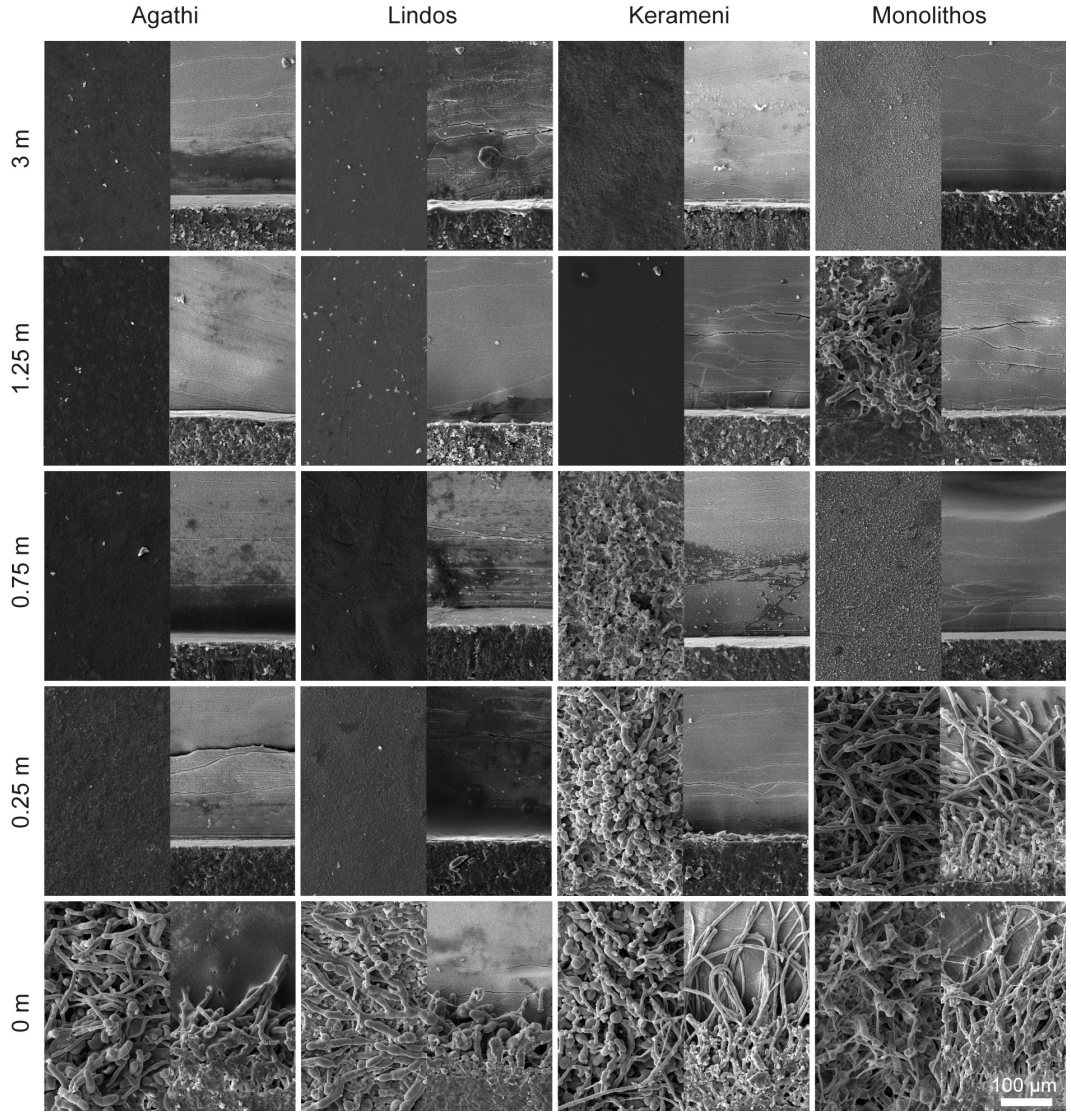


Figure 5.14 The development of bioerosion traces in shells of the bivalve *Callista chione* at the various depth stations in Agathi, Lindos, Kerameni, and Monolithos after 2 year of exposure. In general, no bioerosion traces were found above 3 m during the experiment and are thus not displayed here.

of Schneider (1976). The lower supratidal zone is only periodically wetted by sea spray or higher waves so that the greyish colour could be an effect of salt weathering or salt crystallisation. The rock surface in the lower supratidal subzone shows a distinct surface relief, but is less pronounced as in the upper intertidal subzone, solely produced by microborers, while grazers are missing. Partly smooth surfaces are developed that can originate from the presence of very thin and nearly stationary films of water isolating the rock from erosive agents or be a result of polishing by wind-blown sand grains (Taboroši and Kázmér, 2013). In the lower supratidal subzone, we only found sporadically specimens of *F. dactylus* and *F. frutex*. Studies on endolithic biotaxa, in contrast, revealed a distinct change in the occurrence of endolithic biotaxa with a dominance of the cyanobacteria *Hormathonema violaceo-nigrum*, *H. luteo-brunneum*, *S. foveolarum*, *H. balani*, *H. caespitosa*, *Scytonema endolithicum*, and *Kyrtuthrix dalmatica* (Schneider, 1976; Le Campion-Alsumard, 1979;

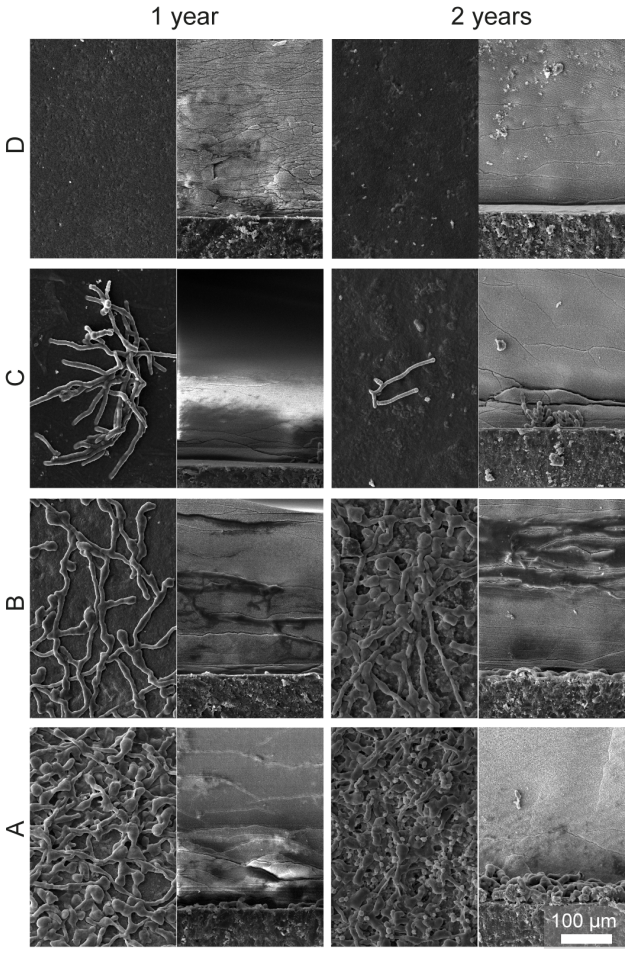


Figure 5.15 The development of bioerosion traces in shells of the bivalve *Callista chione* deployed in solution pans in Agathi after 1 and 2 years of exposure.

Hoffman, 1985; Radtke et al., 1996; Radtke and Golubic, 2011). According to Radtke and Golubic (2005, 2011), however, a differentiation of traces produced by cyanobacteria such as *Solentia* (including *Hormathonema*) and *Hyella* based on morphological differences is difficult. The differentiation of these cyanobacteria is mostly based on colour pigments that are incorporated in the gelatinous EPS-envelopes to absorb UV radiation and protect the cyanobacteria from intense solar radiation (Ehling-Schulz and Scherer, 1999; Castenholz and Garcia-Pichel, 2012). Traces produced by these endoliths fall into the range of the ichnogenus *Fascichnus* (Radtke and Golubic, 2005, 2011). Also for *K. dalmatica* no corresponding bioerosion trace has been identified yet, but it has been similarly been reported to produce *Fascichnus*-like traces (Wisshak et al., 2011). The low abundance of microborings in our substrates is due to the irregular wetting by wave splash and larger waves at high tide. Salt crystallisation indicates evaporative conditions and an extreme environment for settling organisms. Nonetheless, colour zonation on the rock surface indicated endolithic settlement and we assume that with ongoing exposure the abundance of microborings will increase. This shows that endolithic settlement is strongly connected to regular water supply and is much slower under aerial conditions. This becomes clear in solution pans, where sea water is retained and the abundance of microborings increased. Here, however, a distinct difference in bioerosion trace assemblages in solution pans close to the shore and

further afield occurred: in solution pans that show a short distance to the shoreline, mostly chlorophyte traces were observed, while in solution pan C, similarly to vertical walls, solely *F. dactylus* were documented. This suggests that endolithic cyanobacteria show a much higher tolerance against temperature and salinity fluctuations (i.e., evaporation) than chlorophytes. Studies on euendoliths in hypersaline settings are scarce, but the observed microborings *Planopola* isp., *F. dactylus*, *S. filosa*, and *R. catenata* are in good agreement with the endolithic cyanobacteria *Cyanosaccus atticus*, *H. caespitosa* var. *arbuscula*, *H. inconstans*, *H. reptans*, and *Leptolyngbya terebrans* (former *P. terebrans*) as well as the endolithic chlorophytes *Gomontia polyriza*, *O. quekettii*, and *P. dendroides* that were described in a saline lagoon in Milos, Greece (Pantazidou et al., 2006).

### 5.4.2 Palaeoenvironmental implications

Recent bioerosion traces provide important information for the reconstruction of palaeoenvironmental conditions. Especially microbioerosion ichnocoenoses have been shown to be a strong tool for judging light availability and hence relative bathymetry (see Wisshak, 2012 for a review). According to the scheme of index ichnocoenoses developed for the reconstruction of light conditions and relative bathymetry (Glaub, 1994; Glaub et al., 2001; Vogel et al., 1995, 2008; Wisshak, 2012), subtidal ranges are typically dominated by *F. dactylus* and *R. catenata* and intertidal ranges by *F. acinosus* and *F. dactylus*, while for the supratidal range no index ichnocoenoses has yet been described. In general, bioerosion traces observed in -0.25 and 0 m are in good agreement with the shallow subtidal ichnocoenosis. In substrates mounted in 0 and 0.25 m in the intertidal zone, *F. dactylus* was common, but no specimens of *F. acinosus* occurred. However, in the Mediterranean Sea, *H. balani* as trace maker of *F. acinosus* has been reported to show a high morphological variability under different environmental conditions (Le Campion-Alsumard and Golubic, 1985). Specimens of *F. rogus*, whose trace maker *H. racemus* typically occurs in deeper waters (0.5–5 m; Al-Thukair et al., 1994), could represent traces of *H. balani* in its globular morphology (status "gloecapsoides"). In the supratidal zone during our experiment solely *F. dactylus* traces have been observed, which might be produced by several cyanobacterial species within the genera *Hyella* or *Solentia*, but cannot be deciphered based on morphological characteristics alone (see above). According to this, a reconstruction of the coastal zonation based on microbioerosion trace assemblages seems difficult. Nevertheless, our results show that also the absence of certain species helps to understand bathymetric conditions. For instance, the cyanobacterial boring *E. nodosum* was only monitored in the lower intertidal zone indicating a preference for fully marine conditions.

## 5.5 Conclusions and outlook

In conclusion, the experiment shows that microbioerosion in the inter- and supratidal zone is mostly limited by sea water supply. Pace of microborer settlement in the upper intertidal and particularly in the supratidal zone was found surprisingly slow, with a complete lack of bioerosion traces above 0.75 m after 2 years of exposure. This implies that the mature bioerosion traces present in these zones take many years to develop. For that reason a complete set of our experimental substrates remained in place, to be recovered and analysed in a couple of years' time, allowing better insight into the sequence and pace of microborer succession in the intertidal and supratidal zone. While most microbioerosion traces can be assigned to their living trace maker from morphological characteristics and are thus useful

indicators for palaeoenvironmental conditions, coastal endoliths are classified based on pigment variations, which are not provided in the fossil record. This makes the reconstruction of fossil rocky shore zonation patterns by means of microbioerosion trace assemblages difficult.

## Acknowledgements

We thank Nicol Mahnken and Marco Persicke (Senckenberg am Meer, Wilhelmshaven) for technical and logistic support. We are indebted to Neele Meyer for student assistance during lab and fieldwork, and Jürgen Titschack (MARUM, Bremen) for pointing out potential study sites. This study was funded by the Deutsche Forschungsgemeinschaft (Wi 3754/2-1).

# 6 Long-term development of macrobioerosion in the Mediterranean Sea assessed by micro-computed tomography

Claudia Färber[1], Jürgen Titschack[1,2], Christine H. L. Schönberg[3,4], Karsten Ehrig[5], Karin Boos[2], Daniel Baum[6], Bernhard Illerhaus[5], Ulla Asgaard[7], Richard G. Bromley[7], André Freiwald[1], Max Wisshak[1]

[1]Senckenberg am Meer, Abteilung Meeresforschung, Südstrand 40, 26382 Wilhelmshaven, Germany
[2]MARUM, Center for Marine Environmental Sciences, Leobener Straße, 28359 Bremen, Germany
[3]Oceans Institute, The University of Western Australia, Crawley, WA 6009, Australia
[4]Western Australian Museum, Welshpool, WA 6106, Australia
[5]BAM, Bundesanstalt für Materialforschung und -prüfung, Unter den Eichen 87, 12205 Berlin, Germany
[6]ZIB, Zuse Institute Berlin, Takustraße 7, 14195 Berlin, Germany
[7]Rønnevej 97, DK-3720 Aakirkeby, Denmark

Submitted to Biogeosciences[1]

## Abstract

Biological erosion is a key process for the recycling of carbonate and the formation of calcareous sediments in the oceans. Experimental studies showed that bioerosion is subject to distinct temporal variability, but previous long-term studies were restricted to tropical waters. Here, we present results from a 14 year bioerosion experiment that was carried out along the rocky limestone coast of the island of Rhodes, Greece, in the Eastern Mediterranean Sea, in order to monitor the pace at which bioerosion affects carbonate substrate and the sequence of colonisation by bioeroding organisms. Internal macrobioerosion was visualised and quantified by micro-computed tomography and computer-algorithm based segmentation procedures. Analysis of internal macrobioerosion traces revealed a dominance of bioeroding sponges producing eight types of characteristic *Entobia* cavity networks, which were matched to five different clionaid sponges by spicule identification in extracted tissue. The morphology of the entobians strongly varied depending on the species of the producing sponge, its ontogenetic stage, available space, and competition by other bioeroders. An early community developed during the first 5 years of exposure with initially very low macrobioerosion rates and was followed by an intermediate stage when sponges formed large and more diverse entobians and bioerosion rates increased. After 14 years, 30 % of the block volumes were occupied by boring sponges, yielding maximum bioerosion rates of 900 g $m^{-2}$ $yr^{-1}$. A high spatial variability in macrobioerosion prohibited clear conclusions about the onset of macrobioerosion equilibrium conditions. This highlights the necessity of even longer experimental exposures and higher replication at various factor levels in order to better understand and quantify temporal patterns of macrobioerosion in marine carbonate environments.

1 Text, figures, and tables were reformatted to the layout of this thesis. There are minor orthographic changes in the text.

## 6.1 Introduction

Bioerosion, the erosion of hard substrate by living organisms (Neumann, 1966), generally comprises (i) internal microbioerosion by boring cyanobacteria, algae, and fungi, (ii) internal macrobioerosion by boring sponges, worms, and bivalves, and (iii) external bioerosion by grazing gastropods, echinoids, and fish (e.g., Glynn, 1997; Tribollet et al., 2011). Experimental studies showed that the succession of bioerosion agents is subject to distinct temporal variability: Under favourable conditions, microborers can reach stable communities within 1 year of exposure (Tribollet and Golubic, 2005; Grange et al., 2015), whereas establishment of macrobioeroders may take several years to form mature communities (e.g., Kiene and Hutchings, 1992, 1994; Pari et al., 1998, 2002; Chazottes et al., 2002; Tribollet and Golubic, 2005). Most bioerosion experiments were conducted over a period of only 1–2 years, giving a detailed picture on microbioerosion in different geographical settings (e.g., Kiene, 1988; Vogel et al., 1996, 2000; Wisshak, 2006; Wisshak et al., 2010, 2011). Experimental studies on the succession of macrobioeroders were previously limited to tropical coral reef systems and commonly lasted about 4–8 years (Kiene and Hutchings, 1992, 1994; Pari et al., 2002; Carreiro-Silva and McClanahan, 2012). The longest experiments have been conducted over 12 years at the Great Barrier Reef (Kiene and Hutchings, 1992) and 13 years at Jamaica (Scott et al., 1988). To date, no experimental data on long-term bioerosion from non-tropical settings are available, but would constitute important information for evaluating global patterns of bioerosion and for modelling future impacts of bioerosion. This is particularly relevant since bioerosion is considered to increase with ongoing ocean acidification (Tribollet et al., 2009), a trend that is especially true for bioeroding sponges (e.g., Wisshak et al., 2012, 2013, 2014b; Fang et al., 2013), with potentially detrimental effects on carbonate-dominated ecosystems (Kennedy et al., 2013).

In the Mediterranean Sea, bioerosion affects sensitive ecosystems such as limestone coasts, deposits of coralline algae, and cold-water coral reefs, as well as molluscs in aquaculture, submerged man-made materials, and artefacts (see Schönberg and Wisshak, 2014 for a review). Experimental data on Mediterranean bioerosion are only available in form of short-term observations on microendoliths (Le Campion-Alsumard, 1979; Färber et al., 2015). Here, we present results from a long-term bioerosion experiment that was carried out over 14 years along the limestone rocky shore of Rhodes (Greece) in order to analyse the succession of bioeroders in the Eastern Mediterranean Sea. A preliminary summary on macroscopic observations during the first 6 years was provided by Bromley et al. (1990). For the visualisation of internal macrobioerosion traces and quantification of macrobioerosion rates, micro-computed tomographic analysis was chosen as a non-destructive approach. Computed tomography is increasingly used to visualise bioerosion traces in three dimensions (Beuck et al., 2007, 2008; Bromley et al., 2008; Schönberg and Shields, 2008), but quantitative approaches are still scarce and comparatively new (Crook et al., 2013; Silbiger et al., 2014; DeCarlo et al., 2015). Aim of this paper is (i) to introduce a novel approach to visualise and quantify internal bioerosion using computer-algorithm based segmentation procedures, (ii) to provide an inventory of macrobioerosion traces, (iii) to identify trace making boring sponges through spicule analysis, and (iv) to assess the long-term development of bioerosion rates and ontogenetic development of sponge borings in terms of a possible onset of macrobioerosion equilibrium conditions.

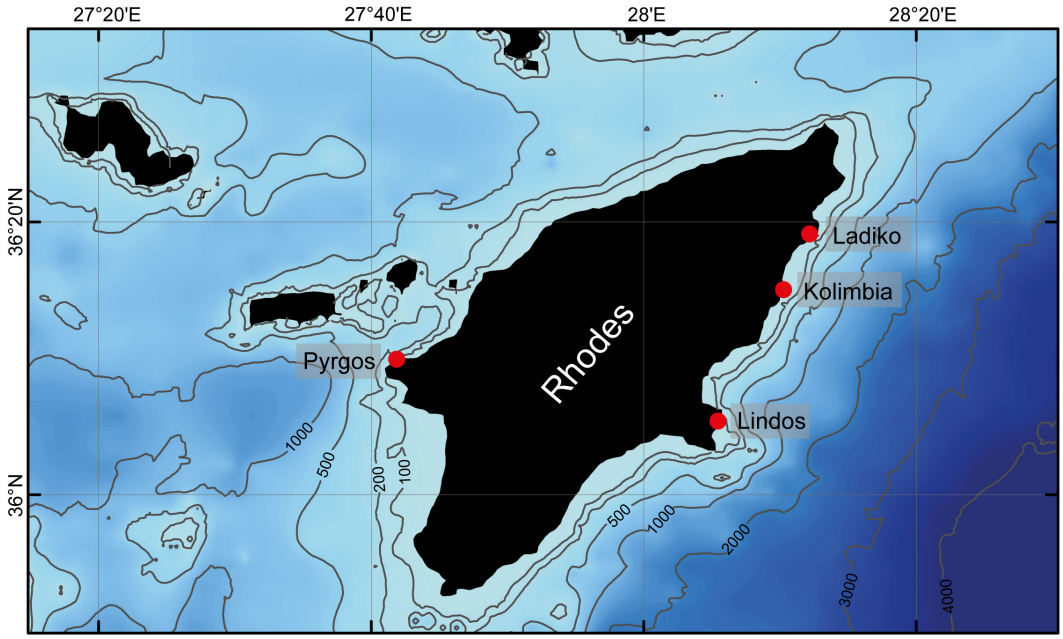


Figure 6.1 Location of the long-term experiment at Rhodes, Greece, in the Eastern Mediterranean Sea. Between 1982 and 1996, experimental blocks were deployed at four sites on the east and west coast of Rhodes in 3 to 17 m water depth. Bathymetric data were derived from the EMODnet Portal for Bathymetry (EMODnet, 2015).

## 6.2 Material and Methods

### 6.2.1 Experimental design

Experimental blocks were deployed in the vicinity of four limestone cliffs at the east and west coast of the island of Rhodes, Greece (Fig. 6.1): (i) at the south and east edge of Ladiko Bay (36°19'5"N, 28°12'17"E; 36°19'10"N, 28°12'29"E), (ii) south of Kolimbia (36°14'26"N, 28°9'44"E; 36°14'21"N, 28°9'47"E), (iii) north of St. Paul's Bay near Lindos (36°5'17"N, 28°5'20"E), and (iv) in Pyrgos (36°10'10"N, 27°43'55"E). All localities were characterised by limestone rock ground or boulder fields, and were free from local pollution. Annual monitoring in October showed no indication of interference of the experiment by human activities. The blocks were of pure calcium carbonate (marble and limestone), and respective lithology was confirmed by petrographic thin sections. Between 1982 and 1989, 46 blocks were placed directly on the sea floor, in water depths between 3 and 17 m, and until 1996 each year some blocks were retrieved, all by skin diving and using floatation devices. Recovered blocks were rinsed in fresh water and soft epiliths were removed. The blocks were subsequently photographed and dried. From all retrieved blocks, for the present approach twelve were chosen from different depths (3 to 17 m) and exposure times (1 to 14 years), all with a surface area of 11 x 11 cm or more. Most of these showed no evidence for having been dislocated during the experiment, however, some blocks had slightly moved and for some the information about recovery date and/or water depth was incomplete (Table 6.1). This was reviewed case by case, and ultimately the latter blocks were included in the study.

Table 6.1 Metadata of experimental blocks deployed during the experiment and analysed via micro-computed tomography (E = east, W = west, Ma = marble, Mi = micritic limestone).

| Exposure (yrs) | Site | Coast | Water depth (m) | Deployment | Recovery | Block lithology |
|---|---|---|---|---|---|---|
| 1 | Lindos | E | 3–8 | 21 October 1982 | 25 October 1983 | Ma |
| 1 | Pyrgos | W | 3–6 | 20 October 1982 | 26 October 1983 | Ma |
| 2 | Pyrgos | W | 8 | 26 October 1983 | 15 October 1985 | Ma |
| 3 | Ladiko | E | 3–4 | 28 October 1983 | 22 October 1986 | Ma |
| 4 | Lindos | E | 16–17 | 19 October 1982 | 19 October 1986 | Mi |
| 4 | Ladiko | E | 3.5 | 28 October 1983 | October 1987 | Ma |
| 5 | Ladiko | E | 3 | 28 October 1983 | 14 October 1988 | Mi |
| 6 | Lindos | E | 12 | 18 October 1985 | 18 October 1991 | Ma |
| 7 * | Kolimbia | E | 3 | 17 October 1982 | 13 October 1989 | Ma |
| 8 | Lindos | E | 12 | 18 October 1985 | 1993 | Ma |
| 8–9 | Pyrgos | W | 3 or 8 m | 20 October 1982/83 | 16 October 1991 | Ma |
| 14 | Pyrgos | W | 7 | 20 October 1982 | 1996 | Ma |

* three replicates scanned

### 6.2.2 Micro-computed tomography

Internal bioerosion in the blocks was investigated by micro-computed tomographic analysis (micro-CT). In order to yield spatial resolutions of about 70 µm, blocks were cut with a rock saw to a uniform surface area of 10 x 10 cm. The 7-year block was cut into three such replicates to obtain an impression of the spatial variability of bioerosion within a single block. In this way, a total of 14 samples (in the following called blocks) were selected for micro-CT analysis.

Micro-CT scanning was carried out at the Bundesanstalt für Materialforschung und -prüfung (BAM), Berlin, Germany, using the 225 kV system (Badde and Illerhaus, 2008). An X-ray source voltage of 210 kV, a current of 90 µA, and a pre-filter of 1 mm copper was applied. Attenuation images were taken at smallest possible resolution due to specimen size. To achieve the best signal-to-noise-ratio, 2400 projections over 360 degrees with a total measuring time of 16 h were taken. Images were reconstructed using BAM software generated from the original Feldkamp algorithm (Feldkamp et al., 1984). The resulting voxel size was 72 µm.

Post-processing of micro-CT data was conducted using the Amira software edition from the Zuse Institute Berlin, ZIBAmira version 2014.51 (Stalling et al., 2005). In an initial segmentation step all encrusting epiliths on the surface of the blocks were excluded from the dataset using the *Segmentation Editor*. Limestone substrate was distinguished from the surrounding air and organic tissue (borings were partially filled by air and organic remains of the sponges) using the marker-based *Watershed segmentation* module. Segmentation of the borings from the space surrounding the block was carried out with the *AmbientOcclusionField* module (Baum and Titschack, subm.). Resulting micro-CT images of the blocks were cropped to uniform sizes of 90 x 90 x 18 mm with the *CropEditor* to obtain comparable volumes. The respective volumes of substrate and bioerosion per block were quantified with the *MaterialStatistics* module using the results from the latter segmentation. To quantify the total surface area of each block, bioerosion and substrate

were selected together and the surface was calculated using the *SurfaceGen* module. After removing all other surfaces except the upper surface with the *SurfaceEditor*, this surface area was quantified with the *SurfaceStatistics* module. To further evaluate the bioerosion constituents, a third segmentation step was performed based on a *DistanceMap* of the segmented bioerosion traces employing the *ContourTreeSegmentation* module to gain an automatic separation of different bioerosion traces in the blocks (threshold: 0, persistence value: 0.05; see Titschack et al., 2015). Subsequently, each trace was parameterised with the *ShapeAnalysis* module. The maximum trace extent defined microbioerosion patterns as < 1 mm and macrobioerosion patterns as > 1 mm, following the definition by Wisshak (2012). Bioerosion rates (including micro- and macrobioerosion; g $m^{-2}$ $yr^{-1}$) were calculated by multiplying the volume of bioerosion ($cm^3$) with the mean density of limestone/marble of 2.7 g $cm^{-3}$ (Schön, 2011) and expressing the result per surface area ($m^2$) per duration of exposure (years). These rates include the residual internal micro- and macrobioerosion, since the volume of substrate removed by grazers (potentially also including micro- and macrobioerosion) was impossible to quantify without a reference to the original substrate surface.

### 6.2.3 Bioerosion inventory

Bioerosion ichnotaxa were identified following descriptions of Bromley (1970) and Bromley and D'Alessandro (1983, 1984, 1989). Ontogenetic stages of sponge borings were classified into putative growth phases A–E according to characterisations in Bromley and D'Alessandro (1984).

### 6.2.4 Sponge spicule analysis and species identification

For the identification of the trace makers of *Entobia* cavity networks, sponge spicule preparations were made from dry sponge tissue. To extract the tissue from the equivalent positions as in micro-CT reconstruction, the blocks were fragmented with hammer and chisel, and tissue was carefully removed with a dissecting needle. For spicule preparations sponge tissue was digested in 68 % concentrated nitric acid in test tubes in a heated sand-bath (60–70 °C) for about 2 h, then leaving the solutions in place over night without heat application. On the next day, acid-cleaned spicules were washed three times in distilled water and dehydrated three times in laboratory-grade ethanol, each wash occurring after centrifugation and pipetting off the supernatant, taking care not to accidentally remove spicules. Spicules were then mounted for scanning electron microscopy (SEM) by drying aliquots of re-suspended spicules directly on SEM stubs, followed by sputter-coating with gold, and analysis with the SEM (VEGA3, TESCAN). In some cases, colour of the dry tissue helped with classification efforts (e.g., Christomanos and Norton, 1974), but in most cases species identification had to rely exclusively on spicules. We mostly referred to descriptions of Mediterranean bioeroding sponges by Rosell and Uriz (2002). Tylostyle measurements were obtained from 20 spicules per specimen. Spirasters and amphiasters were scarce and often broken, so that only five microscleres were measured where possible. Measurements were carried out using ImageJ v.1.48 (Rasband, 1997–2015).

## 6.3 Results

### 6.3.1 Bioerosion traces

Analysis of bioerosion patterns in the experimental blocks revealed ten different ichnotaxa, eight of which were attributed to the activity of excavating sponges and two to polychaete worms (Table 6.2). In respect to general patterns, the boring intensity distinctly increased with exposure time (Fig. 6.2–6.5). In blocks deployed for 2 to 5 years, superficial cavity networks were observed (Fig. 6.2–6.3). From 7 years onward, extensive three-dimensional networks had developed (Fig. 6.4–6.5). Diversity increased over time as well, with blocks containing more than one ichnospecies after 5 years (Table 6.2).

In the two blocks deployed for 1 year no macroborings were detected (Fig. 6.2A–B). The first distinct sponge boring was observed in the 2-year block (Fig. 6.2C). The trace was characterised by cylindrical chambers (about 1.4–5.1 mm in length, 0.7–1.3 mm in width) that were arranged in long, sublinear chains that coalesced in cross-, T- or L-shape, which is characteristic for *Entobia cateniformis* Bromley and D'Alessandro, 1984 in the late ontogenetic growth phase C. This system formed one tier in about 0.1–0.2 mm depth in the block parallel to the external surface, extending through the entire block.

In the 3-year block, an early-stage of *Entobia megastoma* (Fischer, 1868) was found. It was composed of a sublinear gallery (about 50 x 4 mm in size) with hand-like extensions (phase A–B; Fig. 6.2D). In the two 4-year blocks no assignable macrobioerosion patterns occurred (Fig. 6.2E–F).

In the 5-year block, a well-developed *Entobia geometrica* Bromley and D'Alessandro, 1984 cavity network was detected (Fig. 6.3A). The trace consisted of subrectangular to subtriangular flattened chambers with rounded corners (about 3.5–9.9 mm in diameter) that were aligned in weakly developed rows (phase D). The system extended in one tier throughout the entire surface of the block, parallel to the substrate surface in about 0.2–0.5 mm depth. In addition, one early-stage and two well-developed specimens of the polychaete bioerosion traces *Caulostrepsis* isp. penetrated from the upper surface into the block (Fig. 6.3A1–3).

In the 6-year block, a well-developed network of *Entobia* cf. *ovula* Bromley and D'Alessandro, 1984 occurred (Fig. 6.3B). The trace was characterised by globose-ovoid to sub-prismatic chambers (about 0.7–1.5 mm in diameter) that were arranged in a crowded boxwork pattern (phase D). The entire system had a diameter of 40–50 mm and was arranged in one tier parallel to the external substrate surface in about 0.2–0.6 mm depth.

In the 7-year block, the bioerosion intensity strongly varied within the three subsamples (Fig. 6.4A–C). In the first subsample only an early-stage sponge boring was found that resembled *Entobia mammilata* Bromley and D'Alessandro, 1984 in growth phase A–B (Fig. 6.4A). In the second subsample, two separate specimens of *E. megastoma* and one of *E. mammilata* occurred (Fig. 6.4B). The first specimen of *E. megastoma* was composed of subcylindrical galleries that formed a three-dimensional system (30 x 40 mm) and penetrated about 1.5 cm into the substrate (phase B–C; Fig. 6.4B1). The second specimen of *E. megastoma* was connected with *E. mammilata* (Fig. 6.4B2). This specimen of *E. megastoma* appeared to be an earlier growth stage than the other specimens in the same block (phase B). *Entobia mammilata* formed chains of turnip-shaped chambers (about 1.3–1.7 mm; in phase B). The galleries extended over an area of about 42 x 40 mm and were arranged in two tiers in about 10 mm depth of the block. The third subsample was crowded with bioerosion traces that were identified as two entobian ichnospecies (Fig. 6.4C). Here, a well-developed network of *E. mammilata* was composed of clusters of tubercle-like

Table 6.2 Inventory of bioerosion traces. Sponge borings (trace = *Entobia* ispp.) and boring sponges (trace maker = *Cliona* spp.) in the scanned experimental blocks were assigned via spicule analysis. Ontogenetic phases of sponge boring traces were determined according to Bromley and D'Alessandro (1984) with most mature stages in brackets. Measurements of sponge spicules are given as ranges, with length before widths, and means in parenthesis. Number of tylostyles n = 20, number of spirasters n = 5, unless otherwise indicated in square brackets.

| Exposure (yrs) | Boring | | Phase | Producer | | Tylostyles (µm) | Spiraster (µm) |
|---|---|---|---|---|---|---|---|
| 2 | *Entobia cateniformis* | Fig. 6.2C | C (D) | *Cliona schmidtii* | Fig. 6.6A | 170–247 (198) x 3–8 (5) | a) 57–71 (66) x 2–3 (2) |
| | | | | | | | b) 28–52 (36) x 2–3 (3) |
| | | | | | | | c) 17 x 3 [1] |
| 3 | *Entobia megastoma* | Fig. 6.2D | A–B (D) | Sponge | - | - | - |
| 5 | *Entobia geometrica* | Fig. 6.3A | D (D) | *Cliona* cf. *celata* 1 | Fig. 6.6C | 243–373 (320) x 6–13 (10) | - |
| | *Caulostrepsis* isp. | Fig. 6.3A1–A3 | | Worm | | | |
| 6 | *Entobia* cf. *ovula* | Fig. 6.3B | D (D) | *Cliona* cf. *viridis* | Fig. 6.6H | 217–356 (273) x 3–6 (4) | 20–32 x 1 [2] |
| 7 | *Entobia* cf. *mammilata* | Fig. 6.4A | A–B (E) | Sponge | - | - | - |
| 7 | *Entobia megastoma* | Fig. 6.4B1 | B–C (D) | *Cliona* cf. *celata* 2 | Fig. 6.6D | 218–369 (316) x 4–8 (6) | - |
| | *Entobia megastoma* | Fig. 6.4B2 | B (D) | *Cliona* cf. *celata* 2 | Fig. 6.6E | 208–339 (283) x 3–9 (6) | |
| | *Entobia mammilata* | Fig. 6.4B2 | B (E) | Sponge | - | - | - |
| 7 | *Entobia mammilata* | Fig. 6.4C1 | D (E) | *Cliona* cf. *viridis* | Fig. 6.6G | 234–394 (324) x 4–9 (7) | a) 30–44 (35) x 1–2 (1) |
| | | | | | | | b) 18 x 1 [1] |
| | *Entobia megastoma* | Fig. 6.4C2 | B (D) | *Cliona* cf. *celata 2* | Fig. 6.6F | 235–358 (321) x 5–9 (7) | - |
| 8 | *Entobia* cf. *ovula* | Fig. 6.5A1 | D (D) | *Cliona* cf. *schmidtii* | Fig. 6.6B | 179–275 (220) x 3–6 (5) | a) 58–84 (75) x 1–2 (2) |
| | | | | | | | b) 25–46 (35) x 2 (2) |
| | | | | | | | c) 21 x 7 [1] |
| | *Entobia* cf. *magna* | Fig. 6.5A2 | B (D) | *Cliona rhodensis* | Fig. 6.6I | 245–356 (289) x 6–10 (8) | 23 x 1 [1] |
| | *Entobia* cf. *parva* | Fig. 6.5A3 | D (D) | Sponge | - | - | - |
| 8–9 | *Entobia megastoma* | Fig. 6.5B | B (D) | Sponge | - | - | - |
| 14 | *Entobia* cf. *cretacea* | Fig. 6.5C | C–D (D) | Sponge | - | - | - |
| | *Trypanites* isp. | Fig. 6.5C3-5 | | Worm | | | |

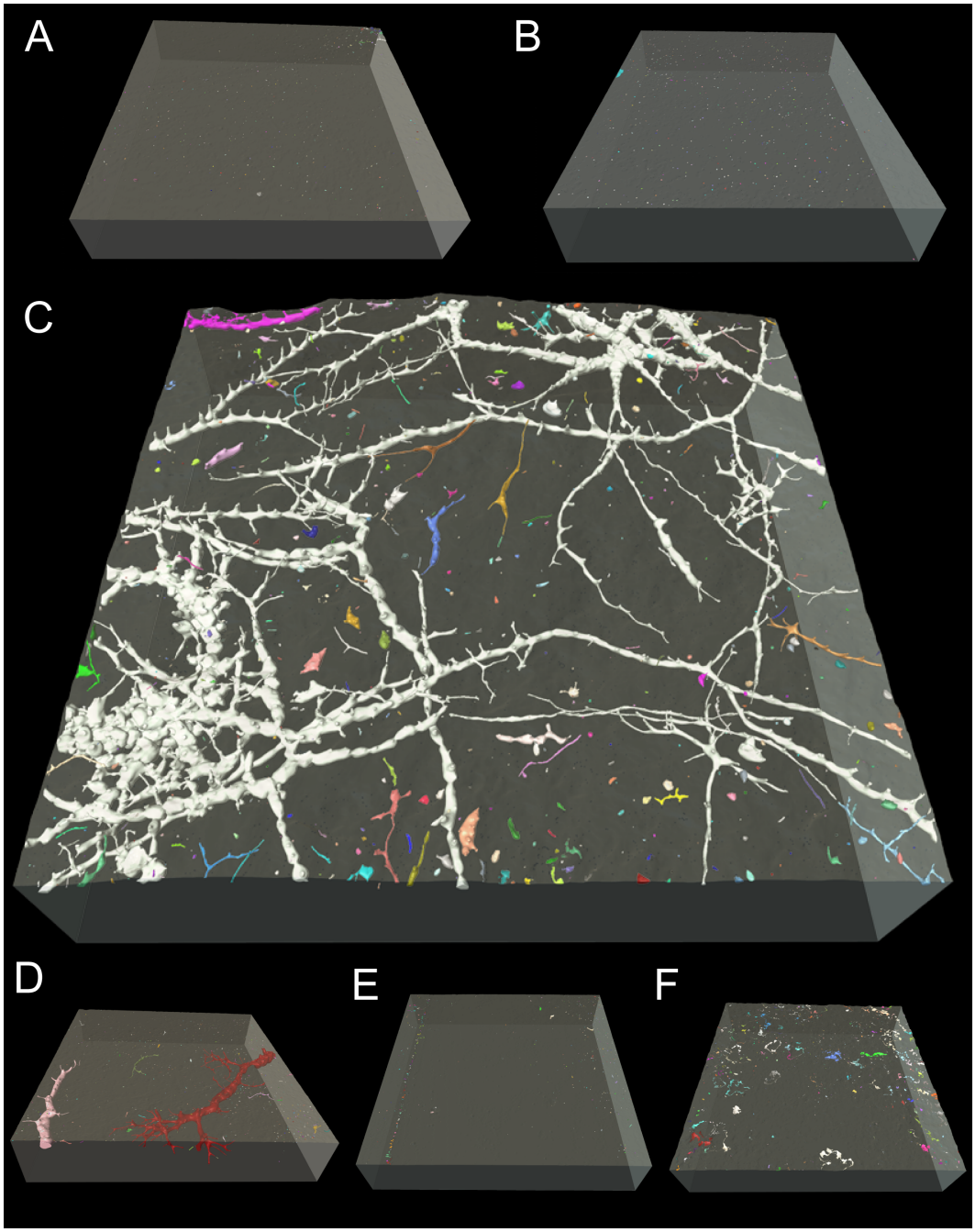


Figure 6.2 Micro-computed tomographic visualisation of bioerosion traces in experimental blocks deployed for 1–4 years. (A–B) 1-year blocks showed no macrobioerosion traces. First bioerosion traces were observed (C) in the 2-year block with *Entobia cateniformis* and (D) in the 3-year block with *E. megastoma*. (E–F) The 4-year blocks showed no distinct macrobioerosion traces (size of blocks = 90 x 90 x 18 mm).

chambers in about 1.2–1.4 mm of the block (phase D; Fig. 6.4C1). The network extended over an area of 30 x 90 mm and had penetrated the entire depth of the block (18 mm). In addition, several juvenile specimens of *E. megastoma* occurred. The largest specimen was 25 x 50 mm in size and had a subcylindrical gallery of about 3 mm in diameter with long exploratory threads (phase B; Fig. 6.4C2).

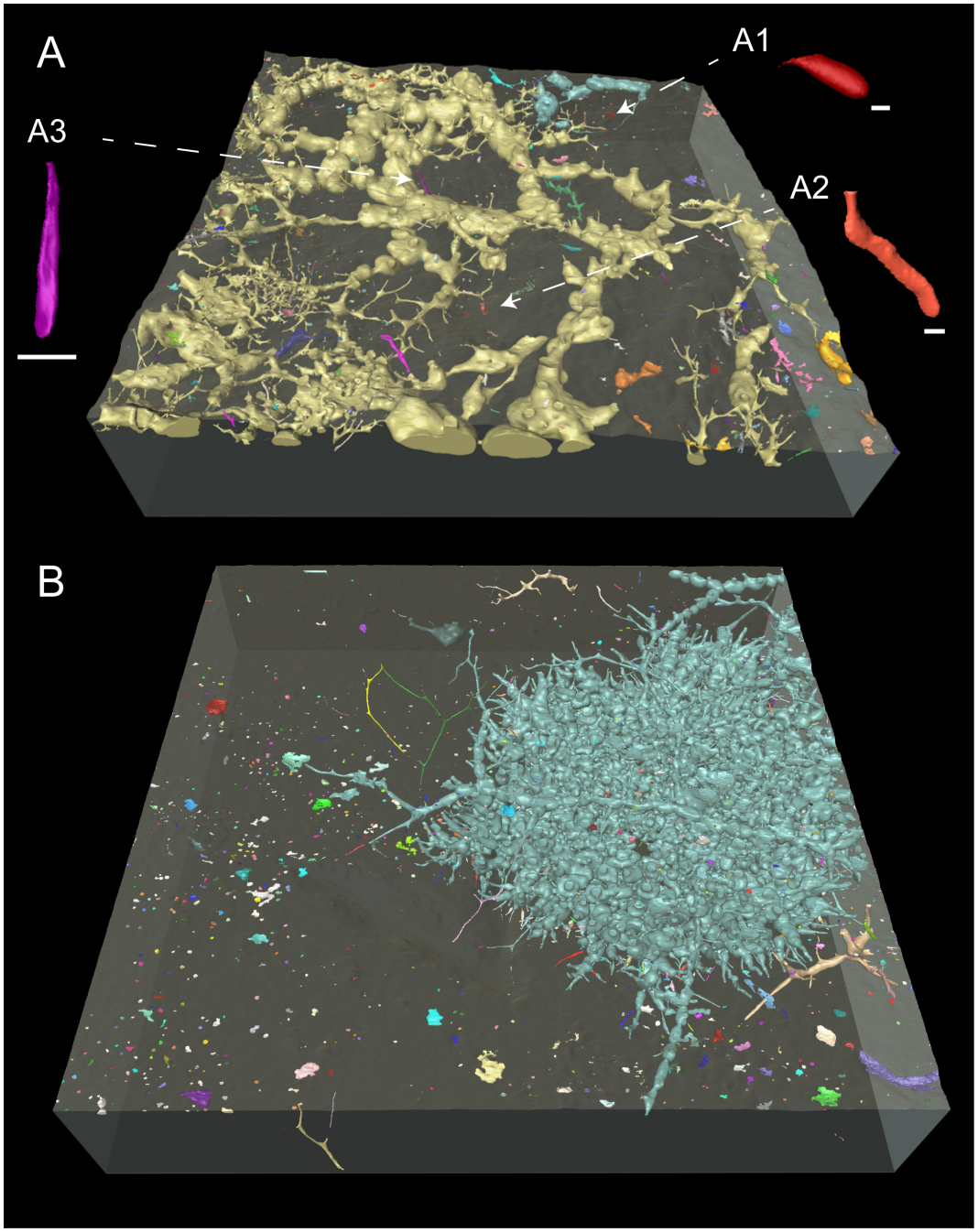


Figure 6.3 Micro-computed tomographic visualisation of bioerosion traces in experimental blocks deployed for 5–6 years. (A) The 5-year block showed a network of *Entobia geometrica* and specimens of *Caulostrepsis* isp. (A1–A3). (B) The 6-year block showed a cluster of *E.* cf. *ovula* (scales A1–A3 = 2 mm, size of blocks = 90 x 90 x 18 mm).

The 8-year block showed a dense network of shallow bioerosion (Fig. 6.5A), which was composed of three different entobians, dominated by a large network of *E.* cf. *ovula* clusters that were interconnected by long galleries in growth phase D. The largest cluster was about 25 x 40 mm in size and extended in about 0.2–0.6 mm depth of the block in one tier parallel to the external substrate surface (Fig. 6.5A1). In addition, four large chambers of

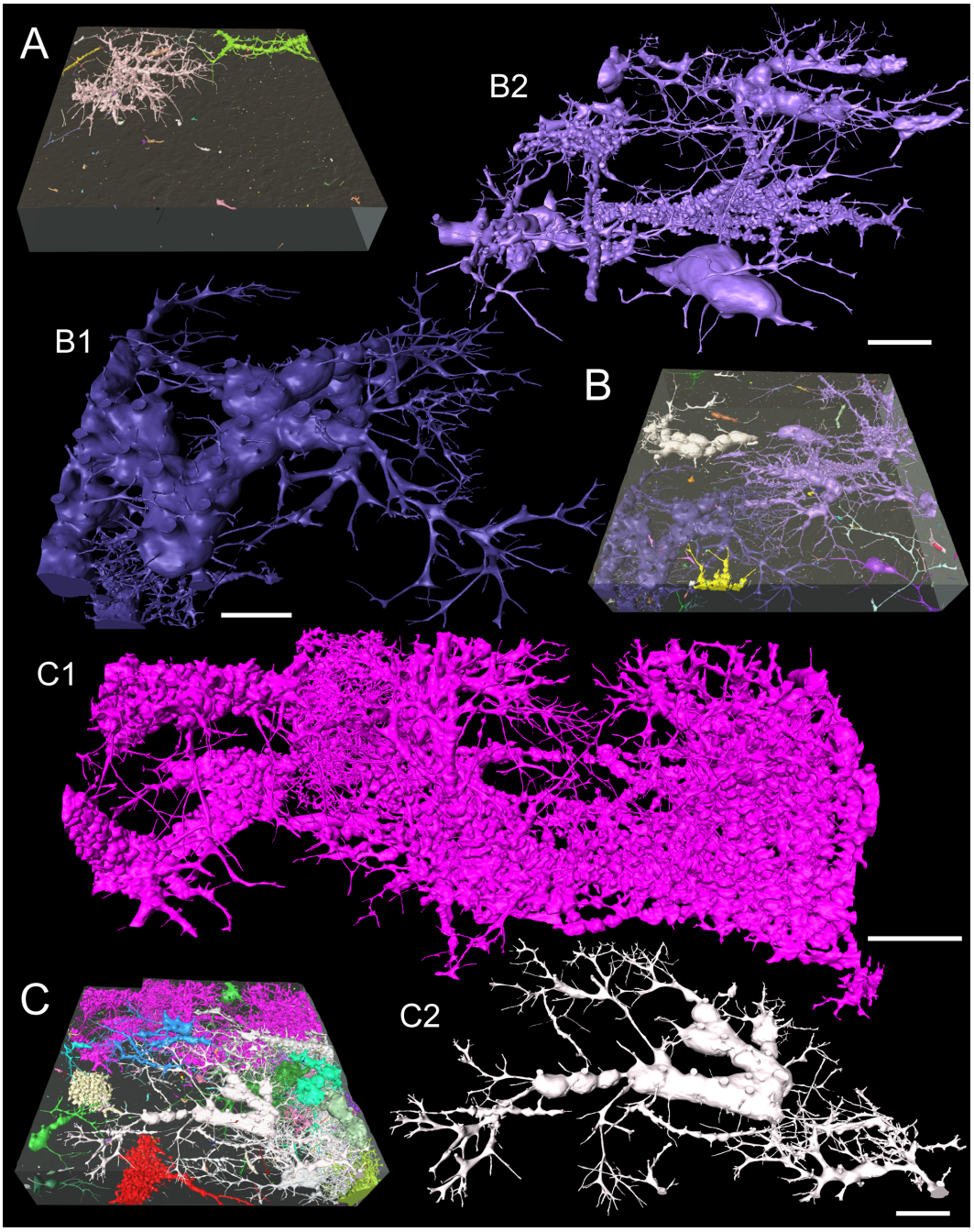


Figure 6.4 Micro-computed tomographic visualisation of bioerosion traces in three subsamples of the 7-year block. (A) First subsample of the block with *Entobia* cf. *mammilata*, B) second subsample of the block showing two specimens of *E. megastoma* (B1 and large chambers B2) and *E. mammilata* (small chambers B2), and C) third subsample of the block with *E. mammilata* (C1) and *E. megastoma* (C2) (scales = 10 mm, size of blocks = 90 x 90 x 18 mm).

about 6 mm in diameter being connected by numerous exploratory threads were found that resembled *E. magna* Bromley and D'Alessandro, 1989 in phase B (Fig. 6.5A2). The third entobian was a specimen of *Entobia* cf. *parva* Bromley and D'Alessandro, 1989, which was identified through its compact boxwork of densely distributed, inflated chambers of

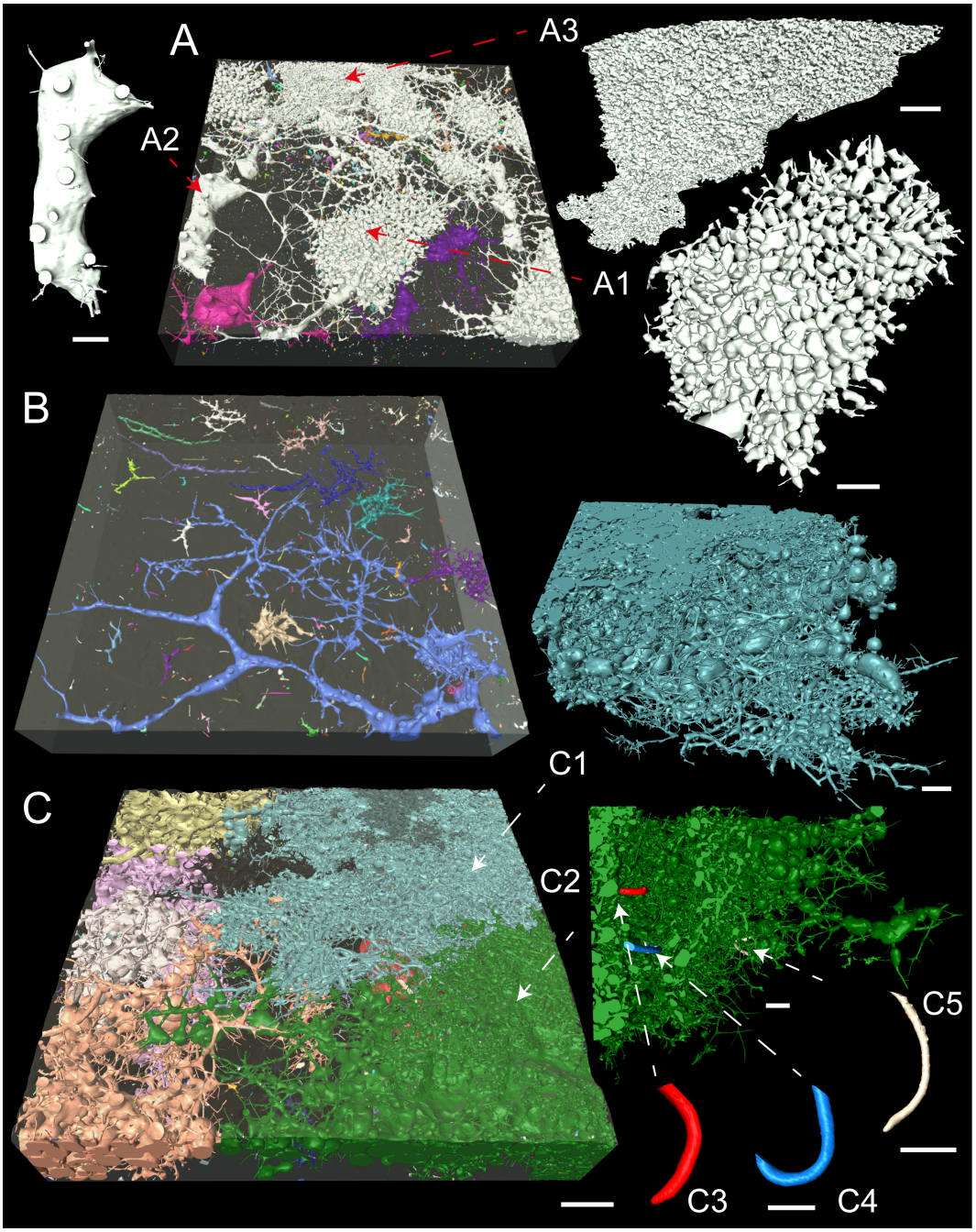


Figure 6.5 Micro-computed tomographic visualisation of bioerosion traces in experimental blocks deployed for 8–14 years. (A) 8-year block with *Entobia* cf. *ovula* (A1), *E. magna* (A2), and *E.* cf. *parva* (A3), B) 8–9-year block with *E. megastoma*, and C) 14-year block with *E.* cf. *cretacea* (C1–C2) and *Trypanites* isp. (C3–C5) (scales A1–A3, C1–C2 = 5 mm, scales C3–C5 = 1 mm, size of blocks = 90 x 90 x 18 mm).

about 0.2–0.6 mm that were arranged in a 15 x 40 mm tier in about 10 mm depth of the block (phase D; Fig. 6.5A3).

In the 8- to 9-year block, an advanced network of *E. megastoma* and several scattered early-stage galleries co-occurred (Fig. 6.5B). The 1–4 mm, subcylindrical galleries of the advanced specimen extended over an area of about 50 x 90 mm and were distributed in

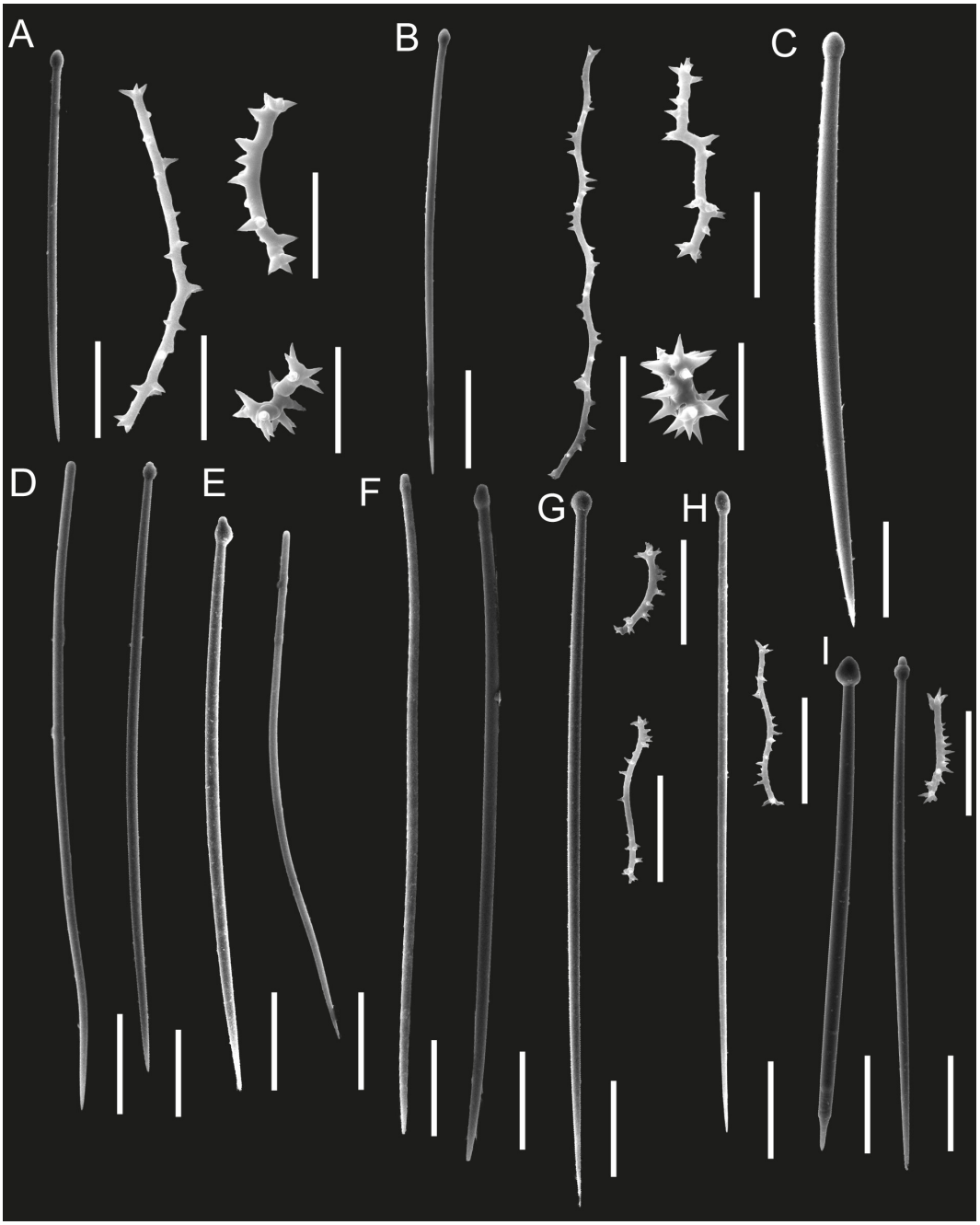


Figure 6.6 Spicules of boring sponges extracted from sponge tissue preserved in cavity networks in the scanned blocks. (A-B) Tylostyles and spirasters of *Cliona schmidtii*, (C) tylostyles of *C.* cf. *celata* 1, (D-F) tylostyles of *C.* cf. *celata* 2, (G-H) tylostyles and spirasters of *C.* cf. *viridis*, (I) tylostyles and spirasters of *C. rhodensis* (scales: tylostyles = 50 µm, spirasters = 20 µm).

parallel to the block surface (phase B). The smaller specimens were about 10–15 mm in size and formed characteristic hand-like cavities (phase A).

The 14-year block was extensively bioeroded and entobians difficult to separate (Fig. 6.5C). Several specimens of *Entobia* cf. *cretacea* Bromley, 1970 exhibited large polygonal chambers of about 1.3–4.2 mm in diameter, being connected by numerous canals, and with the entobians extending through the entire depth of the block (18 mm; Fig. 6.5C1–C2).

Bromley (1970) did not define distinct phases for *E. cretacea*, but we considered the detected traces to reflect phase C–D. Apart from entobians, three galleries of the worm boring *Trypanites* isp. extended as slim sack-like cavities into the blocks (Fig. 6.5C3–C5). The software initially attributed these to the surrounding *E. cretacea* cavity network and the worm borings were afterwards separated manually from the sponge borings.

### 6.3.2 Identification of boring sponges

We recognised spicules of five clionaid bioeroding sponge species that could be assigned as trace makers of eight different entobians (Fig. 6.6, Table 6.2, Table C1). However, not from every cavity network spicules could be extracted, and other, rare, broken or non-diagnostic spicules occurred that could not conclusively be matched to smaller entobians or used to identify bioeroding sponges at species level (these possibly included spicules from the genera *Pione*, *Cliothosa*, *Spirastrella*, *Siphonodictyon*, and *Thoosa*).

*Cliona schmidtii* (Ridley, 1881) was recognised as the trace maker of *E. cateniformis* and *E. ovula* in the 2-year and the 8-year blocks (Fig. 6.6A–B, Table 6.2). Even when dry, the sponge tissue retained its characteristic purple colour that was an immediate indicator for *C. schmidtii*. Tylostyles were 170–275 µm in length and 3–8 µm in thickness, and had a slightly bent shaft. A spectrum of spiraster sizes was observed: We distinguished (i) relatively thin and long spirasters with small spines distributed along the convex sides of the helical shaft (axis 57–84 µm in length and 1–3 µm in thickness), (ii) relatively short and thick spirasters with conical spines (axis 25–52 µm in length and 2–3 µm in thickness), and (iii) short, thick amphiaster-like spirasters (axis 17–21 µm in length and 3–7 µm in thickness).

Two morphospecies of *Cliona* cf. *celata* Grant, 1826 were distinguished as trace makers of two different entobians. *Cliona* cf. *celata* 1 was trace maker of *E. geometrica* in the 5-year block (Fig. 6.6C, Table 6.2), and *Cliona* cf. *celata* 2 was matched to *E. megastoma* in the 7-year block (Fig. 6.6D–F, Table 6.2). Both morphospecies had brown dry sponge tissue and exclusively tylostyles. Tylostyles of *C.* cf. *celata* 1 were 243–373 µm in length and 6–13 µm in thickness, were comparatively robust with well-formed tyles that were occasionally subterminal, and had mostly straight or subtly bent shafts. Tylostyles of *C.* cf. *celata* 2 were comparatively slim, often with subterminal, occasionally multiple tyles, and tyles could be strongly displaced or weakly pronounced, and occasional near-stylar modifications occurred. The tylostyle shafts of *C.* cf. *celata* 2 were occasionally flexuous, being on 208–369 µm in length, but only about 3–9 µm in thickness.

Based on scarce spirasters *Cliona* cf. *viridis* (Schmidt, 1862) was tentatively identified as trace maker of *E. ovula* and *E. mammilata* in the 6- and 7-year blocks (Fig. 6.6G–H, Table 6.2). The colour of the dry sponge tissue was brown. Tylostyles were 217–394 µm in length and about 3–9 µm in thickness, fusiform, slightly bent and had round, oval or subterminal tyles. Two types of spirasters were distinguished: (i) straight, 20–44 µm in length and 1–2 µm in thickness, with relatively long spines that were mainly clustered at the ends of the shaft and (ii) helical, 18 µm in length and 1 µm in thickness, with small spines.

*Cliona rhodensis* Rützler and Bromley, 1981 was identified as trace maker of *E. magna* in the 8-year block (Fig. 6.6I, Table 6.2). The colour of the dry sponge tissue was brown. Tylostyles were near straight and fusiform, 245–356 µm in length and about 6–10 µm in thickness, and had distinct tyles. Only one complete, undamaged spiraster was found, which was 23 µm in length and 1 µm in thickness, and had discrete, relatively long spines slightly recurving at their tips.

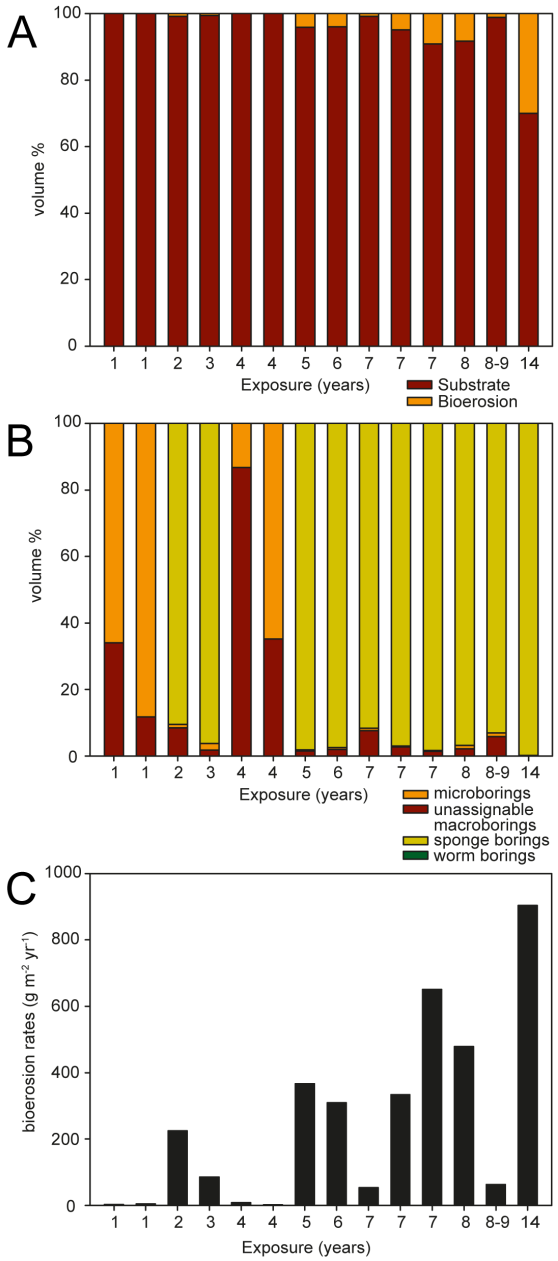


Figure 6.7 (A) Proportion of retained substrate vs. internal bioerosion in the scanned blocks, (B) proportional contribution of the different groups of boring organisms to the internal bioerosion in A, and (C) internal bioerosion rates (g $m^{-2}$ $yr^{-1}$) measured in experimental substrates during the experiment.

### 6.3.3 Bioerosion intensity and rates

Quantification of bioerosion in the experimental blocks revealed that in blocks deployed for 1 to 4 years only small volumes of substrate were removed by bioerosion (<1 %; Fig. 6.7A, Table C2). In the 5- to 8-year blocks, the volume of bioerosion increased to 4–9 %. The highest bioerosion intensity was measured in the block that was deployed for 14 years (30 %). With respect to the proportional contribution of the different groups of bioeroding organisms to total bioerosion, the largest part of bioerosion in the 1- and 4-year blocks was

represented by microbioerosion and unassignable macrobioerosion patterns (Fig. 6.7B). In all other blocks, bioerosion was predominantly produced by boring sponges. Only in the 5- and 14-year blocks complementary worm bioerosion was observed, but it contributed less than 1 % to the total volume of bioerosion. Analogous to the gradual increase in total volume of bioerosion, total bioerosion rates (i.e. residual micro- and macrobioerosion) increased with exposure time (Fig. 6.7C, Table C2). Lowest values were found in the 1- to 4-year blocks (1.5–85 g $m^{-2}$ $yr^{-1}$), except in the 2-year block, where bioerosion rates tallied with 224 g $m^{-2}$ $yr^{-1}$. In the 5- to 7-year blocks bioerosion was elevated compared to blocks retrieved after shorter periods and reached values of 308–648 g $m^{-2}$ $yr^{-1}$. However, in 7- and 8 to 9-year blocks lower values of 53 and 62 g $m^{-2}$ $yr^{-1}$ were observed. Highest bioerosion rates were measured in the 14-year block, resulting in a maximum value of 900 g $m^{-2}$ $yr^{-1}$. Overall, observed bioerosion patterns suggest that not only the bioerosion intensity, i.e. the absolute volume removed by bioerosion, but also the bioerosion rates, i.e. bioerosion normalised to a time span of one year, increased with time of exposure. An additional statistical evaluation was not considered feasible, however, due to the limited amount of available blocks suitable for micro-CT analysis.

## 6.4 Discussion

### 6.4.1 Micro-CT as a tool for the visualisation and quantification of internal macrobioerosion

Methods used in this study represent a new approach and perspective for precise and automatic differentiation and quantification of internal structures of bioerosion, and they can be employed for similar aspects in biogeoscience research. Previously, evaluation of internal bioerosion by tomographic analysis was restricted to two-dimensional image analysis of consecutive layers (e.g., Sammarco and Risk, 1990; Becker and Reaka-Kudla, 1997; Hassan, 1998; Schönberg, 2001), and only recently included also three-dimensional measurement tools (Crook et al., 2013). Above methods are suitable for comparatively simple bioerosion structures, but show clear limitations in the differentiation of complex cavity networks. In our study we took advantage of program algorithms that help to distinguish different traces. This function needs to be manually revised, however, as it does not automatically identify ichnotaxa according to morphological differences. This becomes especially clear where morphological distinct traces were identified as fused to one connected cavity network (Fig. 6.4B2, 6.5A), an effect likely caused by insufficient separation of traces due to different generations of endoliths overprinting earlier borings or galleries of bioeroding sponges that can closely mingle with other species or individuals (unlike observations in Bromley and Tendal, 1973).

Another restriction of micro-CT analysis is the correlation of sample size and spatial resolution. Based on the sample dimensions of 10 x 10 cm spatial resolutions of 72 µm were possible, which allowed preserving large cavity networks, as well as capturing thin exploratory threads of the sponges. However, where connecting galleries were near or below this resolution, occasionally different units of the same trace were split into apparently different specimens (Fig. 6.4C). Neither was the present resolution high enough to capture smaller microborings. Subsequent manual separation or joining of specimens needs to be assessed case-by-case. That is comparatively easy and feasible for cylindrical borings such as *Trypanites* isp. (Fig. 6.5C3–C5), but for complex cavity networks, such as sponge borings, this can potentially become very time-consuming.

Apart from microborings and thin exploratory threads, a small proportion of deeper borings was also neglected due to the digital cropping of the blocks. In addition, some proportion of bioerosion became unavailable for quantification when grazers simultaneously removed surface layers and micro- as well as macrobioerosion traces within them. This substrate loss cannot be quantified without a reference that indicates the original thickness of the experimental blocks. What was actually measured, hence, is the residual internal bioerosion. Particularly in those blocks that were exposed long-term, bioerosion rates thus were somewhat underestimated, in turn implying that the observed increase in bioerosion rates can be expected to be even more pronounced for total bioerosion.

### 6.4.2 The macrobioeroder community

We distinguished *Cliona* cf. *viridis*, *C. schmidtii*, *C.* cf. *celata* morphospecies 1 and 2, and *C. rhodensis* as main producers of the observed bioerosion traces. Apart from these, we assume that other sponges bioeroded the blocks as well, as evidenced by further rare spicules and by few traces that may have differed from the above, but from which no spicules could be extracted. This possibly includes the locally common boring sponges *Pione vastifica* (Hancock, 1849) and *Cliothosa hancocki* (Topsent, 1888), which Rützler and Bromley (1981) and Bromley et al. (1990) reported from Rhodes.

Bioeroding sponge distributions and abundances, as well as their bioerosion rates, are dependent on environmental parameters such as water flow, nutrients, salinity, temperature, and light (see Schönberg, 2008 for a review). Especially *C. viridis* and *C. celata* are very characteristic for the Mediterranean and known to be among the most abundant and destructive sponges in the Mediterranean Sea (e.g., Rosell et al., 1999; Calcinai et al., 2011). Both species, however, are difficult to identify and are members of species complexes that encompass very similar, but taxonomically different species, which means that earlier accounts on their biology may refer to more than one species (e.g., Xavier et al., 2010; Leal et al., 2015). This may also be the case for *C. schmidtii*, because specimens from different sample sites can have somewhat different spicule morphologies (Schönberg, pers. obs.). However, *C. schmidtii* and *C. rhodensis* were the presently best confirmed species, but little is known about their ecological requirements: Both can be found in light and shade, and occur in moderately clear water and may avoid sedimentation (Rützler and Bromley, 1981; Carballo et al., 1994; Corriero et al., 2000), but it is not known what else characterises their ecological niches. To draw conclusions about environmental conditions from our data is difficult, because blocks were from different depths and current regimes, and the lack of replication prevented us from matching species distributions with environmental conditions.

Although on the surrounding sea floor also boring bivalves and worms (sipunculans, polychaetes) were reported to be very common, our experimental blocks were dominated by boring sponges. We assume that this dominance of sponges is an effect of the high spatial variability of macroborers and that locally sponges were most prevalent and determined the predominant larval supply. This assumption is in good agreement with results from other long-term experiments in the tropics, where macrobioerosion strongly varied with water depth and nutrient supply (Kiene and Hutchings, 1992, 1994; Peyrot-Clausade et al., 1995b; Pari et al., 1998, 2002; Osorno et al., 2005; Carreiro-Silva and McClanahan, 2012). The low occurrence of polychaete borings in the blocks may be also explained by the fact that polychaetes have comparatively short life spans and that their vacant burrows became inhabited and overprinted by newly settled larvae of other boring species (Hutchings et al., 1992). To draw a direct comparison between bioerosion rates from these studies and our experiment,

however, is difficult, because these experiments were based on coral substrates and assessed via image analysis.

### 6.4.3 Palaeoenvironmental implications

In the fossil record, sponge borings are preserved as trace fossils in calcareous hard substrates such as rocky shores, hardgrounds, or shells providing important information about palaeoenvironmental conditions (Wilson, 2007). Whereas recent boring sponges can be identified by their spicules or other morphological and molecular characters, the description of fossil entobians mostly relies on the morphological characterisation of their bioerosion traces. This is, because the preservation potential of the boring is much higher than that of the siliceous spicules, which are only rarely preserved within the borings (e.g., Reitner and Keupp, 1991; Blissett et al., 2006; Bromley and Schönberg, 2008). Thus, in order to allow conclusions about past environmental conditions drawn in an actualistic approach from the ecophysiology studied in extant sponges, traces of recent sponges need to be matched with the sponge spicule record, so that deductions about fossil trace makers can be made where a close morphological resemblance is found between fossil and recent traces.

This study is one of the few that allowed matching sponge borings (bioerosion traces) and boring sponges (trace makers) by combining micro-CT with spicule analysis, providing respective information for five species of recent sponges. This information furthers an earlier detailed inventory of Mediterranean sponge borings and boring sponges by Bromley and D'Alessandro (1989). These authors were also able to obtain some clear matches between sponge species and ichnospecies, but in accordance with our results they also showed that one sponge species can produce different traces. Especially *C. celata* was described several times as producing traces that vary morphologically (De Groot, 1977; Bromley and D'Alessandro, 1989), *E. geometrica* and *E. megastoma*, even in the same type of substrate. However, as mentioned above, *C. celata* is not a single species, but a species complex of several morphologically indistinct species, and a proper separation of species presently relies on molecular taxonomy (Xavier et al., 2010; De Paula et al., 2012). While spicular morphology can be variable with different environmental conditions (Hoeksema, 1983; Rosell and Uriz, 1991; Bavestrello et al., 1993), we recognised subtle but consistent differences in spicule morphology between *C.* cf. *celata* 1 (producing *E. geometrica*) and *C.* cf. *celata* 2 (producing *E. megastoma*), and in this case different traces may in fact represent different trace makers. A similar situation may be the case for the two borings found in the other difficult species, *C.* cf. *viridis* (*E. ovula* and *E. mammilata*), but as present samples were not preserved for molecular analysis, we cannot confirm or reject this assumption.

In contrast to *C. celata*, we distinguished two different entobians for *C. schmidtii*: *E. cateniformis* and *E.* cf. *ovula*. Bromley and D'Alessandro (1989) also identified *C. schmidtii* as trace maker of *E. ovula*, but in their study *E. cateniformis* was produced by *P. vastifica* (formerly *C. vastifica*). We furthermore identified *C.* cf. *viridis* as trace maker for *E. ovula* and *E. mammilata*, which led to the conclusion that not only the same species can produce different traces, but the same trace can be produced by different species — which is not a surprise but in accordance to basic ichnological principles (e.g., Bromley and Fürsich, 1980). Our results thus also agree with the assumption of Bromley and D'Alessandro (1984) that the morphology of entobians can strongly vary with the nature and structure of the substrate, the quality of the surrounding environment, the proximity of other endoliths, the species of the boring sponge, and the ontogeny of the borer. However, we lack comparative data as all presently available research on the correlation of sponge borings and boring

sponges was carried out in Mediterranean Sea. Further studies are needed in order to ascertain whether the observed correlations also apply to different biogeographic realms, and to better understand the application and limitations of sponge bioerosion traces as palaeoenvironmental indicators.

### 6.4.4 Long-term succession of boring sponges: Are 14 years long enough to develop equilibrium communities in a warm-temperate environment?

This study provides one of the longest records for a bioerosion experiment, and is one of the few available from the Mediterranean. It included quantitative analyses and observations on succession dynamics of macrobioeroders, all of which represents vital information to assess the impact of macrobioerosion on marine carbonate environments. Using the approach of micro-CT in combination with sponge spicule analysis revealed that during the experiment the blocks were predominantly bioeroded by sponges. The present study from a warm-temperate habitat confirms findings from tropical coral reefs that sponges require a few years to colonise newly available substrates and may only form larger infestations after more than 7 years (e.g., Kiene and Hutchings, 1992, 1994). Based on the present results and taking earlier macroscopic observations of the same blocks into account (Bromley et al., 1990), we recognised two developmental phases during our experiment: (1) an early community stage with initial sponge bioerosion and comparatively low macrobioerosion rates between years 1 and 5 and (2) an intermediate stage starting in year 6 or 7 when boring sponges become firmly established and bioerosion rates increase. Especially in the latter phase, our material displayed much variability, which we expect to decrease at later stages, when a stable bioeroding community has established. Across the early and intermediate stages, bioerosion rates increased over time, but can be expected to slow down to a relatively stable rate when equilibrium conditions are eventually reached. Based on the present dataset, a sound prediction about the onset of these equilibrium conditions is not feasible, and would require even longer exposures combined with a higher number of replicates, and such experiments would be necessary to determine whether bioerosion rates peak at an equilibrium plateau, or, more likely, that highest bioerosion rates are reached in the intermediate stage of colonisation, when substrate is not yet limited and competition not yet restricting further growth.

The analysis of ontogenetic stages of the observed entobians, nevertheless, suggests a distinct development of sponge bioerosion over time. Having settled down on suitable substrates and finding ample space, boring sponges can rapidly mature, preferentially by lateral extension. With more specimens colonising the blocks, boring sponges formed increasingly three-dimensional patterns, but less developed ontogenetic stages. This is in good agreement with observations by Rützler (1975), who showed that with sufficient space and little competition, sponge borings mostly spread laterally and progressively bore vertically when the substrate edges are reached or lateral spreading is compromised by neighbouring competitors or other limitations. The presence of an increasing number of vertical borings during the intermediate stage in our experiment could indicate the gradual onset of a saturation phase. Similar observations with macrobioerosion rates proceeding at lower rates when free substrates became scarce and crowded with borings were demonstrated during long-term studies from the tropical realm (Kiene and Hutchings, 1994; Lescinsky et al., 2008; Carreiro-Silva and McClanahan, 2012). At present, however, we cannot conclude how much time is needed in warm-temperate environments to reach equilibrium phases. This again underlines the necessity for further long-term studies, especially outside the tropical realm.

## 6.5 Conclusions

This study presents the first record on long-term bioerosion from the warm-temperate realm and showcases the use of micro-CT to study internal bioerosion. In contrast to previous studies, experimental blocks were almost exclusively colonised by boring sponges, while only few worm and no bivalve borings were observed. Analyses of bioerosion traces and rates suggested an early community development stage during the first 5 years of exposure, where first boring sponges settle, but yield low rates of macrobioerosion, and an intermediate stage commencing in years 6 to 7 when boring sponges matured and bioerosion rates increase. After 14 years, 30 % of the block volumes were occupied by boring sponges. Analysis of ontogenetic stages of sponge borings suggested that successful settlement of boring sponges is strongly dependent on the availability of space and on competition by other bioeroders. A high spatial variability in macrobioerosion prohibited clear conclusions about the onset of macrobioerosion equilibrium conditions. More long-term experiments are needed in order to identify equilibrium conditions and to assess the impact of macrobioerosion in different biogeographic realms.

## Acknowledgements

We thank Nicol Mahnken (Senckenberg am Meer, Wilhelmshaven) for technical support and Ines Pyko (Erlangen) for her help in inventorying the experimental blocks. This study was funded by the Deutsche Forschungsgemeinschaft (DFG Wi 3754/2-1). This paper is published with the permission of the Director of the Institute of Geology and Mineral Exploration, Athens, Greece.

# 7 Synthesis

In the course of this thesis three bioerosion experiments were investigated, presenting a detailed inventory and record on the succession of bioerosion agents and development of bioerosion rates in the Eastern Mediterranean Sea (Chapters 4–6). According to the main objectives (Chapter 1.2), each manuscript (1) analysed the spatio-temporal variability of bioerosion in the Eastern Mediterranean Sea and its effect on the carbonate budget, (2) assessed the application of bioerosion traces as palaeoenvironmental indicators, and (3) draw a longitudinal and latitudinal comparison to previous studies. In the following, the main findings and conclusions of the three manuscripts are summarised.

## 7.1 Spatio-temporal variability of bioerosion in the Eastern Mediterranean Sea and its effect on the carbonate budget

In total, the analysis of bioerosion traces yielded 44 different ichnotaxa that were assigned to bioeroding cyanobacteria (7), chlorophytes (6), fungi (6), foraminifera (2), bacteria (1), sponges (11), polychaetes (3), bivalves (1), gastropods (1), diatoms (1), echinoids (1), chitons (1), and other unknown producers (2). During the short-term experiments mostly microbioerosion traces were observed, but only initial macroborings and grazing traces (Chapters 4 and 5). During the long-term experiment first distinct macroborings were developed after 2 years (Chapter 6). This development pattern is in general in good agreement with previous studies where microbioerosion agents were considered to mature within 1 to 2 years of exposure, while macroborers with longer development cycles such as sponges and bivalves need about 2 to 3 years to develop (e.g., Kiene and Hutchings, 1992, 1994; Pari et al., 1998, 2002; Chazottes et al., 2002; Tribollet and Golubic, 2005). However, the results of the present study show that the succession and boring intensity of micro- and macrobioeroders is complex and distinctly varies within the water column.

With respect to the short-term development of bioerosion in the subtidal realm, the carbonate cycling experiment indicated that the distribution and boring intensity of microbioeroders in the Eastern Mediterranean Sea is mostly controlled by the availability of light in the water column, but secondary, for the first time, a distinct seasonal variability was documented (Chapter 4). Highest bioerosion rates were recorded in the shallow euphotic zone (83 g $m^{-2}$ $yr^{-1}$), largely driven by the boring activity of phototrophic cyanobacteria and chlorophytes, while towards the chlorophyte-dominated deep euphotic to dysphotic zones and the organotroph-dominated aphotic zone the intensity of bioerosion and the diversity of bioerosion traces strongly decreased. During summer, the activity of phototrophs was higher than during winter, which was likely stimulated by enhanced light availability due to more hours of daylight and increased irradiance angels. The observed patterns in overall bioeroder distribution and abundance were mirrored by the calculated carbonate budget with bioerosion rates exceeding carbonate accretion rates in shallow water, yielding to a significant net loss of carbonate in 15 m water depth (27–100 g $m^{-2}$ $yr^{-1}$). According to results from a similar settlement experiment in the Azores this effect may even increase across the intertidal zone, where 4–5 times higher microbioerosion rates were recorded (Wisshak et al., 2010), resulting in probable maximum values of 350–450 g $m^{-2}$ $yr^{-1}$ in intertidal ranges of the Eastern Mediterranean Sea. Towards and within the supratidal zone, the coastal experiment revealed a distinct decrease of microbioerosion activity and ichnodiversity, with

only initial bioerosion traces having been observed after 1 to 2 years (Chapter 5). A higher vertical distribution of borings on substrates on the west coast than substrates on the east coast, and thriving microbioerosion assemblages in water-filled solution pans indicated sea water supply as one of the limiting factors of coastal bioerosion.

With respect to macroborers, surprisingly during the long-term experiment mostly traces of boring sponges were observed, although on the surrounding sea floor also boring worms and bivalves were reported to be very common (Bromley et al., 1990; Chapter 6). Analysis of bioerosion traces and rates suggested an early community development stage during the first 5 years of exposure, where first boring sponges settled, but yielded low macrobioerosion rates, and an intermediate stage after 6–7 years when boring sponges matured and bioerosion rates increased. After 14 years, 30 % of the block volumes were occupied by boring sponges, but due to the high spatial variability in macrobioerosion no clear conclusions about the onset of macrobioerosion equilibrium conditions and distribution patterns could be drawn. Comparable problems were similarly observed during long-term experiments in the tropics (e.g., Kiene and Hutchings, 1992, 1994; Pari et al., 1998, 2002; Chazottes et al., 2002; Tribollet and Golubic, 2005). This underlines the necessity of long-time exposures and high replication at various factor levels in order to better understand and quantify the impact of macrobioerosion on marine carbonate environments.

## 7.2 Palaeoenvironmental implications

The observed record on bioerosion traces documented during the experiments contributes important information to the application of micro- and macrobioerosion traces for palaeoenvironmental reconstruction. Due to the photoautotrophic character of many euendoliths and their specific low-light tolerance limit and light optimum, particularly the investigation of microendolithic ichnocoenoses has become a strong tool for judging light availability and relative bathymetry (e.g., Wisshak, 2012). In general, microbioerosion traces observed during the carbonate cycling experiment in the Eastern Mediterranean Sea were in good agreement with the bathymetric index ichnocoenoses that were developed for reconstruction of light and relative bathymetry (Glaub, 1994; Glaub et al., 2001; Vogel et al., 1995; 2000; Wisshak, 2012). The dominance of *Fascichnus dactylus*/*Rhopalia catenata* in 15 m corresponds to a typical shallow euphotic zone III ichnocoenosis, the dominance of *F. dactylus*/*Scolecia filosa*/*Ichnoreticulina elegans* in 50 m to a typical deep euphotic ichnocoenosis, the dominance of *I. elegans* and fungal microborings form a typical dysphotic ichnocoenosis albeit *Saccomorpha clava* was not observed, and the exclusive occurrence of organotrophic microborings in 250 m substrates in the aphotic zone corresponds to a typical aphotic ichnocoenosis although the index ichnotaxon *S. clava* was rare and *Orthogonum lineare* was not found (Chapter 4). This however, is not surprising, as they are known from other experiments to show only initial borings even after 1 and 2 years of exposure (Wisshak, 2006; Wisshak et al., 2011). The comparison of up- versus down-facing and summer versus winter exposure indicated that turbidity and shade can cause settlement of low-light adapted ichnocoenoses that can be wrongly interpreted as deep water ichnocoenoses. Similar results were also found in reef environments, were turbidity and shadow produced cryptic subhabitats (Perry and Macdonald, 2002; Heindel et al., 2009).

Previously the scheme of ichnocoenoses for bathymetric reconstruction, however, is restricted to the intertidal zone and until now the composition of ichnocoenoses in the intertidal and particularly the supratidal zone is poorly understood (e.g., Wisshak, 2012).

At present, the cyanobacterial boring *F. acinosus* is defined as index ichnotaxon for the intertidal zone, but during the coastal experiment in the intertidal zone mostly *F. dactylus* and *R. catenata* were observed (resembling more a shallow subtidal ichnocoenoses), but no distinct specimens of *F. acinosus*. The only indication of *Hyella balani*, the trace maker of *F. acinosus*, was provided by specimens of *F. rogus*, which typically occur in more deeper water (0.5-5 m; Al-Thukair et al., 1994). Traces of *H. balani*, however, are known to show a high morphological variability in the Mediterranean Sea (Le Campion-Alsumard and Golubic, 1985), resembling in its globular morphology (status "gloecapsoides") strongly *F. rogus*. The application of *F. acinosus* as index ichnotaxon, hence, seems difficult and needs further investigation.

Although recent rocky coasts show a distinct colour zonation pattern, which is produced by different cyanobacterial species within the genera *Hyella* or *Solentia* (Schneider, 1976; Le Campion-Alsumard, 1979; Hoffman, 1985; Radtke et al., 1996; Radtke and Golubic, 2011), during the coastal bioerosion experiment in the supratidal zone mostly traces of *F. dactylus* were observed, but no distinct zonation of endolithic traces could be reconstructed. This phenomenon, however, is due to the effect that the differentiation of coastal endoliths is mostly based on colour pigments, but their traces morphologically fall all within the ichnogenus *Fascichnus* (Radtke and Golubic, 2005, 2011). The application of microbioerosion trace assemblages for coastal reconstruction, hence, seems difficult, but could be supported by traces of macrobioeroders and grazers, which are also known to produce characteristic trace fossil assemblages on rocky shores (e.g., De Gibert et al., 2012). Due to short exposure, only few grazing traces were observed during the coastal bioerosion experiment, but are expected, alongside with macroborers, to arrive with ongoing exposure. For that purpose, a whole set of substrates remained in place and will be recovered in later years. In contrast to microbioerosion traces, the correlation of macrobioerosion traces and living macrobioerosion agents, however, is much more difficult and often leaves even the phylum in doubt (Bromley, 2004). This was also demonstrated by the assessment of traces of boring sponges, *Entobia* ispp., during the long-term experiment, who showed a high variability with the nature and structure of the substrate, the quality of the surrounding environment, the proximity of other endoliths, the species of the boring sponge, and the ontogeny of the borer (Chapter 6).

In contrast to the application of microbioerosion ichnocoenoses for the reconstruction of relative bathymetry, previously only few ichnotaxa have been identified that could serve as proxy for the reconstruction of palaeotemperature, -salinity or -trophodynamics (Wisshak, 2012). One of them is the cold-water indicating fungal boring *Flagrichnus baiulus*, which has been observed in surprisingly high abundances during the summer, but was absent during the winter, presumably due to comparatively low temperatures during the summer (15–19 °C) and a distinct increase during winter (17–22 °C). This highlights that care must be taken to interpreting the occurrence of "cold-water species" as winter conditions. However, the experiment demonstrated that it is difficult to distinguish distinct effects of water temperature, salinity, and nutrient variations in field experiment, because they are often mutually interlinked. Further potential is here also offered from macrobioeroders such as boring sponges, which distributions and abundances, as well as their bioerosion rates, are dependent on environmental parameters such as water flow, nutrients, salinity, temperature, and light (see Schönberg, 2008 for a review). Previously, however, all presently available research on the correlation of sponge borings and boring sponges was carried out in Mediterranean Sea. Further studies are needed in order to ascertain whether

the observed correlations also apply to different biogeographic realms, and to better understand the application and limitations of sponge bioerosion traces as palaeoenvironmental indicators.

## 7.3 Longitudinal and latitudinal comparison to previous studies

Since the last two decades, a series of bioerosion experiments has been conducted investigating the effect of bioerosion within different environmental settings (see Wisshak, 2006 for a review). While long-term studies are previously limited to the tropical realm, based on short-term data from own experiments and the literature, Wisshak et al. (2010, 2011) have shown that microbioerosion follows a distinct latitudinal gradient with highest bioerosion intensities in the tropical Bahamas (Vogel et al., 1996, 2000), intermediate values in the warm-temperate Azores (Wisshak et al., 2010, 2011), and lowest values in the cold-temperate Swedish Kosterfjord (Wisshak, 2006). Because the herein presented short-experiments were carried out on a very similar approach as the latter experiments, the available data can be directly compared against each other. This is especially interesting as the Eastern Mediterranean Sea shows, in consequence of its restricted position, a distinctly different oceanographic setting than the North Atlantic Ocean (Chapter 2).

With respect to ichnodiversity, the Eastern Mediterranean Sea (34 ichnotaxa) shows comparatively similar values as the Kosterfjord (31 ichnotaxa), while the Azores show distinctly higher values than the Eastern Mediterranean (56 ichnotaxa), and lowest ichnodiversity was observed in the tropical Bahamas (14-25 ichnotaxa). This is likely an effect of the ultra-oligotrophic setting of the Eastern Mediterranean Sea, which is often called a marine desert (Azov, 1991), while the Azores on the other hand are located in the area of the Gulf Stream and are a biodiversity hotspot (Wisshak et al., 2010).

With respect to bioerosion rates, bioerosion rates measured during the carbonate cycling in the Eastern Mediterranean Sea (85 g $m^{-2}$ $yr^{-1}$), on a first glance appear very low in comparison to those reported from the tropical Bahamas (ca. 200 g $m^{-2}$ $yr^{-1}$), the warm-temperate Azores (640 g $m^{-2}$ $yr^{-1}$), and the Swedish Kosterfjord (144 g $m^{-2}$ $yr^{-1}$). However, it must be considered that the carbonate cycling experiment refers to 15 m water depth, but all other experiments to 0 m. As towards the intertidal microbioerosion rates, however, may increase 4–5 times (Wisshak et al., 2010), maximum values of about 350–450 g $m^{-2}$ $yr^{-1}$ can be expected in the Eastern Mediterranean Sea, lying intermediate between the Bahamas and the Azores. The limiting effect of nutrients may be thus balanced, for instance, by warmer temperature and better light illumination, but to identify the main reason is difficult because the effects of water temperature, salinity, and nutrients in the realm are closely interlinked and difficult to distinguish in the field. Future indication will be provided through an ongoing short-term experiment in the Western Mediterranean Sea (pers. comm. Wisshak), which will complete the first longitudinal transect spanning the oligotrophic Eastern Mediterranean marginal sea, over the mesotrophic Western Mediterranean, to the mesotrophic open oceanic Azores Archipelago.

Corresponding to the latitudinal gradient in microbioerosion, it may be suspected that also the diversity and intensity of macrobioeroders decreases towards higher latitudes. Some of the most active bioeroders in tropical environments are absent or play a minor role in high latitude settings, such as lithophag bivalves or sipunculid worms, and especially grazing fish, so that also macrobioerosion may reach highest values in tropical settings (Wisshak et al., 2011). To draw direct comparison between bioerosion rates from previous

long-term experiments in the tropics (Kiene and Hutchings, 1992, 1994; Peyrot-Clausade et al., 1995b; Pari et al., 1998, 2002; Osorno et al., 2005; Carreiro-Silva and McClanahan, 2012) and the herein presented long-term experiment, however, is difficult, because these experiments were based on coral substrates and assessed via image analysis. This underlines the necessity for further long-term studies, especially outside the tropical realm.

# 8 Outlook

Based on an interdisciplinary approach, this thesis contributed important information to the understanding of bioerosion in the marine realm. However, the results show that the process of bioerosion is complex and further research is needed to improving the application of bioerosion traces for palaeoenvironmental reconstruction, for deciphering global patterns in bioerosion, and for modelling the impact of bioerosion under different environmental conditions in the future. The main aspects are:

- The carbonate cycling experiment indicated indirect effects of water temperature, salinity, and nutrients on phototrophic and organotrophic microbioerosion agents. However, these are often mutually interlinked and difficult to distinguish in the field. Laboratory experiments are needed to deciphering these effects and for enhancing the reconstruction of palaeoenvironmental conditions based on bioerosion traces.
- While the application of microbioerosion trace assemblages for the reconstruction of light and relative bathymetry is quite advanced, this study revealed difficulties for the reconstruction of coastal zonation patterns. In order to further the application of microbioerosion assemblages for the reconstruction of coastal zonation patterns (probably based on macrobioerosion traces), a complete set of experimental substrates from the coastal bioerosion experiment remained in place, to be recovered and analysed in a couple of years.
- Bioerodering sponge distribution and abundance are dependent on environmental parameters such as water flow, nutrients, salinity, temperature, and light. Previously, however, the record on sponge bioerosion traces is limited to the Mediterranean Sea and an assignment of bioerosion trace and trace maker is difficult due to the high morphological variance of boring sponges. Further studies from different biogeographical regions are needed to better understand the application and limitations of sponge bioerosion traces as palaeoenvironmental indicators.
- During the course of this thesis, the application of micro-CT was introduced for the assessment of internal macrobioerosion. To further develop this approach for the automatic differentiation and quantification of bioerosion and accretion would significantly enhance the possibility for carbonate budgeting in different marine environments.
- Studies in the tropics showed that grazing significantly contributes to total bioerosion, but previously the record on grazing in the Mediterranean Sea is scarce (Sartoretto and Francour, 1997). Because from the material of the long-term experiment, no reference to the original substrate surface was provided, the volume of substrate removed by grazers was impossible to quantify. Assessing grazing rates would contribute important information to the understanding of bioerosion processes in the non-tropical realm
- In the last years, a series of experimental studies was carried out investigating bioerosion under different environmental conditions. While the understanding of microbioerosion patterns in different biogeographic realm is quite advanced, the record on macrobioerosion is previously almost limited to the tropical realm. Further long-term studies from the non-tropical realm are needed in order to better understand the impact of macrobioerosion in different environmental settings.

# 9 References


Acker, J.G., Leptoukh, G., 2007. Online analysis enhances use of NASA earth science data. Eos, Transactions American Geophysical Union 88, 14–17.

Akpan, E.B., Farrow, G.E., 1984. Shell-boring algae on the Scottish continental shelf: identification, distribution, bathymetric zonation. Transactions of the Royal Society of Edinburgh: Earth Sciences 75, 1–12.

Al-Thukair, A.A., Golubic, S., Rosen, G., 1994. New euendolithic cyanobacteria from the Bahama Bank and the Arabian Gulf: *Hyella racemus* sp. nov. Journal of Phycology 30, 764–769.

Anderson, M.J., Gorley, R.N., Clarke, K.R., 2008. PERMANOVA+ for PRIMER: Guide to Software and Statistical Methods. PRIMER-E, Plymouth, UK.

Azov, Y., 1991. Eastern Mediterranean—a marine desert? Marine Pollution Bulletin 23, 225–232.

Badde, A., Illerhaus, B., 2008. Three dimensional computerized microtomography in the analysis of sculpture. Scanning 30, 16–26.

Basso, D., Granier, B., 2012. Calcareous algae in changing environments. Geodiversitas 34, 5–11.

Bates, N.R., Astor, Y.M., Church, M.J., Currie, K., Dore, J.E., González-Dávila, M., Lorenzoni, L., Muller-Karger, F., Olafsson, J., Santa-Casiano, J.M., 2014. A time-series view of changing ocean chemistry due to ocean uptake of anthropogenic $CO_2$ and ocean acidification. Oceanography 27, 126–141.

Baum, D., Titschack, J., subm. Cavity and pore segmentation in 3D images with ambient occlusion, Eurographics Conference on Visualization (EuroVis), Cagliari, Italy, 25–29 May 2015.

Bavestrello, G., Bonito, M., Sarà, M., 1993. Influence of depth on the size of sponge spicules. Scientia Marina 57, 415–420.

Becker, L.C., Reaka-Kudla, M.L., 1997. The use of tomography in assessing bioerosion in corals, in: Lessios, H.A., Macintyre, I.G. (Eds.), Proceedings of the 8th International Coral Reef Symposium Vol. 2, Smithsonian Tropical Research Institute, Panama, 24–29 June 1996, 1819–1824.

Bertling, M., Braddy, S.J., Bromley, R.G., Demathieu, G.R., Genise, J., Mikuláš, R., Nielsen, J.K., Nielsen, K.S.S., Rindsberg, A.K., Schlirf, M., Uchman, A., 2006. Names for trace fossils: a uniform approach. Lethaia 39, 265–286.

Betzler, C., Brachert, T.C., Nebelsick, J., 1997. The warm temperate carbonate province: a review of the facies, zonations, and delimitations. Courier Forschungsinstitut Senckenberg 201, 83–99.

Beuck, L., Vertino, A., Stepina, E., Karolczak, M., Pfannkuche, O., 2007. Skeletal response of *Lophelia pertusa* (Scleractinia) to bioeroding sponge infestation visualised with micro-computed tomography. Facies 53, 157–176.

Beuck, L., Wisshak, M., Munnecke, A., Freiwald, A., 2008. A giant boring in a Silurian stromatoporoid analysed by computer tomography. Acta Palaeontologica Polonica 53, 149–160.

Blissett, D.J., Pickerill, R.K., Rigby, J.K., 2006. A new species of boring sponge from the White Limestone Group, Jamaica. Caribbean Journal of Science 42, 247–251.

Bongiorni, L., Dini, F., 2002. Distribution and abundance of thraustochytrids in different Mediterranean coastal habitats. Aquatic Microbial Ecology 30, 49–56.

Bornet, E., Flahault, C., 1888. Note sur deux nouveaux genres d'algues perforantes. Journal de Botanique [Morot] 2, 161–165.

Bornet, E., Flahault, C., 1889. Sur quelques plantes vivant dans le test calcaire des mollusques. Bulletin de la Société Botanique de France 36, 147–176.

Boyer, T.P., Antonov, J.I., Baranova, O.K., Coleman, C., Garcia, H.E., Grodsky, A., Johnson, D.R., Locarnini, R.A., Mishonov, A.V., O'Brien, T.D., Paver, C.R., Reagan, J.R., Seidov, D., Smolyar, I.V., Zweng, M.M., 2013. World Ocean Database 2013, in: Levitus, S., Mishonov, A. (Eds.), NOAA Atlas NESDIS 72, Silver Spring, MD, pp. 209.

Bromley, R.G., 1970. Borings as trace fossils and *Entobia cretacea* Portlock, as an example, in: Crimes, T.P., Harper, J.C. (Eds.), Trace Fossils. Geological Journal Special Issue 3, pp. 49–90.

Bromley, R.G., 1975. Comparative analysis of fossil and recent echinoid bioerosion. Palaeontology 18, 725–739.

Bromley, R.G., 1994. The paleoecology of bioerosion, in: Donovan, S.K. (Ed.), The Palaeobiology of Trace Fossils. Wiley, Chichester, pp. 135–154.

Bromley, R.G., 2004. A stratigraphy of marine bioerosion. Geological Society London Special Publications 228, 455–479.

Bromley, R.G., D'Alessandro, A., 1983. Bioerosion in the Pleistocene of southern Italy: ichnogenera *Caulostrepsis* and *Maeandropolydora*. Rivista Italiana di Paleontologia e Stratigrafia 89, 283–309.

Bromley, R.G., D'Alessandro, A., 1984. The ichnogenus *Entobia* from the Miocene, Pliocene and Pleistocene of southern Italy. Rivista Italiana di Paleontologia e Stratigrafia 90, 227–296.

Bromley, R.G., D'Alessandro, A., 1989. Ichnological study of shallow marine endolithic sponges from the Italian coast. Rivista Italiana di Paleontologia e Stratigrafia 95, 279–314.

Bromley, R.G., Fürsich, F.T., 1980. Comments on the proposed amendments to the International Code of Zoological Nomenclature regarding ichnotaxa. Bulletin of Zoological Nomenclature 37, 6–10.

Bromley, R.G., Heinberg, C., 2006. Attachment strategies of organisms on hard substrates: a palaeontological view. Palaeogeography, Palaeoclimatology, Palaeoecology 232, 429–453.

Bromley, R.G., Martinell, J., 1991. *Centrichnus*, new ichnogenus for centrically patterned attachment scars on skeletal substrates. Bulletin of the Geological Society of Denmark 38, 243–252.

Bromley, R.G., Schönberg, C.H.L., 2008. Borings, bodies and ghosts: spicules of the endolithic sponge *Aka akis* sp. nov. within the boring *Entobia cretacea*, Cretaceous, England, in: Wisshak, M., Tapanila, L. (Eds.), Current Developments in Bioerosion. Springer Berlin, pp. 235–248.

Bromley, R.G., Tendal, O.S., 1973. Example of substrate competition and phobotropism between two clionid sponges. Journal of Zoology 169, 151–155.

Bromley, R.G., Hanken, N.-M., Asgaard, U., 1990. Shallow marine bioerosion: preliminary results of an experimental study. Bulletin of the Geological Society of Denmark 38, 85–99.

Bromley, R.G., Wisshak, M., Glaub, I., Botquelen, A., 2007. Ichnotaxonomic review of dendriniform borings attributed to foraminifera: *Semidendrina* igen. nov, in: Miller III, W. (Ed.), Trace fossils: Concepts, Problems, Prospects. Elsevier, Amsterdam, pp. 518–530.

Bromley, R.G., Beuck, L., Ruggiero, E.T., 2008. Endolithic sponge versus terebratulid brachiopod, Pleistocene, Italy: accidental symbiosis, bioclaustration and deformity, in: Wisshak, M., Tapanila, L. (Eds.), Current Developments in Bioerosion. Springer, Berlin, pp. 361–368.

Budd, D.A., Perkins, R.D., 1980. Bathymetric zonation and paleoecological significance of microborings in Puerto Rican shelf and slope sediments. Journal of Sedimentary Research 50, 881–903.

Calcinai, B., Bavestrello, G., Cuttone, G., Cerrano, C., 2011. Excavating sponges from the Adriatic Sea: description of *Cliona adriatica* sp. nov. (Demospongiae: Clionaidae) and estimation of its boring activity. Journal of the Marine Biological Association of the United Kingdom 91, 339–346.

Carannante, G., Esteban, M., Milliman, J.D., Simone, L., 1988. Carbonate lithofacies as paleolatitude indicators: problems and limitations. Sedimentary Geology 60, 333–346.

Carballo, J.L., Sanchez-Moyano, J.E., Garcia-Gomez, J.C., 1994. Taxonomic and ecological remarks on boring sponges (Clionidae) from the Straits of Gibraltar (southern Spain): tentative bioindicators? Zoological Journal of the Linnean Society 112, 407–424.

Carreiro-Silva, M., McClanahan, T.R., 2012. Macrobioerosion of dead branching *Porites*, 4 and 6 years after coral mass mortality. Marine Ecology Progress Series 458, 103–122.

Carreiro-Silva, M., McClanahan, T.R., Kiene, W.E., 2005. The role of inorganic nutrients and herbivory in controlling microbioerosion of carbonate substratum. Coral Reefs 24, 214–221.

Carreiro-Silva, M., McClanahan, T.R., Kiene, W.E., 2009. Effects of inorganic nutrients and organic matter on microbial euendolithic community composition and microbioerosion rates. Marine Ecology Progress Series 392, 1–15.

Carreiro-Silva, M., Kiene, W.E., Golubic, S., McClanahan, T.R., 2012. Phosphorus and nitrogen effects on microbial euendolithic communities and their bioerosion rates. Marine Pollution Bulletin 64, 602–613.

Castenholz, R.W., Garcia-Pichel, F., 2012. Cyanobacterial responses to UV radiation, in: Whitton, B.A. (Ed.), Ecology of Cyanobacteria II. Springer, Netherlands, 481–499.

Chazottes, V., 1996. Étude expérimentale de la bioérosion et de la sédimentogénèse en milieu récifal, effects de l'eutrophisation (Île de la Réunion, Océan Indien). Océanographic (Géologie Marine) 323, 787–794.

Chazottes, V., Le Campion-Alsumard, T., Peyrot-Clausade, M., 1995. Bioerosion rates on coral reefs: interactions between macroborers, microborers and grazers (Moorea, French Polynesia). Palaeogeography, Palaeoclimatology, Palaeoecology 113, 189–198.

Chazottes, V., Le Campion-Alsumard, T., Peyrot-Clausade, M., Cuet, P., 2002. The effects of eutrophication-related alterations to coral reef communities on agents and rates of bioerosion (Reunion Island, Indian Ocean). Coral Reefs 21, 375–390.

Christomanos, A.A., Norton, A.B., 1974. Beiträge zur Kenntnis der Pigmente der Schwämme *Aplysina aerophoba* und *Clione schmidtii*. Folia Biochemica et Biologica Graeca 11, 10–20.

Clarke, K.R., 1993. Non-parametric multivariate analyses of changes in community structure. Australian Journal of Ecology 18, 117–143.

Clarke, K.R., Gorley, R.N., 2006. PRIMER v6: User Manual/Tutorial. PRIMER-E, Plymouth.

Corriero, G., Scalera Liaci, L., Ruggiero, D., Pansini, M., 2000. The sponge community of a semi-submerged Mediterranean cave. Marine Ecology 21, 85–96.

Crook, E.D., Cohen, A.L., Rebolledo-Vieyra, M., Hernandez, L., Paytan, A., 2013. Reduced calcification and lack of acclimatization by coral colonies growing in areas of persistent natural acidification. PNAS 110, 11044–11049.

Davies, P.J., Hutchings, P.A., 1983. Initial colonization, erosion and accretion of coral substrate. Coral Reefs 2, 27–35.

DeCarlo, T.M., Cohen, A.L., Barkley, H.C., Cobban, Q., Young, C., Shamberger, K.E., Brainard, R.E., Golbuu, Y., 2015. Coral macrobioerosion is accelerated by ocean acidification and nutrients. Geology 43, 7–10.

De Gibert, J.M., Domènech, R., Martinell, J., 2012. Rocky Shorelines, in: Knaust, D., Bromley, R.G. (Eds.), Trace Fossils as Indicators of Sedimentary Environments, Elsevier, Amsterdam, pp. 441–462.

De Groot, R.A., 1977. Boring sponges (Clionidae) and their trace fossils from the coast near Rovinj (Yugoslavia). Geologie en Mijnbouw 56, 168–181.

De Paula, T.S., Zilberberg, C., Hajdu, E., Lôbo-Hajdu, G., 2012. Morphology and molecules on opposite sides of the diversity gradient: Four cryptic species of the *Cliona celata* (Porifera, Demospongiae) complex in South America revealed by mitochondrial and nuclear markers. Molecular Phylogenetics and Evolution 62, 529–541.

De Waele, J., Furlani, S., 2013. Seawater and biokarst effects on coastal limestones, in: Shroder, J.F., Frumkin, A. (Eds.), Treatise on Geomorphology. Academic Press, San Diego, pp. 341–350.

Devescovi, M., Iveša, L., 2008. Colonization patterns of the date mussel *Lithophaga lithophaga* (L., 1758) on limestone breakwater boulders of a marina. Periodicum Biologorum 110, 339–346.

Ehling-Schulz, M., Scherer, S., 1999. UV protection in cyanobacteria. European Journal of Phycology 34, 329–338.

EMODnet, 2015. Portal for Bathymetry, available at: http://www.emodnet-bathymetry.eu.

Ercegovic, A., 1927. Tri nova roda litofiskih cijanoiceja sa jadranske obale. Acta Botanica Instituti Botanici Universitatis Zagrebensis 2, 78–84.

Ercegovic, A., 1929. Sur quelques nouveaux types des Cyanophycées lithophytes de la côte Adriatique. Archiv für Protistenkunde 66, 164–174.

Ercegovic, A., 1932. Ekoloske i socioloske studije o litofitskim cijanoficejama sa Jugoslavenske obale Jadrana. Bulletin international de l'Académie Yougoslave des Sciences et des beaux-arts. Classe des sciences mathématiques et naturelles 26, 129–220.

Fang, J.K.H., Mello-Athayde, M.A., Schönberg, C.H.L., Kline, D.I., Hoegh-Guldberg, O., Dove, S., 2013. Sponge biomass and bioerosion rates increase under ocean warming and acidification. Global Change Biology 19, 3581–3591.

Färber, C., Wisshak, M., Pyko, I., Bellou, N., Freiwald, A., 2015. Effects of water depth, seasonal exposure, and substrate orientation on microbial bioerosion in the Ionian Sea (Eastern Mediterranean). PLoS ONE 10, e0126495.

Färber, C., Titschack, J., Schönberg, C.H.L., Ehrig, K., Boos, K., Baum, D., Illerhaus, B., Asgaard, U., Bromley, R.G., Freiwald, A., Wisshak, M., subm. Long-term development of macrobioerosion in the Mediterranean Sea assessed by micro-computed tomography. Biogeosciences.

Feldkamp, L.A., Davis, L.C., Kress, J.W., 1984. Practical cone-beam algorithm. Journal of the Optical Society of America A 1, 612–619.

Fischer, M.P., 1868. Recherches sur les éponges perforantes fossiles. Nouvelles Archives du Museum d'Histoire Naturelle de Paris 4, 117–174.

Fornós, J.J., Ahr, W.M., 2006. Present-day temperate carbonate sedimentation on the Balearic Platform, western Mediterranean: compositional and textural variation along a low-energy isolated ramp. Geological Society, London, Special Publications 255, 71–84.

Garcia-Pichel, F., 2006. Plausible mechanisms for the boring on carbonates by microbial phototrophs. Sedimentary Geology 185, 205–213.

Garcia-Pichel, F., Ramírez-Reinat, E., Gao, Q., 2010. Microbial excavation of solid carbonates powered by P-type ATPase-mediated transcellular $Ca^{2+}$ transport. PNAS 107, 21749–21754.

Glaub, I., 1994. Mikrobohrspuren in ausgewählten Ablagerungsräumen des europäischen Jura und der Unterkreide (Klassifikation und Palökologie). Courier Forschungsinstitut Senckenberg 174, 1–324.

Glaub, I., Vogel, K., 2004. The stratigraphic record of microborings. Fossils and Strata 51, 126–135.

Glaub, I., Vogel, K., Gektidis, M., 2001. The role of modern and fossil cyanobacterial borings in bioerosion and bathymetry. Ichnos 8, 185–195.

Glaub, I., Golubic, S., Gektidis, M., Radtke, G., Vogel, K., 2007. Microborings and microbial endoliths: geological implications, in: Miller III, W. (Ed.), Trace Fossils: Concepts, Problems, Prospects. Elsevier, Amsterdam, pp. 368–381.

Glynn, P.W., 1997. Bioerosion and coral-reef growth: a dynamic balance, in: Birkeland, C. (Ed.), Life and Death of Coral Reefs. Chapman and Hall, New York, pp. 68–95.

Golubic, S., Radtke, G., 2008. The trace *Rhopalia clavigera* isp. n. reflects the development of its maker *Eugomontia sacculata* Kornmann, 1960, in: Wisshak, M., Tapanila, L. (Eds.), Current Developments in Bioerosion. Springer, Berlin, pp. 95–108.

Golubic, S., Brent, G., Le Campion, T., 1970. Scanning electron microscopy of endolithic algae and fungi using a multipurpose casting-embedding technique. Lethaia 3, 203–209.

Golubic, S., Perkins, R.D., Lukas, K.J., 1975. Boring microorganisms and microborings in carbonate substrates, in: Frey, R.W. (Ed.), The Study of Trace Fossils. Springer, Berlin, pp. 229–259.

Golubic, S., Krumbein, W., Schneider, J., 1979. The carbon cycle, in: Trudinger, P.A., Swaine, D.J. (Eds.), Biogeochemical Cycling of Mineral-forming Elements. Elsevier, Amsterdam, pp. 29–45.

Golubic, S., Friedmann, E.I., Schneider, J., 1981. The lithobiontic ecological niche, with special reference to microorganisms. Journal of Sedimentary Research 51, 475–478.

Golubic, S., Radtke, G., Le Campion-Alsumard, T., 2005. Endolithic fungi in marine ecosystems. Trends in Microbiology 13, 229–235.

Grange, J.S., Rybarczyk, H., Tribollet, A., 2015. The three steps of the carbonate biogenic dissolution process by microborers in coral reefs (New Caledonia). Environmental Science and Pollution Research International 22, 13625–13637.

Grant, R.E., 1826. Notice of a new zoophyte (*Cliona celata*, Gr.) from the Firth of Forth. Edinburgh New Philosophical Journal 1, 78–81.

Greuter, W., McNeill, J., Barrie, F.R., Burdet, H.M., Demoulin, V., Filgueiras, T.S., Nicholson, D.H., Silva, P.C., Skog, J.E., Trehane, P., Turland, N.J., Hawksworth D.L., 2000. International Code of Botanical Nomenclature (Saint Louis Code), Proceedings of the 16th International Botany Congress, St. Louis, Missouri, July–August 1999, Koelz Scientific Books, Königstein.

Günther, A., 1990. Distribution and bathymetric zonation of shell-boring endoliths in recent reef and shelf environments: Cozumel, Yucatan (Mexico). Facies 22, 233–261.

Hancock, A., 1849. On the excavating powers of certain sponges belonging to the genus *Cliona*; with descriptions of several new species, and an allied generic form. Annals and Magazine of Natural History, 3, 321–348.

Hanken, N.-M., Bromley, R.G., Miller, J., 1996. Plio-Pleistocene sedimentation in coastal grabens, north-east Rhodes, Greece. Geological Journal 31, 393–418.

Hassan, M., 1998. Modification of Carbonate Substrata by Bioerosion and Bioaccretion on Coral reefs of the Red Sea. Shaker, Aachen.

Heindel, K., Wisshak, M., Westphal, H., 2009. Microbioerosion in Tahitian reefs: a record of environmental change during the last deglacial sea-level rise (IODP 310). Lethaia 42, 322–340.

Hoegh-Guldberg, O., Mumby, P.J., Hooten, A.J., Steneck, R.S., Greenfield, P., Gomez, E., Harvell, C.D., Sale, P.F., Edwards, A.J., Caldeira, K., Knowlton, N., Eakin, C.M., Iglesias-Prieto, R., Muthiga, N., Bradbury, R.H., Dubi, A., Hatziolos, M.E., 2007. Coral reefs under rapid climate change and ocean acidification. Science 318, 1737–1742.

Hoeksema, B.W., 1983. Excavation patterns and spiculae dimensions of the boring sponge *Cliona celata* from the SW Netherlands. Senckenbergiana maritima 15, 55–85.

Hoffman, E.J., 1985. Distribution patterns of recent microbial endoliths in the intertidal and supratidal zones, Bermuda. SEPM Special Publications 35, 179–194.

Hoffman, L., 1999. Marine cyanobacteria in tropical regions: diversity and ecology. European Journal of Phycology 34, 371–379.

Hoskin, C.M., Reed, J.K., Mook, D.H., 1986. Production and off-bank transport of carbonate sediment, Black Rock, southwest Little Bahama Bank. Marine Geology 73, 125–144.

Hutchings, P.A., 1986. Biological destruction of coral reefs: a review. Coral Reefs 4, 239–252.

Hutchings, P.A., Kiene, W.E., Cunningham, R.B., Donnelly, C., 1992. Spatial and temporal patterns of non-colonial boring organisms (polychaetes, sipunculans and bivalve molluscs) in *Porites* at Lizard Island, Great Barrier Reef. Coral Reefs 11, 23–31.

Hutchings, P., Peyrot-Clausade, M., Osnorno, A., 2005. Influence of land runoff on rates and agents of bioerosion of coral substrates. Marine Pollution Bulletin 51, 438–447.

International Commission on Zoological Nomenclature, 1999. International Code of Zoological Nomenclature, Fourth Edition. Natural History Museum, London.

Johnson, M.E., 1988. Why are ancient rocky shores so uncommon? The Journal of Geology 96, 469–480.

Kennedy, E.V., Perry, C.T., Halloran, P.R., Iglesias-Prieto, R., Schönberg, C.H.L., Wisshak, M., Form, A.U., Carricart-Ganivet, J.P., Fine, M., Eakin, C.M., Mumby, P.J., 2013. Avoiding coral reef functional collapse requires local and global action. Current Biology 23, 912–918.

Khanaev, S.A., Kuleshov, A.F., 1992. Measurements of water transparency south-west of Greece, in: Resvanis, L.K. (Ed.), Proceedings of the 2nd NESTOR International Workshop, Pylos, Greece, 19–21 October 1992, pp. 253–269.

Kiene, W.E., 1985. Biological destruction of experimental coral substrates at Lizard Island (Great Barrier Reef, Australia). in: Harmelin Vivien, M., Salvat, B. (Eds.), Proceedings of the Fifth International Coral Reef Congress, Tahiti, pp. 339–344.

Kiene, W.E., 1988. A model of bioerosion on the Great Barrier Reef, in: Choat, J.H., Barnes, D., Borowitzka, M.A., Coll, J.C., Davies, P.J., Flood, P., Hatcher, B.G., Hopley, D., Hutchings, P.A., Kinsey, D., Orme, G.R., Pichon, M., Sale, P.F., Sammarco, P.W., Wallace, C.C., Wilkinson, C., Wolanski, E., Bellwood, O. (Eds.), Proceedings of the 6th International Coral Reef Symposium 3, Townsville, Australia, 8–12 August 1988, pp. 449–454.

Kiene, W.E., 1997. Enriched nutrients and their impact on bioerosion: results from ENCORE, in: Lessios, H.A., Macintyre, I.G. (Eds.), Proceedings of the 8th International Coral Reef Symposium 1, Smithsonian Tropical Research Institute, Panama, 24–29 June 1996, pp. 897–902.

Kiene, W.E., Hutchings, P.A., 1992. Long-term bioerosion of experimental coral substrates from Lizard Island, Great Barrier Reef, in: Richmond, R.H. (Ed.), Proceedings of the 7th International Coral Reef Symposium 1, UOG Station, Guam, 22–27 June 1992, pp. 397–403.

Kiene, W.E., Hutchings, P.A., 1994. Bioerosion experiments at Lizard Island, Great Barrier Reef. Coral Reefs 13, 91–98.

Klein, B., Roether, W., Manca, B.B., Bregant, D., Beitzel, V., Kovacevic, V., Luchetta, A., 1999. The large deep water transient in the Eastern Mediterranean. Deep Sea Research Part I 46, 371–414.

Kobluk, D.R., Risk, M.J., 1977. Rate and nature of infestation of a carbonate substratum by a boring alga. Journal of Experimental Marine Biology and Ecology 27, 107–115.

Kroeker, K.J., Kordas, R.L., Crim, R.N., Singh, G.G., 2010. Meta-analysis reveals negative yet variable effects of ocean acidification on marine organisms. Ecology Letters 13, 1419–1434.

Krom, M.D., Brenner, S., Kress, N., Neori, A., Gordon, L.I., 1992. Nutrient dynamics and new production in a warm-core eddy from the Eastern Mediterranean Sea. Deep Sea Research Part A 39, 467–480.

Krom, M.D., Groom, S., Zohary, T., 2012. The Eastern Mediterranean, in: Black, K.D., Shimmield, G.B. (Eds.), Biogeochemistry of Marine Systems. Blackwell, Cornwall, pp. 91–126.

Krom, M., Kress, N., Berman-Frank, I., Rahav, E., 2014. Past, present and future patterns in the nutrient chemistry of the Eastern Mediterranean, in: Goffredo, S., Dubinsky, Z. (Eds.), The Mediterranean Sea. Springer, Netherlands, pp. 49–68.

Kucuksezgin, F., Balci, A., Kontas, A., Altay, O., 1995. Distribution of nutrients and chlorophyll-a in the Aegean Sea. Oceanologica Acta 18, 343–352.

Le Campion-Alsumard, T., 1975. Etude expérimentale de la colonisation d'éclats de calcite par les cyanophycées endolithes marines. Cahiers de Biologie Marine 16, 177–185.

Le Campion-Alsumard, T., 1978. Les cyanophycées endolithes marines. Systématique, ultrastructure, écologie et biodestruction. Thèse University Aix-Marseille II.

Le Campion-Alsumard, T., 1979. Les cyanophycées endolithes marines. Systématique, ultrastructure, écologie et biodestruction. Oceanologica Acta 2, 143–156.

Le Campion-Alsumard, T., Golubic, S., 1985. *Hyella caespitosa* Bornet et Flahault and *Hyella balani* Lehmann (Pleurocapsales, Cyanophyta): a comparative study. Algological Studies/Archiv für Hydrobiologie Supplement Volumes 38–39, 119–148.

Leal, C.V., De Paula, T.S., Lôbo-Hajdu, G., Schönberg, C.H.L., Esteves, E.L., 2015. Morphological and molecular systematics of the '*Cliona viridis* complex' from south-eastern Brazil. Journal of the Marine Biological Association of the United Kingdom, doi: 10.1017/S0025315415001642.

Lekkas, E., Papanikolaou, D., Sakellariou, D., 1993. Neotectonic map of Greece, Rhodes island (scale: 1:100.000). University of Athens, Athens.

Lescinsky, H.L., Hill, M., Hoedt, B.A., 2008. Results of long-term bioerosion study: Belize patch reefs, Proceedings of the 11th International Coral Reef Symposium, Florida, 26–30.

Lionello, P., Malanotte-Rizzoli, P., Boscolo, R., 2006. Mediterranean climate variability. Elsevier, Amsterdam.

Lionello, P., Abrantes, F., Congedi, L., Dulac, F., Gacic, M., Gomis, D., Goodess, C., Hoff, H., Kutiel, H., Luterbacher, J., Planton, S., Reale, M., Schröder, K., Struglia, M.V., Toreti, A., Tsimplis, M., Ulbrich, U., Xoplaki, E., 2012. Introduction: Mediterranean Climate—Background Information, in: Lionello, P. (Ed.), The Climate of the Mediterranean Region: from the Past to the Future. Elsevier, Oxford, pp. 35–90.

Lüning, K., 1985. Meeresbotanik: Verbreitung, Ökophysiologie und Nutzung der marinen Makroalgen. Thieme, Stuttgart.

Malanotte-Rizzoli, P., Manca, B.B., D'Alcalà, M.R., Theocharis, A., Bergamasco, A., Bregant, D., Budillon, G., Civitarese, G., Georgopoulos, D., Michelato, A., Sansone, E., Scarazzato, P., Souvermezoglou, E., 1997. A synthesis of the Ionian Sea hydrography, circulation and water mass pathways during POEM-Phase I. Progress in Oceanography 39, 153–204.

Mater Group, 2001. MTP II-MATER Database. Field observation inventories, data sets and documentation. A project of the European Commission's Marine Science and Technology Programme (MAS3-CT96-0051). CD-ROM. IFREMER, Brest.

Mayoral, E., 1987. Acción bioerosiva de Mollusca (Gastropoda, Bivalvia) en el Plioceno inferior de la Cuenca del Bajo Guadalquivir. Revista Española de Paleontología 2, 49–58.

Millot, C., Taupier-Letage, I., 2005. Circulation in the Mediterranean Sea, in: Saliot, A. (Ed.), The Mediterranean Sea. Springer, Berlin, pp. 29–66.

Mutti, E., Orombelli, G., Pozzi, R., 1970. Geological studies on the Dodecanese Islands (Aegean Sea) IX: Geological map of the island of Rhodos (Greece); Explanatory Notes. Annales Géologiques des Pays Helléniques 22, 77–226.

Neumann, A.C., 1966. Observations on coastal erosion in Bermuda and measurements of the boring rate of the sponge, *Cliona lampa*. Limnology and Oceanography 11, 92–108.

Nittis, K., Pinardi, N., Lascaratos, A., 1993. Characteristics of the summer 1987 flow field in the Ionian Sea. Journal of Geophysical Research: Oceans 98, 10171–10184.

Osler, E., 1826. On burrowing and boring marine animals. Philosophical Transactions of the Royal Society of London 116, 342–371.

Osorno, A., Peyrot-Clausade, M., Hutchings, P.A., 2005. Patterns and rates of erosion in dead *Porites* across the Great Barrier Reef (Australia) after 2 years and 4 years of exposure. Coral Reefs 24, 292–303.

Paerl, H.W., Huisman, J., 2008. Blooms like it hot. Science 320, 57–58.

Pantazidou, A., Louvrou, I., Economou-Amilli, A., 2006. Euendolithic shell-boring cyanobacteria and chlorophytes from the saline lagoon Ahivadolimni on Milos Island, Greece. European Journal of Phycology 41, 189–200.

Pari, N., Peyrot-Clausade, M., Le Campion-Alsumard, T., Hutchings, P., Chazottes, V., Golubic, S., Le Campion, J., Fontaine, M.F., 1998. Bioerosion of experimental substrates on high islands and on atoll lagoons (French Polynesia) after two years of exposure. Marine Ecology Progress Series 166, 119–130.

Pari, N., Peyrot-Clausade, M., Hutchings, P.A., 2002. Bioerosion of experimental substrates on high islands and atoll lagoons (French Polynesia) during 5 years of exposure. Journal of Experimental Marine Biology and Ecology 276, 109–127.

Pérès, J.-M., Picard, J., 1964. Nouveau manuel de bionomie benthique de la Mer Méditerranée. Recueil des Travaux de la Station marine d'Endoume, 31, 1-137.

Perkins, R.D., Tsentas, C.I., 1976. Microbial infestation of carbonate substrates planted on the St. Croix shelf, West Indies. Geological Society of America Bulletin 87, 1615–1628.

Perry, C.T., Macdonald, I.A., 2002. Impacts of light penetration on the bathymetry of reef microboring communities: implications for the development of microendolithic trace assemblages. Palaeogeography, Palaeoclimatology, Palaeoecology 186, 101–113.

Peyrot-Clausade, M., Le Campion-Alsumard, T., Harmelin-Vivien, M., Romano, J.-C., Chazottes, V., Pari, N., Le Campion, J., 1995a. La bioérosion dans le cycle des carbonates: essais de quantification des precessus en Polynésie francaise. Bulletin de la Société Géologique de France 166, 85–94.

Peyrot-Clausade, M., Le Campion-Alsumard, T., Hutchings, P., Le Campion, J., Payri, C., Fontaine, M.-F., 1995b. Initial bioerosion and bioaccretion on experimental substrates in high island and atoll lagoons (French Polynesia). Oceanologica Acta 18, 531–541.

Poulos, S.E., Drakopoulos, P.G., Collins, M.B., 1997. Seasonal variability in sea surface oceanographic conditions in the Aegean Sea (Eastern Mediterranean): an overview. Journal of Marine Systems 13, 225–244.

Radtke, G., 1991. Die mikroendolithischen Spurenfossilien im Alt-Tertiär West-Europas und ihre palökologische Bedeutung. Courier Forschungsinstitut Senckenberg 138, 1–185.

Radtke, G., Golubic, S., 2005. Microborings in mollusk shells, Bay of Safaga, Egypt: Morphometry and ichnology. Facies 51, 118–134.

Radtke, G., Golubic, S., 2011. Microbial euendolithic assemblages and microborings in intertidal and shallow marine habitats: insight in cyanobacterial speciation, in: Reitner, J., Quéric, N.-V., Arp, G. (Eds.), Advances in Stromatolite Geobiology. Springer, Berlin, pp. 233–263.

Radtke, G., Le Campion-Alsumard, T., Golubić, S., 1996. Microbial assemblages of the bioerosional "notch" along tropical limestone coasts. Algological Studies/Archiv für Hydrobiologie, Supplement Volumes 83, 469–482.

Rasband, W.S., 1997–2015. ImageJ. U. S. National Institutes of Health, Bethesda, http://imagej.nih.gov/ij/.

Reaka-Kudla, M.L., Feingold, J.S., Glynn, W., 1996. Experimental studies of rapid bioerosion of coral reefs in the Galápagos Islands. Coral Reefs 15, 101–107.

Reitner, J., Keupp, H., 1991. The fossil record of the haplosclerid excavating sponge *Aka* de Laubenfels, in: Reitner, J., Keupp, H. (Eds.), Fossil and Recent Sponges. Springer, Berlin, pp. 102–120.

Ridgwell, A.J., Zeebe, R.E., 2005. The role of the global carbonate cycle in the regulation and evolution of the Earth system. Earth and Planetary Science Letters 234, 299–315.

Ridley, S.O., 1881. Account of the zoological collections made during the surveys of the H. M. S. "Alert" in the Strait of Magellan and on the coast of Patagonia X. Spongida, Proceedings of the Zoological Society of London, pp. 107–139.

Robinson, A.R., Leslie, W.G., Theocharis, A., Lascaratos, A., 2001. Ocean circulation currents: Mediterranean Sea circulation, in: Turekian, K.K., Thorpe, S.A. (Eds.), Encyclopedia of Ocean Sciences. Academic Press, London, pp. 1689–1706.

Roether, W., Manca, B.B., Klein, B., Bregant, D., Georgopoulos, D., Beitzel, V., Kovačević, V., Luchetta, A., 1996. Recent changes in Eastern Mediterranean deep waters. Science 271, 333–335.

Rosell, D., Uriz, M.-J., 1991. *Cliona viridis* (Schmidt, 1862) and *Cliona nigricans* (Schmidt, 1862)(Porifera, Hadromerida): evidence which shows they are the same species. Ophelia 33, 45–53.

Rosell, D., Uriz, M.-J., 2002. Excavating and endolithic sponge species (Porifera) from the Mediterranean: species descriptions and identification key. Organisms Diversity & Evolution 2, 55–86.

Rosell, D., Uriz, M.-J., Martin, D., 1999. Infestation by excavating sponges on the oyster (*Ostrea edulis*) populations of the Blanes littoral zone (north-western Mediterranean Sea). Journal of the Marine Biological Association of the UK 79, 409–413.

Rützler, K., 1975. The role of burrowing sponges in bioerosion. Oecologia 19, 203–216.

Rützler, K., Bromley, R.G., 1981. *Cliona rhodensis*, new species (Porifera: Hadromerida) from the Mediterranean. Proceedings of the Biological Society of Washington 94, 1219–1225.

Sammarco, P.W., Risk, M.J., 1990. Large-scale patterns in internal bioerosion of *Porites*: cross continental shelf trends on the Great Barrier Reef. Marine Ecology Progress Series 59, 145–156.

Sartoretto, S., 1998. Bioérosion des concrétions coralligènes de Méditerranée par les organismes perforants: essai de quantification des processus. Comptes Rendus de l'Académie des Sciences - Series IIA - Earth and Planetary Science 327, 839–844.

Sartoretto, S., Francour, P., 1997. Quantification of bioerosion by Sphaerechinus granularis on 'coralligene' concretions of the western Mediterranean. Journal of the Marine Biological Association UK 77, 565-568.

Schlitzer, R., 2014–2015. Ocean Data View, https://odv.awi.de/.

Schmidt, H., 1992. Mikrobohrspuren ausgewählter Faziesbereiche der tethyalen und germanischen Trias (Beschreibung, Vergleich und bathymetrische Interpretation). Frankfurter Geowissenschaftliche Arbeiten A 12, 1–228.

Schmidt, O., 1862. Die Spongien des Adriatischen Meeres. Engelmann, Leipzig.

Schneider, J., 1976. Biological and inorganic factors in the destruction of limestone coasts, Contributions to Sedimentology 6, 1–112.

Schön, J.H., 2011. Physical Properties of Rocks: a Workbook, Elsevier, Amsterdam.

Schönberg, C.H.L., 2001. Estimating the extent of endolithic tissue of a Great Barrier Reef clionid sponge. Senckenbergiana maritima 31, 29–39.

Schönberg, C.H.L., 2008. A history of sponge erosion: from past myths and hypotheses to recent approaches, in: Wisshak, M., Tapanila, L. (Eds.), Current Developments in Bioerosion. Springer, Berlin, pp. 165–202.

Schönberg, C.H.L., Shields, G., 2008. Micro-computed tomography for studies on *Entobia*: transparent substrate versus modern technology, in: Wisshak, M., Tapanila, L. (Eds.), Current Developments in Bioerosion. Springer, Berlin, pp. 147–164.

Schönberg, C.H.L., Tapanila, L., 2006. Bioerosion research before and after 1996 – a discussion of what has changed since the First International Bioerosion Workshop. Ichnos 13, 99–102.

Schönberg, C.H.L., Wisshak, M., 2014. Marine bioerosion, in: Goffredo, S., Dubinsky, Z. (Eds.), The Mediterranean Sea. Springer, Netherlands, pp. 449–461.

Scott, P.J.B., Moser, K.A., Risk, M.J., 1988. Bioerosion of concrete and limestone by marine organisms: a 13 year experiment from Jamaica. Marine Pollution Bulletin 19, 219–222.

Silbiger, N.J., Guadayol, O., Thomas, F.I.M., Donahue, M.J., 2014. Reefs shift from net accretion to net erosion along a natural environmental gradient. Marine Ecology Progress Series 515, 33–44.

Skliris, N., 2014. Past, present and future patterns of the thermohaline circulation and characteristic water masses of the Mediterranean Sea, in: Goffredo, S., Dubinsky, Z. (Eds.), The Mediterranean Sea. Springer, Netherlands, pp. 29–48.

Smith, A., Lott, N., Vose, R., 2011. The Integrated Surface Database: recent developments and partnerships. Bulletin of the American Meteorological Society 92, 704–708.

Smith, S.V., Kimmerer, W.J., Laws, E.A., Brock, R.E., Walsh, T.W., 1981. Kaneohe Bay sewage diversion experiment: perspectives on ecosystem responses to nutritional perturbation. Pacific Science 35, 279–395.

Stalling, D., Westerhof, M., Hege, H.-C., 2005. Amira: a highly interactive system for visual data analysis, in: Hansen, C.D., Johnson, C.R. (Eds.), The Visualization Handbook. Elsevier Butterworth-Heinemann, Burlington, pp. 749–767.

Stambler, N., 2014. The Mediterranean Sea – primary productivity, in: Goffredo, S., Dubinsky, Z. (Eds.), The Mediterranean Sea. Springer, Netherlands, pp. 113–121.

Stavrakakis, S., Gogou, A., Krasakopoulou, E., Karageorgis, A.P., Kontoyiannis, H., Rousakis, G., Velaoras, D., Perivoliotis, L., Kambouri, G., Stavrakaki, I., Lykousis, V., 2013. Downward fluxes of sinking particulate matter in the deep Ionian Sea (NESTOR site), eastern Mediterranean: seasonal and interannual variability. Biogeosciences 10, 7235–7254.

Stephenson, T.A., Stephenson, A., 1949. The universal features of zonation between tide-marks on rocky coasts. Journal of Ecology 37, 289–305.

Stubler, A.D., Furman, B.T., Peterson, B.J., 2014. Effects of $pCO_2$ on the interaction between an excavating sponge, *Cliona varians*, and a hermatypic coral, *Porites furcata*. Marine Biology 161, 1851–1859.

Taboroši, D., Kázmér, M., 2013. Erosional and depositional textures and structures in coastal karst landscapes, in: Lace, M.J., Mylroie, J.E. (Eds.), Coastal Karst Landforms. Springer, Netherlands, pp. 15–57.

Titschack, J., Baum, D., De Pol-Holz, R., López Correa, M., Forster, N., Flögel, S., Hebbeln, D., Freiwald, A., 2015. Aggradation and carbonate accumulation of Holocene Norwegian cold-water coral reefs. Sedimentology 62, 1873–1898.

Topsent, E., 1888. Contribution à l'étude des Clionides. Archives de zoologie expérimentale et générale 5, 1–165.

Tribollet, A., 2008. The boring microflora in modern coral reef ecosystems: a review of its roles, in: Wisshak, M., Tapanila, L. (Eds.), Current Developments in Bioerosion. Springer, Berlin, pp. 67–94.

Tribollet, A., Golubic, S., 2005. Cross-shelf differences in the pattern and pace of bioerosion of experimental carbonate substrates exposed for 3 years on the northern Great Barrier Reef, Australia. Coral Reefs 24, 422–434.

Tribollet, A., Decherf, G., Hutchings, P., Peyrot-Clausade, M., 2002. Large-scale spatial variability in bioerosion of experimental coral substrates on the Great Barrier Reef (Australia): importance of microborers. Coral Reefs 21, 424–432.

Tribollet, A., Godinot, C., Atkinson, M., Langdon, C., 2009. Effects of elevated $pCO_2$ on dissolution of coral carbonates by microbial euendoliths. Global Biogeochemical Cycles 23, GB3008.

Tribollet, A., Radtke, G., Golubic, S., 2011. Bioerosion, in: Reitner, J., Thiel, V. (Eds.), Encyclopedia of Geobiology. Springer, Netherlands, pp. 117–134.

Trimonis, E., Rudenko, M., 1992. Geomorphology and bottom sediments of the Pylos area, in: Resvanis, L.K. (Ed.), Proceedings of the 2nd NESTOR International Workshop, Pylos, Greece, 19–21 October 1992, pp. 321–339.

UNEP/MAP, 2012. State of the Mediterranean Marine and Coastal Environment, UNEP/MAP, Barcelona Convention, Athens.

Vogel, K., Bundschuh, M., Glaub, I., Hofmann, K., Radtke, G., Schmidt, H., 1995. Hard substrate ichnocoenoses and their relations to light intensity and marine bathymetry. Neues Jahrbuch fur Geologie und Paläontologie-Abhandlungen 195, 49–61.

Vogel, K., Kiene, W.E., Gektidis, M., Radtke, G., 1996. Scientific results from investigations of microbial borers and bioerosion in reef environments. Göttinger Arbeiten zur Geologie und Paläontologie Sonderband 2, 139–143.

Vogel, K., Gektidis, M., Golubic, S., Kiene, W.E., Radtke, G., 2000. Experimental studies on microbial bioerosion at Lee Stocking Island, Bahamas and One Tree Island, Great Barrier Reef, Australia: implications for paleoecological reconstructions. Lethaia 33, 190–204.

Vogel, K., Schäfer, H., Glaub, I., 2008. Spurengemeinschaften bohrender Mikroorganismen. Natur und Museum 138, 184–189.

Voigt, E., 1977. On grazing traces produced by the radula of fossil and recent gastropods and chitons, in: Crimes, T.P., Harper, J.C. (Eds.), Trace Fossils 2. Geological Journal Special Issue 9, pp. 335–346.

Walker, S.E., 2007. Traces of gastropod predation on molluscan prey in tropical reef environments, in: Miller III, W. (Ed.), Trace Fossils: Concepts, Problems, and Prospects. Elsevier, Amsterdam, pp. 324–344.

Warme, J.E., 1975. Borings as trace fossils, and the processes of marine bioerosion, in: Frey, R.W. (Ed.), The Study of Trace Fossils. Springer, Berlin, pp. 181–227.

Wilson, M.A., 2007. Macroborings and the evolution of marine bioerosion, in: Milller, W. (Ed.), Trace Fossils: Concepts, Problems, Prospects. Elsevier, Amsterdam, pp. 356–367.

Wilson, S., Blake, C., Berges, J.A., Maggs, C.A., 2004. Environmental tolerances of free-living coralline algae (maerl): implications for European marine conservation. Biological Conservation 120, 279–289.

Wisshak, M., 2006. High-latitude Bioerosion: the Kosterfjord Experiment. Springer, Berlin.

Wisshak, M., 2008. Two new dwarf *Entobia* ichnospecies in a diverse aphotic ichnocoenosis (Pleistocene/Rhodes, Greece), in: Wisshak, M., Tapanila, L. (Eds.), Current Developments in Bioerosion. Springer, Berlin, pp. 213–233.

Wisshak, M., 2012. Microbioerosion, in: Knaust, D., Bromley, R.G. (Eds.), Trace Fossils as Indicators of Sedimentary Environments. Elsevier, Amsterdam, pp. 213–243.

Wisshak, M., Porter, D., 2006. The new ichnogenus *Flagrichnus* – a paleoenvironmental indicator for cold-water settings? Ichnos 13, 135–145.

Wisshak, M., Gektidis, M., Freiwald, A., Lundälv, T., 2005. Bioerosion along a bathymetric gradient in a cold-temperate setting (Kosterfjord, SW Sweden): an experimental study. Facies 51, 93–117.

Wisshak, M., Form, A., Jakobsen, J., Freiwald, A., 2010. Temperate carbonate cycling and water mass properties from intertidal to bathyal depths (Azores). Biogeosciences 7, 2379–2396.

Wisshak, M., Tribollet, A., Golubic, S., Jakobsen, J., Freiwald, A., 2011. Temperate bioerosion: ichnodiversity and biodiversity from intertidal to bathyal depths (Azores). Geobiology 9, 492–520.

Wisshak, M., Schönberg, C.H.L., Form, A., Freiwald, A., 2012. Ocean acidification accelerates reef bioerosion. PLoS ONE 7, e45124.

Wisshak, M., Schönberg, C.H.L., Form, A., Freiwald, A., 2013. Effects of ocean acidification and global warming on reef bioerosion – lessons from a clionaid sponge. Aquatic Biology 19, 111–127.

Wisshak, M., Alexandrakis, E., Hoppenrath, M., 2014a. The diatom attachment scar *Ophthalmichnus lyolithon* igen. et isp. n. Ichnos 21, 111–118.

Wisshak, M., Schönberg, C.H.L., Form, A., Freiwald, A., 2014b. Sponge bioerosion accelerated by ocean acidification across species and latitudes? Helgoland Marine Research 68, 253–262.

Wisshak, M., Berning, B., Jakobsen, J., Freiwald, A., 2015. Temperate carbonate production: biodiversity of calcareous epiliths from intertidal to bathyal depths (Azores). Marine Biodiversity, 87–112.

Xavier, J.R., Rachello-Dolmen, P.G., Parra-Velandia, F., Schönberg, C.H.L., Breeuwer, J.A.J., van Soest, R.W.M., 2010. Molecular evidence of cryptic speciation in the "cosmopolitan" excavating sponge *Cliona celata* (Porifera, Clionaidae). Molecular Phylogenetics and Evolution 56, 13–20.

Zavatarelli, M., Mellor, G.L., 1995. A numerical study of the Mediterranean Sea circulation. Journal of Physical Oceanography 25, 1384–1414.

Zervakis, V., Georgopoulos, D., Karageorgis, A.P., Theocharis, A., 2004. On the response of the Aegean Sea to climatic variability: a review. International Journal of Climatology 24, 1845–1858.

# Appendix

## Appendix A: Supplementary information for Chapter 4

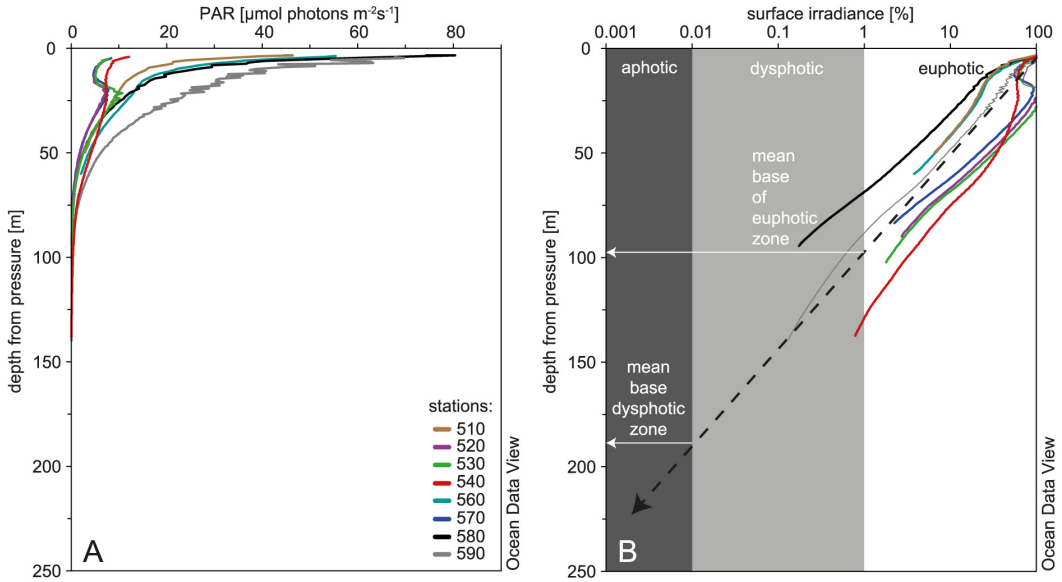


Figure A1 (A) Measurements of the photosynthetically active radiation (PAR; unit: µmol photons $m^{-2}$ $s^{-1}$), which were carried out during the MATER cruise in May 1996 in the Ionian Sea (38). (B) Semi-logarithmic plot of corrected PAR values expressed as percent of the surface irradiance measured just below the water surface. Dashed line suggests a mean base of the euphotic zone (1% surface irradiance) in ca. 100 m of water depth and a base of the dysphotic zone (0.01 % surface irradiance) in ca. 180 m. Graphs were displayed with Ocean Data View (Schlitzer, 2014–2015).

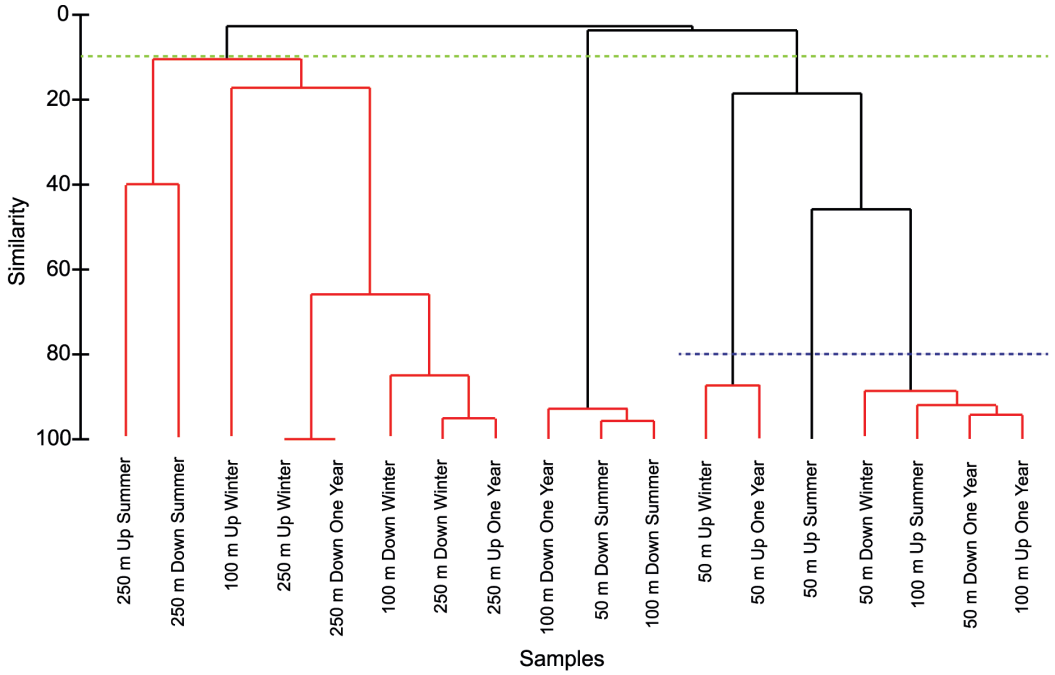


Figure A2 Group-average cluster analysis of bioerosion traces from 50–250 m water depth calculated based on Bray-Curtis-Similarity. Homogenous groups were coloured red during a similarity profile routine (SIMPROF) identifying three main clusters (green line = similarity of 10). The right cluster can be further subdivided in three subclusters (blue line = similarity of 80).

Table A1 Mean values of water temperature measurements during the carbonate cycling experiment in 15, 50, 100, and 250 m. Due to the loss of a platform no data is available from the 15 m winter deployment. Due to data loss no values are available from the 250 m winter and all one year platforms.

| Exposure | Water temperature (°C) | | | |
|---|---|---|---|---|
| | 15 m | 50 m | 100 m | 250 m |
| February 2008 | 15.19 | 15.15 | 14.95 | 14.63 |
| March 2008 | 15.51 | 15.22 | 14.94 | 14.57 |
| April 2008 | 15.93 | 15.13 | 14.83 | 14.48 |
| May 2008 | 17.44 | 15.13 | 14.84 | 14.52 |
| June 2008 | 18.60 | 15.36 | 14.90 | 14.54 |
| July 2008 | 21.74 | 15.96 | 14.91 | 14.51 |
| August 2008 | 24.45 | 17.26 | 14.93 | 14.52 |
| September 2008 | 24.44 | 17.07 | 14.83 | 14.46 |
| October 2008 | 21.67 | 18.25 | 15.00 | 14.41 |
| November 2008 | | 18.89 | 14.91 | |
| December 2008 | | 17.97 | 15.50 | |
| January 2009 | | 16.64 | 16.29 | |
| Februrary 2009 | | 15.69 | 15.36 | |
| March 2009 | | 15.07 | 15.04 | |
| April 2009 | | 15.11 | 15.07 | |

Table A2 Bioerosion, accretion, and net limestone erosion rates measured during the carbonate cycling experiment experiment.

| Depth (m) | Orientation | Exposure | Substrate | # Panel | Accretion rates ($g\ m^{-2}\ yr^{-1}$) | Bioerosion rates ($g\ m^{-2}\ yr^{-1}$) | Net limestone erosion rates ($g\ m^{-2}\ yr^{-1}$) |
|---|---|---|---|---|---|---|---|
| 15 | Down | Summer | Limestone | 357 | 190.31 | 18.24 | 172.07 |
| 15 | Down | Summer | Limestone | 339 | 130.71 | 26.53 | 104.18 |
| 15 | Down | Summer | Limestone | 412 | 99.07 | 21.55 | 77.51 |
| 15 | Down | Summer | Limestone | 330 | 219.05 | 28.19 | 190.86 |
| 15 | Down | Summer | Limestone | 498 | 110.97 | 23.21 | 87.76 |
| 15 | Down | Summer | Limestone | 367 | 148.73 | 26.53 | 122.20 |
| 15 | Down | Summer | PVC | 574 | 57.75 | | |
| 15 | Down | Summer | PVC | 473 | 62.61 | | |
| 15 | Down | Summer | PVC | 439 | 72.97 | | |
| 15 | Down | Summer | PVC | 479 | 82.54 | | |
| 15 | Down | Summer | PVC | 386 | 84.79 | | |
| 15 | Down | Summer | PVC | 444 | 64.15 | | |
| 15 | Up | Summer | Limestone | 353 | 28.19 | 81.25 | -53.06 |
| 15 | Up | Summer | Limestone | 362 | 33.16 | 79.59 | -46.43 |
| 15 | Up | Summer | Limestone | 414 | 29.85 | 77.93 | -48.08 |
| 15 | Up | Summer | Limestone | 411 | 36.48 | 92.85 | -56.37 |
| 15 | Up | Summer | Limestone | 337 | 28.19 | 54.72 | -26.53 |
| 15 | Up | Summer | Limestone | 342 | 34.82 | 101.14 | -66.32 |
| 15 | Up | Summer | PVC | 452 | 13.56 | | |
| 15 | Up | Summer | PVC | 480 | 16.46 | | |
| 15 | Up | Summer | PVC | 401 | 8.36 | | |
| 15 | Up | Summer | PVC | 477 | 23.00 | | |
| 15 | Up | Summer | PVC | 405 | 11.46 | | |
| 15 | Up | Summer | PVC | 403 | 14.14 | | |
| 15 | Down | One Year | Limestone | 177 | 185.81 | 37.72 | 148.09 |
| 15 | Down | One Year | Limestone | 190 | 164.69 | 34.90 | 129.79 |
| 15 | Down | One Year | Limestone | 91 | 115.52 | 36.78 | 78.74 |
| 15 | Down | One Year | Limestone | 214 | 200.07 | 26.41 | 173.67 |
| 15 | Down | One Year | Limestone | 440 | 337.64 | 40.55 | 297.08 |
| 15 | Down | One Year | Limestone | 157 | 274.04 | 27.35 | 246.69 |
| 15 | Down | One Year | PVC | 365 | 54.38 | | |
| 15 | Down | One Year | PVC | 368 | 52.42 | | |
| 15 | Down | One Year | PVC | 321 | 36.81 | | |
| 15 | Down | One Year | PVC | 493 | 40.54 | | |
| 15 | Down | One Year | PVC | 511 | 38.52 | | |
| 15 | Down | One Year | PVC | 508 | 53.72 | | |
| 15 | Up | One Year | Limestone | 301 | 19.60 | 94.31 | -74.71 |
| 15 | Up | One Year | Limestone | 407 | 20.98 | 120.72 | -99.73 |
| 15 | Up | One Year | Limestone | 194 | 21.10 | 69.79 | -48.69 |

Table A2 Continued.

| Depth (m) | Orientation | Exposure | Substrate | # Panel | Accretion rates ($g\ m^{-2}\ yr^{-1}$) | Bioerosion rates ($g\ m^{-2}\ yr^{-1}$) | Net limestone erosion rates ($g\ m^{-2}\ yr^{-1}$) |
|---|---|---|---|---|---|---|---|
| 15 | Up | One Year | Limestone | 410 | 21.13 | 83.94 | -62.81 |
| 15 | Up | One Year | Limestone | 456 | 23.26 | 85.82 | -62.57 |
| 15 | Up | One Year | Limestone | 155 | 17.11 | 61.30 | -44.19 |
| 15 | Up | One Year | PVC | 521 | 5.07 | | |
| 15 | Up | One Year | PVC | 517 | 6.48 | | |
| 15 | Up | One Year | PVC | 518 | 6.49 | | |
| 15 | Up | One Year | PVC | 516 | 8.66 | | |
| 15 | Up | One Year | PVC | 523 | 7.43 | | |
| 15 | Up | One Year | PVC | 331 | 9.71 | | |
| 50 | Down | Summer | Limestone | 496 | 72.57 | 16.58 | 55.99 |
| 50 | Down | Summer | Limestone | 495 | 291.52 | 21.55 | 269.97 |
| 50 | Down | Summer | Limestone | 454 | 139.61 | 18.24 | 121.37 |
| 50 | Down | Summer | Limestone | 372 | 146.37 | 18.24 | 128.14 |
| 50 | Down | Summer | Limestone | 446 | 155.86 | 14.92 | 140.94 |
| 50 | Down | Summer | Limestone | 510 | 97.26 | 16.58 | 80.68 |
| 50 | Down | Summer | PVC | 500 | 420.52 | | |
| 50 | Down | Summer | PVC | 499 | 160.30 | | |
| 50 | Down | Summer | PVC | 564 | 213.43 | | |
| 50 | Down | Summer | PVC | 504 | 63.62 | | |
| 50 | Down | Summer | PVC | 407 | 45.55 | | |
| 50 | Down | Summer | PVC | 408 | 139.99 | | |
| 50 | Up | Summer | Limestone | 368 | 61.35 | 29.85 | 31.50 |
| 50 | Up | Summer | Limestone | 377 | 86.25 | 26.53 | 59.72 |
| 50 | Up | Summer | Limestone | 453 | 91.06 | 36.48 | 54.58 |
| 50 | Up | Summer | Limestone | 448 | 49.21 | 23.21 | 26.00 |
| 50 | Up | Summer | Limestone | 421 | 83.33 | 26.53 | 56.81 |
| 50 | Up | Summer | Limestone | 383 | 111.80 | 31.50 | 80.30 |
| 50 | Up | Summer | PVC | 530 | 94.24 | | |
| 50 | Up | Summer | PVC | 503 | 56.08 | | |
| 50 | Up | Summer | PVC | 501 | 102.77 | | |
| 50 | Up | Summer | PVC | 561 | 11.46 | | |
| 50 | Up | Summer | PVC | 553 | 35.40 | | |
| 50 | Up | Summer | PVC | 532 | 64.07 | | |
| 50 | Down | Winter | Limestone | 459 | 24.06 | 15.31 | 8.75 |
| 50 | Down | Winter | Limestone | 182 | 47.44 | 4.37 | 43.07 |
| 50 | Down | Winter | Limestone | 213 | 78.28 | 0.00 | 78.28 |
| 50 | Down | Winter | Limestone | 164 | 48.91 | 0.00 | 48.91 |
| 50 | Down | Winter | Limestone | 181 | 0.00 | 0.00 | 0.00 |
| 50 | Down | Winter | Limestone | 3 | 60.35 | 0.00 | 60.35 |

Table A2 Continued.

| Depth (m) | Orientation | Exposure | Substrate | # Panel | Accretion rates (g $m^{-2}$ $yr^{-1}$) | Bioerosion rates (g $m^{-2}$ $yr^{-1}$) | Net limestone erosion rates (g $m^{-2}$ $yr^{-1}$) |
|---|---|---|---|---|---|---|---|
| 50 | Down | Winter | PVC | 460 | 38.74 | | |
| 50 | Down | Winter | PVC | 507 | 47.18 | | |
| 50 | Down | Winter | PVC | 483 | 40.97 | | |
| 50 | Down | Winter | PVC | 424 | 65.25 | | |
| 50 | Down | Winter | PVC | 385 | 32.06 | | |
| 50 | Down | Winter | PVC | 362 | 36.94 | | |
| 50 | Up | Winter | Limestone | 180 | 236.79 | 8.75 | 228.04 |
| 50 | Up | Winter | Limestone | 158 | 44.36 | 17.50 | 26.86 |
| 50 | Up | Winter | Limestone | 86 | 21.89 | 6.56 | 15.33 |
| 50 | Up | Winter | Limestone | 154 | 39.46 | 2.19 | 37.27 |
| 50 | Up | Winter | Limestone | 81 | 34.10 | 2.19 | 31.91 |
| 50 | Up | Winter | Limestone | 191 | 42.80 | 10.94 | 31.87 |
| 50 | Up | Winter | PVC | 462 | 16.64 | | |
| 50 | Up | Winter | PVC | 498 | 39.50 | | |
| 50 | Up | Winter | PVC | 642 | 19.40 | | |
| 50 | Up | Winter | PVC | 425 | 23.27 | | |
| 50 | Up | Winter | PVC | 458 | 34.60 | | |
| 50 | Up | Winter | PVC | 440 | 23.40 | | |
| 50 | Down | One Year | Limestone | 441 | 260.86 | 16.03 | 244.82 |
| 50 | Down | One Year | Limestone | 475 | 283.41 | 20.75 | 262.66 |
| 50 | Down | One Year | Limestone | 434 | 234.27 | 13.20 | 221.07 |
| 50 | Down | One Year | Limestone | 503 | 267.49 | 26.41 | 241.08 |
| 50 | Down | One Year | Limestone | 469 | 319.10 | 16.03 | 303.07 |
| 50 | Down | One Year | Limestone | 479 | 152.40 | 15.09 | 137.31 |
| 50 | Down | One Year | PVC | 349 | 278.34 | | |
| 50 | Down | One Year | PVC | 526 | 254.30 | | |
| 50 | Down | One Year | PVC | 496 | 229.85 | | |
| 50 | Down | One Year | PVC | 641 | 137.65 | | |
| 50 | Down | One Year | PVC | 505 | 225.65 | | |
| 50 | Down | One Year | PVC | 509 | 258.62 | | |
| 50 | Up | One Year | Limestone | 429 | 60.36 | 35.84 | 24.52 |
| 50 | Up | One Year | Limestone | 467 | 84.43 | 37.72 | 46.70 |
| 50 | Up | One Year | Limestone | 436 | 44.99 | 31.12 | 13.86 |
| 50 | Up | One Year | Limestone | 500 | 34.89 | 40.55 | -5.67 |
| 50 | Up | One Year | Limestone | 435 | 27.35 | 30.18 | -2.83 |
| 50 | Up | One Year | Limestone | 461 | 108.65 | 38.67 | 69.98 |
| 50 | Up | One Year | PVC | 495 | 89.50 | | |
| 50 | Up | One Year | PVC | 524 | 29.42 | | |
| 50 | Up | One Year | PVC | 513 | 14.44 | | |

Table A2 Continued.

| Depth (m) | Orientation | Exposure | Substrate | # Panel | Accretion rates ($g\ m^{-2}\ yr^{-1}$) | Bioerosion rates ($g\ m^{-2}\ yr^{-1}$) | Net limestone erosion rates ($g\ m^{-2}\ yr^{-1}$) |
|---|---|---|---|---|---|---|---|
| 50 | Up | One Year | PVC | 323 | 39.69 | | |
| 50 | Up | One Year | PVC | 366 | 52.80 | | |
| 50 | Up | One Year | PVC | 535 | 88.73 | | |
| 100 | Down | Summer | Limestone | 333 | 94.28 | 13.26 | 81.01 |
| 100 | Down | Summer | Limestone | 417 | 128.85 | 4.97 | 123.87 |
| 100 | Down | Summer | Limestone | 352 | 113.21 | 6.63 | 106.58 |
| 100 | Down | Summer | Limestone | 371 | 92.09 | 3.32 | 88.77 |
| 100 | Down | Summer | Limestone | 340 | 89.88 | 6.63 | 83.25 |
| 100 | Down | Summer | Limestone | 328 | 98.21 | 9.95 | 88.26 |
| 100 | Down | Summer | PVC | 427 | 76.87 | | |
| 100 | Down | Summer | PVC | 402 | 49.66 | | |
| 100 | Down | Summer | PVC | 397 | 100.28 | | |
| 100 | Down | Summer | PVC | 478 | 68.25 | | |
| 100 | Down | Summer | PVC | 394 | 52.43 | | |
| 100 | Down | Summer | PVC | 430 | 58.23 | | |
| 100 | Up | Summer | Limestone | 473 | 54.40 | 6.63 | 47.77 |
| 100 | Up | Summer | Limestone | 338 | 68.26 | 13.26 | 55.00 |
| 100 | Up | Summer | Limestone | 359 | 81.64 | 6.63 | 75.01 |
| 100 | Up | Summer | Limestone | 363 | 44.57 | 9.95 | 34.62 |
| 100 | Up | Summer | Limestone | 346 | 36.97 | 0.00 | 36.97 |
| 100 | Up | Summer | Limestone | 365 | 65.16 | 6.63 | 58.53 |
| 100 | Up | Summer | PVC | 573 | 64.76 | | |
| 100 | Up | Summer | PVC | 463 | 60.19 | | |
| 100 | Up | Summer | PVC | 433 | 33.86 | | |
| 100 | Up | Summer | PVC | 578 | 56.41 | | |
| 100 | Up | Summer | PVC | 527 | 47.37 | | |
| 100 | Up | Summer | PVC | 465 | 31.40 | | |
| 100 | Down | Winter | Limestone | 179 | 10.78 | 0.00 | 10.78 |
| 100 | Down | Winter | Limestone | 135 | 18.18 | 0.00 | 18.18 |
| 100 | Down | Winter | Limestone | 299 | 13.58 | 2.19 | 11.40 |
| 100 | Down | Winter | Limestone | 465 | 14.61 | 8.75 | 5.86 |
| 100 | Down | Winter | Limestone | 172 | 13.52 | 2.19 | 11.33 |
| 100 | Down | Winter | Limestone | 185 | 22.48 | 2.19 | 20.30 |
| 100 | Down | Winter | PVC | 450 | 0.94 | | |
| 100 | Down | Winter | PVC | 422 | 6.41 | | |
| 100 | Down | Winter | PVC | 541 | 4.29 | | |
| 100 | Down | Winter | PVC | 461 | 3.22 | | |
| 100 | Down | Winter | PVC | 455 | 6.08 | | |
| 100 | Down | Winter | PVC | 357 | 1.86 | | |

Table A2 Continued.

| Depth (m) | Orientation | Exposure | Substrate | # Panel | Accretion rates (g $m^{-2}$ $yr^{-1}$) | Bioerosion rates (g $m^{-2}$ $yr^{-1}$) | Net limestone erosion rates (g $m^{-2}$ $yr^{-1}$) |
|---|---|---|---|---|---|---|---|
| 100 | Up | Winter | Limestone | 5 | 60.17 | 0.00 | 60.17 |
| 100 | Up | Winter | Limestone | 395 | 12.23 | 2.19 | 10.04 |
| 100 | Up | Winter | Limestone | 409 | 22.66 | 0.00 | 22.66 |
| 100 | Up | Winter | Limestone | 68 | 15.31 | 2.19 | 13.12 |
| 100 | Up | Winter | Limestone | 163 | 9.95 | 15.31 | -5.36 |
| 100 | Up | Winter | Limestone | 12 | 10.94 | 0.00 | 10.94 |
| 100 | Up | Winter | PVC | 475 | 1.66 | | |
| 100 | Up | Winter | PVC | 409 | 7.66 | | |
| 100 | Up | Winter | PVC | 417 | 5.14 | | |
| 100 | Up | Winter | PVC | 423 | 6.10 | | |
| 100 | Up | Winter | PVC | 456 | 3.74 | | |
| 100 | Up | Winter | PVC | 454 | 3.65 | | |
| 100 | Down | One Year | Limestone | 343 | 73.92 | 5.66 | 68.26 |
| 100 | Down | One Year | Limestone | 320 | 44.64 | 1.89 | 42.75 |
| 100 | Down | One Year | Limestone | 325 | 99.87 | 12.26 | 87.61 |
| 100 | Down | One Year | Limestone | 349 | 38.94 | 7.54 | 31.40 |
| 100 | Down | One Year | Limestone | 329 | 29.69 | 4.72 | 24.97 |
| 100 | Down | One Year | Limestone | 322 | 64.91 | 9.43 | 55.48 |
| 100 | Down | One Year | PVC | 393 | 52.92 | | |
| 100 | Down | One Year | PVC | 383 | 47.63 | | |
| 100 | Down | One Year | PVC | 387 | 81.89 | | |
| 100 | Down | One Year | PVC | 392 | 19.57 | | |
| 100 | Down | One Year | PVC | 406 | 35.43 | | |
| 100 | Down | One Year | PVC | 404 | 39.35 | | |
| 100 | Up | One Year | Limestone | 366 | 31.78 | 13.20 | 18.58 |
| 100 | Up | One Year | Limestone | 360 | 29.59 | 4.72 | 24.87 |
| 100 | Up | One Year | Limestone | 324 | 44.66 | 10.37 | 34.28 |
| 100 | Up | One Year | Limestone | 351 | 17.05 | 2.83 | 14.22 |
| 100 | Up | One Year | Limestone | 413 | 21.99 | 6.60 | 15.39 |
| 100 | Up | One Year | Limestone | 326 | 32.37 | 4.72 | 27.65 |
| 100 | Up | One Year | PVC | 575 | 6.27 | | |
| 100 | Up | One Year | PVC | 525 | 20.80 | | |
| 100 | Up | One Year | PVC | 502 | 12.01 | | |
| 100 | Up | One Year | PVC | 563 | 18.40 | | |
| 100 | Up | One Year | PVC | 579 | 12.87 | | |
| 100 | Up | One Year | PVC | 604 | 10.35 | | |
| 250 | Down | Summer | Limestone | 332 | 8.29 | 3.32 | 4.97 |
| 250 | Down | Summer | Limestone | 391 | 0.00 | 8.29 | -8.29 |
| 250 | Down | Summer | Limestone | 452 | 10.16 | 4.97 | 5.19 |

Table A2 Continued.

| Depth (m) | Orientation | Exposure | Substrate | # Panel | Accretion rates (g $m^{-2}$ $yr^{-1}$) | Bioerosion rates (g $m^{-2}$ $yr^{-1}$) | Net limestone erosion rates (g $m^{-2}$ $yr^{-1}$) |
|---|---|---|---|---|---|---|---|
| 250 | Down | Summer | Limestone | 381 | 8.52 | 8.29 | 0.23 |
| 250 | Down | Summer | Limestone | 420 | 6.68 | 0.00 | 6.68 |
| 250 | Down | Summer | Limestone | 476 | 8.29 | 14.92 | -6.63 |
| 250 | Down | Summer | PVC | 580 | 3.81 | | |
| 250 | Down | Summer | PVC | 441 | 4.74 | | |
| 250 | Down | Summer | PVC | 437 | 3.20 | | |
| 250 | Down | Summer | PVC | 435 | 3.55 | | |
| 250 | Down | Summer | PVC | 418 | 0.05 | | |
| 250 | Down | Summer | PVC | 420 | 3.66 | | |
| 250 | Up | Summer | Limestone | 455 | 13.26 | 1.66 | 11.61 |
| 250 | Up | Summer | Limestone | 373 | 9.95 | 3.32 | 6.63 |
| 250 | Up | Summer | Limestone | 449 | 9.95 | 1.66 | 8.29 |
| 250 | Up | Summer | Limestone | 493 | 9.95 | 4.97 | 4.97 |
| 250 | Up | Summer | Limestone | 419 | 8.29 | 0.00 | 8.29 |
| 250 | Up | Summer | Limestone | 489 | 11.92 | 0.00 | 11.92 |
| 250 | Up | Summer | PVC | 494 | 0.12 | | |
| 250 | Up | Summer | PVC | 372 | 0.50 | | |
| 250 | Up | Summer | PVC | 445 | 1.14 | | |
| 250 | Up | Summer | PVC | 474 | 4.39 | | |
| 250 | Up | Summer | PVC | 520 | 0.41 | | |
| 250 | Up | Summer | PVC | 419 | 0.45 | | |
| 250 | Down | Winter | Limestone | 196 | 4.28 | 2.14 | 2.14 |
| 250 | Down | Winter | Limestone | 170 | 4.54 | 0.00 | 4.54 |
| 250 | Down | Winter | Limestone | 304 | 12.91 | 0.00 | 12.91 |
| 250 | Down | Winter | Limestone | 492 | 8.82 | 0.00 | 8.82 |
| 250 | Down | Winter | Limestone | 400 | 15.33 | 0.00 | 15.33 |
| 250 | Down | Winter | Limestone | 408 | 4.28 | 0.00 | 4.28 |
| 250 | Down | Winter | PVC | 451 | 31.14 | | |
| 250 | Down | Winter | PVC | 552 | 4.52 | | |
| 250 | Down | Winter | PVC | 382 | 3.36 | | |
| 250 | Down | Winter | PVC | 360 | 2.48 | | |
| 250 | Down | Winter | PVC | 355 | 1.80 | | |
| 250 | Down | Winter | PVC | 583 | 2.23 | | |
| 250 | Up | Winter | Limestone | 168 | 17.28 | 0.00 | 17.28 |
| 250 | Up | Winter | Limestone | 159 | 17.18 | 0.00 | 17.18 |
| 250 | Up | Winter | Limestone | 464 | 11.12 | 6.43 | 4.69 |
| 250 | Up | Winter | Limestone | 398 | 15.08 | 0.00 | 15.08 |
| 250 | Up | Winter | Limestone | 458 | 17.18 | 2.14 | 15.03 |
| 250 | Up | Winter | Limestone | 240 | 10.73 | 0.00 | 10.73 |

Table A2 Continued.

| Depth (m) | Orientation | Exposure | Substrate | # Panel | Accretion rates (g $m^{-2}$ $yr^{-1}$) | Bioerosion rates (g $m^{-2}$ $yr^{-1}$) | Net limestone erosion rates (g $m^{-2}$ $yr^{-1}$) |
|---|---|---|---|---|---|---|---|
| 250 | Up | Winter | PVC | 358 | 0.00 | | |
| 250 | Up | Winter | PVC | 457 | 0.24 | | |
| 250 | Up | Winter | PVC | 543 | 0.77 | | |
| 250 | Up | Winter | PVC | 356 | 0.00 | | |
| 250 | Up | Winter | PVC | 359 | 0.00 | | |
| 250 | Up | Winter | PVC | 361 | 0.00 | | |
| 250 | Down | One Year | Limestone | 488 | 7.33 | 0.94 | 6.38 |
| 250 | Down | One Year | Limestone | 433 | 6.22 | 0.94 | 5.28 |
| 250 | Down | One Year | Limestone | 512 | 10.63 | 0.00 | 10.63 |
| 250 | Down | One Year | Limestone | 513 | 9.43 | 0.00 | 9.43 |
| 250 | Down | One Year | Limestone | 507 | 8.86 | 1.89 | 6.97 |
| 250 | Down | One Year | Limestone | 478 | 6.40 | 3.77 | 2.63 |
| 250 | Down | One Year | PVC | 335 | 3.20 | | |
| 250 | Down | One Year | PVC | 399 | 0.46 | | |
| 250 | Down | One Year | PVC | 371 | 1.59 | | |
| 250 | Down | One Year | PVC | 344 | 1.33 | | |
| 250 | Down | One Year | PVC | 336 | 0.97 | | |
| 250 | Down | One Year | PVC | 515 | 0.37 | | |
| 250 | Up | One Year | Limestone | 477 | 5.68 | 0.00 | 7.56 |
| 250 | Up | One Year | Limestone | 516 | 4.87 | 1.89 | 2.98 |
| 250 | Up | One Year | Limestone | 450 | 9.58 | 0.00 | 14.30 |
| 250 | Up | One Year | Limestone | 491 | 8.78 | 1.89 | 6.89 |
| 250 | Up | One Year | Limestone | 394 | 11.46 | 1.89 | 9.57 |
| 250 | Up | One Year | Limestone | 514 | 10.40 | 6.60 | 3.80 |
| 250 | Up | One Year | PVC | 566 | 1.06 | | |
| 250 | Up | One Year | PVC | 398 | 1.17 | | |
| 250 | Up | One Year | PVC | 576 | 0.62 | | |
| 250 | Up | One Year | PVC | 531 | 0.75 | | |
| 250 | Up | One Year | PVC | 528 | 1.24 | | |
| 250 | Up | One Year | PVC | 519 | 0.78 | | |

# Appendix B: Supplementary information for Chapter 5

Table B1 Mean values of water temperature measurements during the coastal bioerosion experiment. Due to loss of loggers no data is available from the 15 m winter deployment. Due to data loss no values are available from the 250 m winter and all one year platforms.

| Exposure | Water temperature (°C) | | | | | | | | |
|---|---|---|---|---|---|---|---|---|---|
| | Agathi | | | | Lindos | | Kerameni | | Monolithos |
| | 0 m | 0.75 m | 10 m | solution pan B | 0 m | 10 m | 0 m | 10 m | 0 m |
| May 2013 | 20.74 | 20.87 | 24.09 | 25.89 | 21.43 | 24.58 | 20.63 | 23.63 | 20.40 |
| June 2013 | 22.81 | 22.95 | 26.65 | 28.11 | 23.38 | 27.38 | 22.45 | 26.69 | 22.39 |
| July 2013 | 25.47 | 25.66 | 30.16 | 33.25 | 25.95 | 30.75 | 23.44 | 28.43 | 23.42 |
| August 2013 | 27.67 | 27.87 | 31.62 | 34.08 | 28.07 | 31.92 | 25.15 | 29.27 | 25.17 |
| September 2013 | 25.61 | 25.84 | 28.31 | 30.26 | 25.84 | 27.89 | 23.78 | 27.29 | 23.84 |
| October 2013 | 22.25 | 22.46 | 22.81 | 21.97 | 22.41 | 22.43 | 21.03 | 22.24 | 21.40 |
| November 2013 | 20.52 | 20.80 | 19.63 | 18.46 | 20.73 | 19.70 | 20.43 | 19.54 | 20.39 |
| December 2013 | 17.47 | 18.30 | 14.48 | 14.02 | 17.66 | 14.34 | 15.83 | 13.98 | 16.73 |
| January 2014 | 17.48 | 17.63 | 15.21 | 15.07 | 17.48 | 15.62 | 17.25 | 15.59 | 17.18 |
| February 2014 | 16.75 | 17.22 | 15.78 | 15.74 | 16.79 | 15.83 | 16.50 | 15.78 | 16.63 |
| March 2014 | 16.54 | 17.23 | 16.30 | 16.65 | 16.64 | 16.33 | 16.06 | 16.60 | 16.29 |
| April 2014 | 17.93 | 18.13 | 18.73 | 19.21 | 18.29 | 19.25 | 17.76 | 19.27 | 17.76 |

# Appendix C: Supplementary information for Chapter 6

Table C1 Measurement of sponge spicules from the long-term experiment.

| Identified Sponge | | Tylostyles | | Spirasters | | | | | |
|---|---|---|---|---|---|---|---|---|---|
| | | | | a | | b | | c | |
| | | Length (µm) | Width (µm) | Length (µm) | Width (µm) | Length (µm) | Width (µm) | Length (µm) | Width (µm) |
| *Cliona schmidtii* | Fig. 6.6A | 196 | 5 | 67 | 2 | 35 | 3 | 17 | 3 |
| | | 200 | 5 | 57 | 2 | 31 | 2 | | |
| | | 199 | 3 | 67 | 2 | 28 | 3 | | |
| | | 195 | 6 | 71 | 2 | 34 | 2 | | |
| | | 207 | 5 | 69 | 3 | 52 | 3 | | |
| | | 199 | 4 | | | | | | |
| | | 203 | 5 | | | | | | |
| | | 194 | 6 | | | | | | |
| | | 198 | 5 | | | | | | |
| | | 203 | 6 | | | | | | |
| | | 247 | 5 | | | | | | |
| | | 206 | 5 | | | | | | |
| | | 198 | 5 | | | | | | |
| | | 190 | 6 | | | | | | |
| | | 177 | 5 | | | | | | |
| | | 170 | 4 | | | | | | |
| | | 199 | 4 | | | | | | |
| | | 195 | 5 | | | | | | |
| | | 194 | 8 | | | | | | |
| | | 197 | 5 | | | | | | |
| *Cliona schmidtii* | Fig. 6.6B | 275 | 6 | 84 | 2 | 25 | 2 | 21 | 7 |
| | | 262 | 6 | 58 | 2 | 34 | 2 | | |
| | | 260 | 5 | 78 | 2 | 30 | 2 | | |
| | | 231 | 5 | 73 | 1 | 39 | 2 | | |
| | | 230 | 5 | 80 | 1 | 46 | 2 | | |
| | | 227 | 5 | | | | | | |
| | | 224 | 5 | | | | | | |
| | | 223 | 5 | | | | | | |
| | | 221 | 5 | | | | | | |
| | | 215 | 5 | | | | | | |
| | | 211 | 5 | | | | | | |
| | | 210 | 5 | | | | | | |
| | | 208 | 5 | | | | | | |
| | | 208 | 4 | | | | | | |
| | | 208 | 4 | | | | | | |
| | | 208 | 4 | | | | | | |

Table C1 Continued.

| Identified Sponge | | Tylostyles | | Spirasters | | | | | |
|---|---|---|---|---|---|---|---|---|---|
| | | | | a | | b | | c | |
| | | Length (µm) | Width (µm) | Length (µm) | Width (µm) | Length (µm) | Width (µm) | Length (µm) | Width (µm) |
| | | 207 | 4 | | | | | | |
| | | 205 | 4 | | | | | | |
| | | 199 | 4 | | | | | | |
| | | 179 | 3 | | | | | | |
| *Cliona* cf. *celata* 1 | Fig. 6.6C | 373 | 13 | | | | | | |
| | | 359 | 11 | | | | | | |
| | | 351 | 11 | | | | | | |
| | | 346 | 11 | | | | | | |
| | | 344 | 11 | | | | | | |
| | | 341 | 11 | | | | | | |
| | | 339 | 11 | | | | | | |
| | | 339 | 10 | | | | | | |
| | | 333 | 10 | | | | | | |
| | | 331 | 10 | | | | | | |
| | | 326 | 10 | | | | | | |
| | | 319 | 10 | | | | | | |
| | | 317 | 10 | | | | | | |
| | | 311 | 10 | | | | | | |
| | | 302 | 10 | | | | | | |
| | | 300 | 10 | | | | | | |
| | | 290 | 10 | | | | | | |
| | | 286 | 9 | | | | | | |
| | | 260 | 6 | | | | | | |
| | | 243 | 6 | | | | | | |
| *Cliona* cf. *celata* 2 | Fig. 6.6D | 369 | 8 | | | | | | |
| | | 364 | 7 | | | | | | |
| | | 352 | 7 | | | | | | |
| | | 347 | 7 | | | | | | |
| | | 343 | 7 | | | | | | |
| | | 339 | 7 | | | | | | |
| | | 337 | 6 | | | | | | |
| | | 331 | 6 | | | | | | |
| | | 329 | 6 | | | | | | |
| | | 328 | 6 | | | | | | |
| | | 327 | 6 | | | | | | |
| | | 319 | 6 | | | | | | |
| | | 312 | 6 | | | | | | |
| | | 307 | 6 | | | | | | |

Table C1 Continued.

| Identified Sponge | | Tylostyles | | Spirasters | | | | | |
|---|---|---|---|---|---|---|---|---|---|
| | | | | a | | b | | c | |
| | | Length (µm) | Width (µm) | Length (µm) | Width (µm) | Length (µm) | Width (µm) | Length (µm) | Width (µm) |
| | | 304 | 6 | | | | | | |
| | | 300 | 6 | | | | | | |
| | | 293 | 5 | | | | | | |
| | | 270 | 5 | | | | | | |
| | | 226 | 5 | | | | | | |
| | | 218 | 4 | | | | | | |
| *Cliona* cf. *celata* 2 | Fig. 6.6E | 339 | 9 | | | | | | |
| | | 337 | 8 | | | | | | |
| | | 337 | 8 | | | | | | |
| | | 333 | 7 | | | | | | |
| | | 331 | 7 | | | | | | |
| | | 322 | 6 | | | | | | |
| | | 310 | 6 | | | | | | |
| | | 299 | 6 | | | | | | |
| | | 299 | 6 | | | | | | |
| | | 296 | 6 | | | | | | |
| | | 296 | 5 | | | | | | |
| | | 293 | 5 | | | | | | |
| | | 292 | 5 | | | | | | |
| | | 247 | 5 | | | | | | |
| | | 246 | 5 | | | | | | |
| | | 232 | 5 | | | | | | |
| | | 220 | 4 | | | | | | |
| | | 219 | 4 | | | | | | |
| | | 211 | 4 | | | | | | |
| | | 208 | 3 | | | | | | |
| *Cliona* cf. *celata* 2 | Fig. 6.6F | 358 | 9 | | | | | | |
| | | 351 | 9 | | | | | | |
| | | 351 | 8 | | | | | | |
| | | 349 | 8 | | | | | | |
| | | 347 | 8 | | | | | | |
| | | 341 | 7 | | | | | | |
| | | 337 | 7 | | | | | | |
| | | 336 | 7 | | | | | | |
| | | 334 | 7 | | | | | | |
| | | 333 | 7 | | | | | | |
| | | 332 | 7 | | | | | | |
| | | 332 | 7 | | | | | | |

Table C1 Continued.

| Identified Sponge | | Tylostyles | | Spirasters | | | | | |
|---|---|---|---|---|---|---|---|---|---|
| | | | | a | | b | | c | |
| | | Length (μm) | Width (μm) | Length (μm) | Width (μm) | Length (μm) | Width (μm) | Length (μm) | Width (μm) |
| | | 331 | 7 | | | | | | |
| | | 322 | 6 | | | | | | |
| | | 312 | 6 | | | | | | |
| | | 311 | 6 | | | | | | |
| | | 305 | 6 | | | | | | |
| | | 253 | 6 | | | | | | |
| | | 250 | 6 | | | | | | |
| | | 235 | 5 | | | | | | |
| *Cliona* cf. *viridis* | Fig. 6.6G | 356 | 6 | 32 | 1 | | | | |
| | | 308 | 5 | 20 | 1 | | | | |
| | | 303 | 5 | | | | | | |
| | | 301 | 5 | | | | | | |
| | | 300 | 5 | | | | | | |
| | | 299 | 5 | | | | | | |
| | | 294 | 5 | | | | | | |
| | | 291 | 4 | | | | | | |
| | | 290 | 4 | | | | | | |
| | | 269 | 4 | | | | | | |
| | | 269 | 4 | | | | | | |
| | | 267 | 4 | | | | | | |
| | | 265 | 4 | | | | | | |
| | | 250 | 4 | | | | | | |
| | | 249 | 4 | | | | | | |
| | | 249 | 4 | | | | | | |
| | | 244 | 3 | | | | | | |
| | | 229 | 3 | | | | | | |
| | | 218 | 3 | | | | | | |
| | | 217 | 3 | | | | | | |
| *Cliona* cf. *viridis* | Fig. 6.6H | 394 | 9 | 44 | 2 | 18 | 1 | | |
| | | 378 | 8 | 32 | 1 | | | | |
| | | 360 | 8 | 36 | 1 | | | | |
| | | 356 | 8 | 30 | 1 | | | | |
| | | 351 | 8 | 32 | 1 | | | | |
| | | 348 | 8 | | | | | | |
| | | 341 | 7 | | | | | | |
| | | 341 | 7 | | | | | | |
| | | 341 | 7 | | | | | | |
| | | 340 | 7 | | | | | | |

Table C1 Continued.

| Identified Sponge | | Tylostyles | | Spirasters | | | | | |
|---|---|---|---|---|---|---|---|---|---|
| | | | | a | | b | | c | |
| | | Length (μm) | Width (μm) | Length (μm) | Width (μm) | Length (μm) | Width (μm) | Length (μm) | Width (μm) |
| | | 336 | 7 | | | | | | |
| | | 334 | 6 | | | | | | |
| | | 313 | 6 | | | | | | |
| | | 310 | 6 | | | | | | |
| | | 310 | 6 | | | | | | |
| | | 302 | 6 | | | | | | |
| | | 295 | 6 | | | | | | |
| | | 261 | 5 | | | | | | |
| | | 237 | 5 | | | | | | |
| | | 234 | 4 | | | | | | |
| *Cliona rhodensis* | Fig. 6.6I | 356 | 10 | 23 | 1 | | | | |
| | | 345 | 10 | | | | | | |
| | | 327 | 10 | | | | | | |
| | | 313 | 9 | | | | | | |
| | | 311 | 9 | | | | | | |
| | | 304 | 9 | | | | | | |
| | | 303 | 9 | | | | | | |
| | | 301 | 8 | | | | | | |
| | | 290 | 8 | | | | | | |
| | | 289 | 8 | | | | | | |
| | | 286 | 8 | | | | | | |
| | | 286 | 7 | | | | | | |
| | | 271 | 7 | | | | | | |
| | | 267 | 7 | | | | | | |
| | | 267 | 7 | | | | | | |
| | | 265 | 7 | | | | | | |
| | | 251 | 7 | | | | | | |
| | | 249 | 6 | | | | | | |
| | | 246 | 6 | | | | | | |
| | | 245 | 6 | | | | | | |

Table C2 Volume of bioerosion, surface of marble blocks, and bioerosion rates quantified via micro-computed tomography from the long-term experiment.

| Exposure (years) | Block | Volume ($mm^3$) | | | | | | Surface block ($mm^2$) | Bioerosionsrate ($g\ m^{-2}\ yr^{-1}$) |
|---|---|---|---|---|---|---|---|---|---|
| | | Marble | Total Bio-erosion | Microbio-erosion | Macrobio-erosion unassignable | Sponge | Worm | | |
| 1 | Fig. 6.2A | 147892.30 | 8.99 | 5.93 | 3.06 | 0.00 | 0.00 | 8195.10 | 2.96 |
| 1 | Fig. 6.2B | 139205.59 | 12.36 | 10.92 | 1.44 | 0.00 | 0.00 | 7783.30 | 4.29 |
| 2 | Fig. 6.2C | 160190.72 | 1399.10 | 14.36 | 1384.74 | 1266.47 | 0.00 | 8443.30 | 223.70 |
| 3 | Fig. 6.2D | 147351.59 | 780.63 | 16.15 | 764.49 | 751.18 | 0.00 | 8245.40 | 85.21 |
| 4 | Fig. 6.2E | 152550.53 | 102.59 | 13.58 | 89.01 | 0.00 | 0.00 | 8533.53 | 8.12 |
| 4 | Fig. 6.2F | 144569.38 | 18.61 | 12.07 | 6.54 | 0.00 | 0.00 | 8202.60 | 1.53 |
| 5 | Fig. 6.3A | 135287.11 | 5827.76 | 21.74 | 5806.01 | 5711.59 | 6.49 | 8611.49 | 365.44 |
| 6 | Fig. 6.3B | 138384.08 | 5719.56 | 31.23 | 5688.34 | 5575.66 | 0.00 | 8352.80 | 308.14 |
| 7 | Fig. 6.4A | 144971.63 | 1133.49 | 9.11 | 1124.37 | 1038.85 | 0.00 | 8234.10 | 53.10 |
| 7 | Fig. 6.4B | 139240.78 | 7111.60 | 18.80 | 7092.80 | 6901.71 | 0.00 | 8259.00 | 332.13 |
| 7 | Fig. 6.4C | 136287.44 | 13599.95 | 37.96 | 13561.98 | 13377.67 | 0.00 | 8095.50 | 647.98 |
| 8 | Fig. 6.5A | 130851.24 | 11746.90 | 121.04 | 11625.86 | 11370.66 | 0.00 | 8307.20 | 477.25 |
| 8-9 | Fig. 6.5B | 142975.11 | 1640.60 | 16.98 | 1623.61 | 1468.67 | 0.00 | 8372.20 | 62.25 |
| 14 | Fig. 6.5C | 93275.38 | 40008.29 | 27.96 | 39980.33 | 39896.29 | 48.51 | 8569.50 | 900.39 |